AD-A118 515 NORTH CAROLINA STATE UNIV RALEIGH DEPT OF PHYSICS F/G 20/7
OBSERVATIONS OF COLLECTIVE ION ACCELERATION.(U)
1981 D L MORROW AFOSR-80-0051
UNCLASSIFIED AFOSR-TR-82-0641 NL

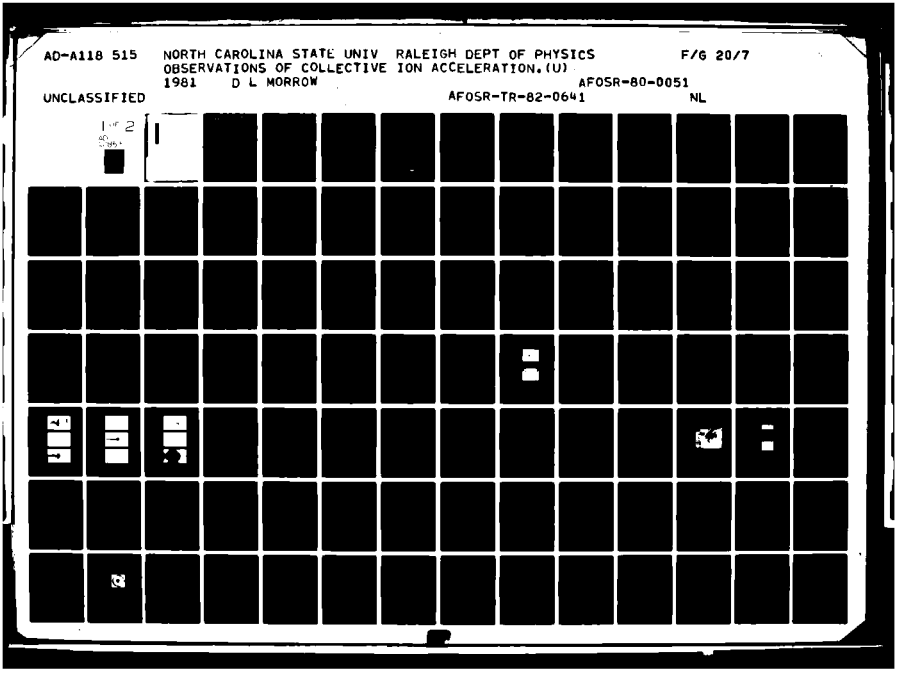

UNCLASSIFIED
SECURITY CLASSIFICATION OF THIS PAGE (When Data Entered)

REPORT DOCUMENTATION PAGE		READ INSTRUCTIONS BEFORE COMPLETING FORM
1. REPORT NUMBER AFOSR-TR- 82-0641	2. GOVT ACCESSION NO. AD-A118515	3. RECIPIENT'S CATALOG NUMBER
4. TITLE (and Subtitle) OBSERVATIONS OF COLLECTIVE ION ACCELERATION		5. TYPE OF REPORT & PERIOD COVERED INTERIM
		6. PERFORMING ORG. REPORT NUMBER
7. AUTHOR(s) David Lee Morrow		8. CONTRACT OR GRANT NUMBER(s) AFOSR-80-0051
9. PERFORMING ORGANIZATION NAME AND ADDRESS North Carolina State University Physics Department Raleigh, NC 27650		10. PROGRAM ELEMENT, PROJECT, TASK AREA & WORK UNIT NUMBERS 61102F 2301/A7
11. CONTROLLING OFFICE NAME AND ADDRESS AFOSR/NP Building 410 Bolling AFB, DC 20332		12. REPORT DATE 1981
		13. NUMBER OF PAGES 128
14. MONITORING AGENCY NAME & ADDRESS(if different from Controlling Office)		15. SECURITY CLASS. (of this report) UNCLASSIFIED
		15a. DECLASSIFICATION/DOWNGRADING SCHEDULE

16. DISTRIBUTION STATEMENT (of this Report)

APPROVED FOR PUBLIC RELEASE; DISTRIBUTION UNLIMITED

17. DISTRIBUTION STATEMENT (of the abstract entered in Block 20, if different from Report)

18. SUPPLEMENTARY NOTES

19. KEY WORDS (Continue on reverse side if necessary and identify by block number)

20. ABSTRACT (Continue on reverse side if necessary and identify by block number)

Linear collective acceleration of protons by a relativistic electron beam (0.5 MeV, 50 kA, 60 ns) was explored in the vacuum diode and vacuum drift tube. Nylon meshes, polyethylene films, and nylon dilaments as proton sources were tested along with the variation of cathode-anode-target spacings. Target activation was used to compare the various arrangements and to yield information concerning proton energies, amounts, and spatial distributions. Proton energies in excess of 7 MeV (12 times the electron energy) were produced with filaments in 30 cm long drift tubes. A few times 10^{10} particles were accelerated at (cont.)

DD FORM 1 JAN 73 1473 EDITION OF 1 NOV 65 IS OBSOLETE

UNCLASSIFIED
SECURITY CLASSIFICATION OF THIS PAGE (When Data Entered)

82 08 23 084

20. Cont.

this level. Activation was localized to a target spot and an axial streak on the drift tube wall. Electron beam behavior in the drift tube was examined with a Rogowski coil to measure the current and PIN diodes to measure bremsstrahlung. In addition, the periodic activation of dielectric cathodes by radially accelerated protons is reported.

ABSTRACT

MORROW, DAVID LEE. Observations of Collective Ion Acceleration. (Under the direction of Wesley O. Doggett.)

Linear collective acceleration of protons by a relativistic electron beam (0.5 MeV, 50 kA, 60 ns) was explored in the vacuum diode and vacuum drift tube. Nylon meshes, polyethylene films, and nylon filaments as proton sources were tested along with the variation of cathode-anode-target spacings. Target activation was used to compare the various arrangements and to yield information concerning proton energies, amounts, and spatial distributions. Proton energies in excess of 7 MeV (12 times the electron energy) were produced with filaments in 30 cm long drift tubes. A few times 10^{10} particles were accelerated at this level. Activation was localized to a target spot and an axial streak on the drift tube wall. Electron beam behavior in the drift tube was examined with a Rogowski coil to measure the current and PIN diodes to measure bremsstrahlung. In addition, the periodic activation of dielectric cathodes by radially accelerated protons is reported.

Accession For	
NTIS GRA&I	X
DTIC TAB	☐
Unannounced	☐
Justification	
By	
Distribution/	
Availability Codes	
Dist	Avail and/or Special
A	

DTIC COPY INSPECTED 2

AIR FORCE OFFICE OF SCIENTIFIC RESEARCH (AFSC)
NOTICE OF TRANSMITTAL TO DTIC
This technical report has been reviewed and is approved for public release IAW AFR 190-12.
Distribution is unlimited.
MATTHEW J. KERPER
Chief, Technical Information Division

OBSERVATIONS OF COLLECTIVE ION ACCELERATION

by

DAVID LEE MORROW

A thesis submitted to the Graduate Faculty of
North Carolina State University at Raleigh
in partial fulfillment of the
requirements for the Degree of
Doctor of Philosophy

DEPARTMENT OF PHYSICS

RALEIGH

1 9 8 1

APPROVED BY:

David F Ullrich — Carter M Armstrong

Allen W Jenkins Jr — [illegible]

Cochairman of Advisory Committee

Wesley A Doggett

Cochairman of Advisory Committee

BIOGRAPHY

David Lee Morrow was born on May 8, 1947, in Monroe North Carolina. He grew up there and graduated from Monroe Senior High School in 1965.

As an undergraduate, he studied at Davidson College where he was a member of Phi Eta Sigma and Sigma Pi Sigma. He received a Bachelor of Science degree cum laude in Physics in 1969. The summer of his junior year he participated in a research program at Oak Ridge National Laboratory.

While a graduate student in Plasma Physics at North Carolina State University, he has held research and teaching assistantships, receiving an Outstanding Teaching Assistant Award. On three occasions he has been a summer research assistant at Los Alamos National Laboratory. He is a member of Phi Kappa Phi and the American Physical Society.

His outside interests include music, concerts, theater, movies, and reading.

ACKNOWLEDGMENTS

The author wishes to especially thank Drs. W. O. Doggett and W. H. Bennett for their support and guidance during his graduate career. He also wishes to acknowledge the help he received from Drs. C. M. Armstrong, A. W. Jenkins, and D. F. Ullrich, the other members of his graduate committee. In addition the assistance of Dr. J. J. Kim is appreciated.

The following fellow graduate student collaborators considerably eased the way: James D. Phillips, Ray M. Stringfield, Stanley P. Converse, Dean E. Pershing, and John R. Smith. For construction of apparatus the author is indebted to Mr. Tom Hill and Mr. Stanley Mezynski. Further technical aid was provided by David Wheeler.

Finally, the author wishes to thank Miss Martha L. Turner for her patience in the preparation of this manuscript.

This work is supported by the Air Force Office of Scientific Research.

TABLE OF CONTENTS

TABLE OF CONTENTS
(continued)

LIST OF TABLES

LIST OF FIGURES

LIST OF FIGURES
(continued)

1. HISTORICAL REVIEW

1.1 Motivation and Objectives

The promise of collective acceleration is one of high energy and high current ion pulses produced in relatively small machines. The ions produced collectively can, in principle, be used for most of the same applications as the ions of more conventional accelerators. Collective and conventional accelerators could even be used together, with one type injecting into the other. Of course, it remains to be seen whether or not sufficient beam quality can be achieved. Even today, though, heavy ions have been accelerated to high energies, and may be useful in studying the reactions between heavy nuclei or the production of superheavy elements.

Collective accelerators may find a use as injectors for other devices. An application of this sort would be the injection of the ion beam into a fusion plasma for heating. However, collective accelerators could find a more direct application such as the focusing of the ion beam onto a pellet for inertial confinement fusion. An advantage is gained here because the ions more efficiently impart their energy to heat the atoms of the target. In a similar vein, the shocks produced in targets when bombarded by ion beams are also of interest.

Some other areas of possible benefit can be listed. In cancer therapy, radiation produced by ion beams may be more selectively directed into tumors. Ion beams in spallation breeders may be used to produce fissile material from fertile material. Particle beams have, in addition, been proposed as weapons.

In view of such applications and the availability of the FX75 in Seattle and the Seven Ohm Line at NCSU, we have undertaken a series of experiments to elucidate the production and control of collective ion acceleration. Our interest has been to maximize the ion energy and minimize the length of the acceleration region. The distribution of ions in space and energy was also of interest, as was the behavior of the electron beam which produced the accelerating fields.

More basically, the opportunity to study new physical processes is of interest in itself apart from any immediate application. Here, instead of trying to minimize collective effects, we are trying to use them to advantage. In the process we can expect to learn much about nonlinear behavior and the interactions between electron beams and ions.

1.2 Early Developments

Reviews of the literature[1-9] indicate that the earliest schemes employing collective effects for particle acceleration were those of Raudorf[10] and Alfven and Wernholm[11]. Even in these initial conceptions, the authors recognized features which were central to later developments.

Raudorf proposed an "electronic ram" which was to function in a manner similar to its hydraulic counterpart. It featured an electron beam in a drift tube with an axial magnetic field. Acceleration was to be achieved by sudden stalling of the beam at an abrupt increase in the magnetic field. The ensuing increase in space charge and the additional induced fields were to provide the accelerating forces. He described the process as one of a large moving charge giving up its energy to a small fraction of that charge. This feature is a basic characteristic of many subsequent proposals.

Alfven and Wernholm described a device in which an electron beam was focussed by external fields. The point of focus was then to be scanned, and its strong space charge fields used to pull ions along. Again, in later developments, the space charge fields of electron beams have figured prominently, as has focussing by means of electrostatic lenses.

General interest was not apparently aroused in collective acceleration per se until the CERN symposium in 1956. At this meeting papers by Budker[12], Veksler, and Fainberg[13], besides proposing particular schemes, addressed features which make collective acceleration attractive in general. Budker pointed out that the requirements of curl B and div E equal to zero in the region of accelerating particles places severe restrictions on field structure which can be eliminated if plasmas or beams are present. These can then provide strong focussing and accelerating fields which would not otherwise be possible. As Veksler[14] pointed out, a great economy in size might also be attained.

At the CERN meeting and elsewhere[15], Veksler proposed two collective acceleration methods which were, in addition, coherent. These methods, known as inverse Cerenkov and impact acceleration, were such that the accelerating force on each particle was proportional to the number of particles being accelerated. Thus the total force on the bunch was proportional to N^2, where N was the number of particles in the ion bunch. It is interesting to note that, although his original schemes had serious practical difficulties[3], the creation of charged particle bunches in its pursuit led to the electron ring accelerator. This latter program has produced several large projects.

The first actual observation of collective ion acceleration appears to be that of Plyutto[16] in a plasma filled diode experiment. His extraction voltage was 9 kV but he obtained H+ and D+ ions of 18 kV, Li+ of 24 kV, and C+ of 35 kV. This work was later extended to a vacuum diode[17-18] in which the acceleration of cathode material ions were observed. The ions were accelerated toward the anode. Maximum ion energies of 10-15 MeV for a breakdown voltage of 300 kV were cited. These were Al and C ions.

The first acceleration of ions by injecting an intense relativistic electron beam into a neutral gas was that of Graybill and Uglam[19]. With a peak beam energy of 1.6 MeV, they observed p and d energies of 5 MeV, He of 9 MeV, and N of 20 MeV. These observations generated considerable subsequent experimental and theoretical work on firing into neutral gas. It is not, however, the purpose of this work to follow these events further, but the previously cited review papers provide a key to the literature.

1.3 Vacuum Diode Work

More germane to the NCSU studies were the observations of Kerns et al.[20-21] Working in a vacuum diode and using a dielectric cathode[22], these workers discovered neutron production when the electron beam irradiated a CD_2 target. The neutron production mechanism was believed to be thermal (i.e. fusion) in origin.

Investigations by Bradley and Kuswa[23-24] also produced neutrons but only with deuterated cathodes. They also observed accelerated H, D, and C ions arriving at the anode. This observation indicated that the neutrons were actually due to accelerated cathode ions interacting at the anode. The debate over thermal vs ion beam neutrons continued in subsequent publications[25-30]. Similar experiments by Freeman et al.[31-33], trying

to optimize the geometry, were simultaneously underway.

With the development of the Luce diode[31, 34], some attention was turned from neutron production to actual ion acceleration. In this diode an insulated anode of CH_2 with an aperture is used. The electron beam fires through the aperture into a target behind the anode. The accelerated ions are generated at the anode and are carried with the beam to the target beyond. Pulses of 10^{14} ions with energies up to 15 MeV were observed using a 2.5 MeV electron beam.

In subsequent work, Luce[35] used an electrostatic lens after the anode and used grounded, as well as insulated, targets. He found that, with the lens, the grounded targets gave better results and higher ion energies. Experiments with the Luce diode and lenses were undertaken by Zorn et al.[36, 37] with similar results. Hoeberling et al.[38, 39] and Williams[40] have also reported investigations with the Luce diode. Hoeberling obtained ions 2-3 times the beam energy while Williams obtained 5 times.

Most recently, Luce[41] has reported accelerating protons to 40 MeV using the Boeing FX75 (3 MeV). Half this acceleration is claimed to have occurred in a region 6-7 cm long. Meanwhile, the Maryland group[42-45] has concentrated on heavy ion acceleration. They have accelerated krypton to 390 MeV. In these last experiments they departed from the Luce diode, using instead a metal anode with an aperture. The ions to be accelerated were provided by a puff of gas into the aperture. Adler and Nation[46, 47] have reported acceleration of metallic ions.

1.4 Other Trends

Other major trends in collective ion acceleration include the following. The previously mentioned electron ring accelerator[48] uses the space charge

of a closed circulating electron beam trapped in a magnetic field to hold ions. The ions are then accelerated with the ring when it is moved by manipulating the magnetic field.

The autoresonant accelerator[49] uses an electron beam in an axial field. Cyclotron waves are induced to grow on the beam producing potential fluctuations. Ions are then trapped in the waves and accelerated by them, much as in a conventional linear accelerator.

The ionization front accelerator[9] uses a beam injected into neutral gas. Such a beam would normally produce its own ionization front. This project hopes to control the advance of the front by external means (lasers). The strong space charge fields at the ionization front accelerate the ions.

Some researchers are trying to produce high current ion beams. One development in this direction is the reflex triode[50] and tetrode[51]. An electron beam is passed through a plastic foil, and creates a virtual cathode beyond. Ions released at the foil then travel in large quantities to the virtual cathode.

Another development in this program is the magnetically insulated diode[52]. Here, strong magnetic fields prevent the electrons from crossing the diode gap, but have no effect on the much more massive ions. Thus an ion beam is created instead. Both of these schemes, however, produce ion energies only equal to the original charging voltage.

Many other ideas have been tried, and many more suggested. Each method has its problems which must be worked out. The reader is again referred to the literature to pursue these matters.

1.5 Overview of Thesis

In the following sections the results of the collective ion acceleration experiments performed since 1971 in Seattle and at NCSU will be presented. The procedure has been to vary those factors of geometry and ion source which might affect the amount and energy of accelerated ions. In addition, observations of the ion distribution and electron beam behavior are reported. Discussed at appropriate places in the text are the various diagnostics, their use, and the analysis of data obtained from them. The general trend has been to accelerate ions with as simple a diode arrangement as possible.

The experimental work divides logically into three sections, and a chapter is devoted to each. The first division concerns the activation of dielectric cathodes. The second involves the acceleration of ions in the vacuum diode of the electron beam generator. Finally, the acceleration of ions in a vacuum drift tube is described. In a chapter on theory, a simple model is presented illustrating the availability of fields capable of producing the observed acceleration in reasonable times and distances.

2. ACTIVATION OF DIELECTRIC CATHODES

2.1 Description of the FX75 Relativistic Electron Beam Generator

The first observations of ion acceleration made by the plasma physics group at NCSU occurred in March of 1971, while performing electron beam experiments using the FX75 flash x-ray machine at the Boeing Radiation Effects Laboratory in Seattle. Persons participating in this research at this time and in 1974-75 (to be discussed later) were (from NCSU) Dr. W. O. Doggett, Dr. W. H. Bennett, J. D. Phillips, R. M. Stringfield, S. P. Converse, the author, (from Boeing) J. L. Adamski, R. A. Zilbert, J. R. Beymer, and R. L. Guay.

There are basically two distinct types of electron beam machines. The FX75 is an example of the dc charged type, while the 7 Ohm Line at NCSU is of the pulse charged type.

The FX75, Fig. 2.1, consists of a large cylindrical pressure vessel (nominally 23 ft long by 10 ft in diameter) filled with an SF_2-CO_2 mixture at 25 atmospheres for insulation. Inside and coaxial with the outer wall is the head of a Van de Graaff generator. The geometry is such that this head forms the inner conductor of a transmission line with about a 15 ns transit time. The head is separated from the cathode of the diode region by a gap, while the anode is electrically part of the outer machine wall. A bulkhead of alternating plastic and aluminum rings separates the evacuated diode region from the high pressure region.

In operation the Van de Graaff head is charged on a time scale of nominally 30 sec to the desired voltage (up to 6 MV). Then the gap between the head and the cathode is broken down by a triggered spark. The head then discharges through the diode. Due to its transmission

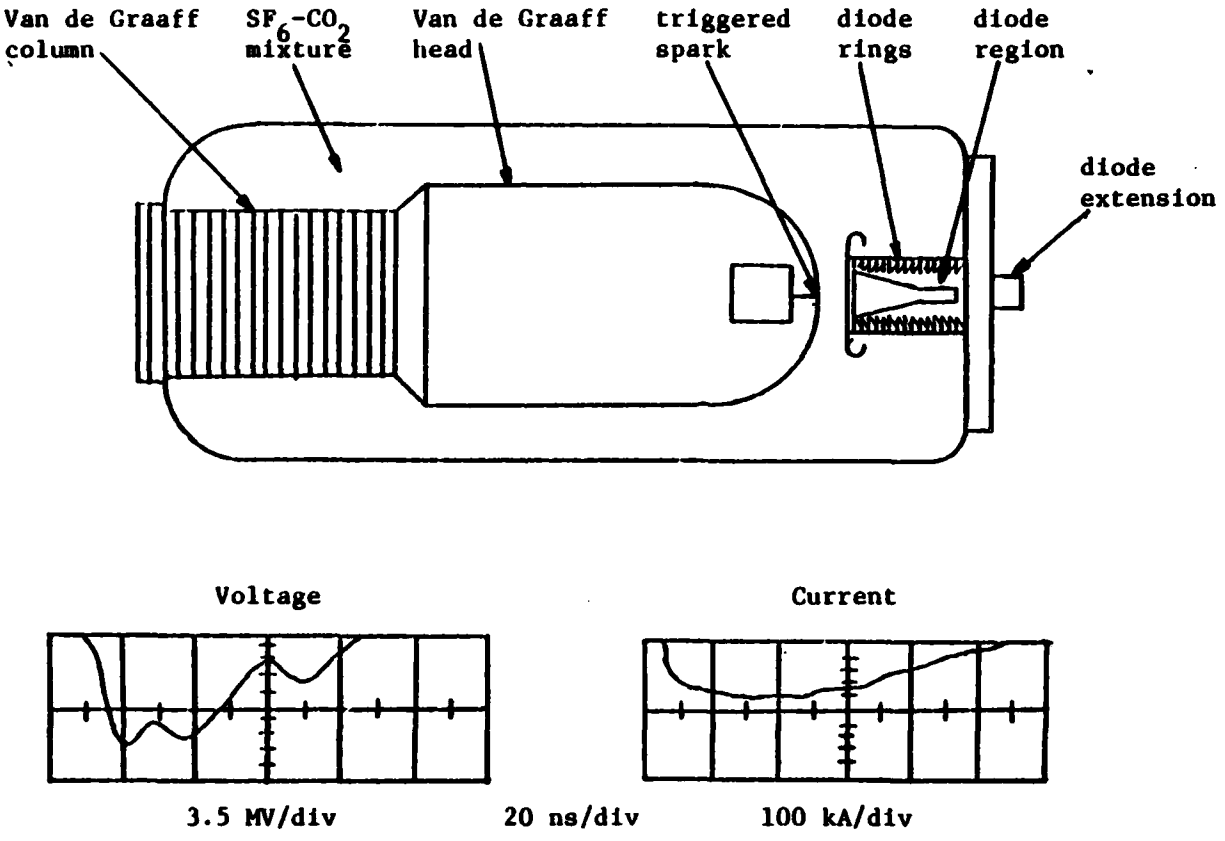

Figure 2.1 The FX75 with typical voltage and current traces

line construction, it tries to maintain a roughly constant voltage on the diode for a time equal to twice its transit time (i.e. 30 ns = 2 x 15 ns). The impedance of the electron beam can, however, have an effect on the actual current and voltage achieved.[53]

The FX75 is capable of voltages of 6 MV, producing a peak electron energy of about 4.5 MeV with a peak current of 50 kA. This gives powers of 225 GW and, in a time of 30 ns, would deliver 6.57 kJ. Typical voltage and current traces are shown in Fig. 2.1. In consequence of being a dc charged machine, no pulse (prepulse) appears in the diode prior to actual firing.

2.2 Experimental Geometry

The general experimental configuration is shown in Fig. 2.2. A metallic cathode came approximately flush with the machine face. A variety of long, narrow shapes of Pyrex could be inserted in cathodes with appropriately matching tips. The dielectric cathode extended beyond the machine face into a glass pipe (10 cm inner diameter) of a suitable length for the cathode. The pipe was terminated in a calorimeter, in the mouth of which the dielectric penetrated without touching. A return current path was provided by 3 copper strips 1 in. wide spaced symmetrically. The assembly was evacuated to pressures in the high 10^{-5} Torr range for firing.

2.3 Initial Activity and Its Identification

It was observed with a hand Geiger counter that the dielectric cathodes were becoming radioactive. In particular, a hollow 6 in. rod of Pyrex 3 mm in diameter was counted with a crystal detector. This measurement was an integral count over the spectrum using time intervals of 100 sec and

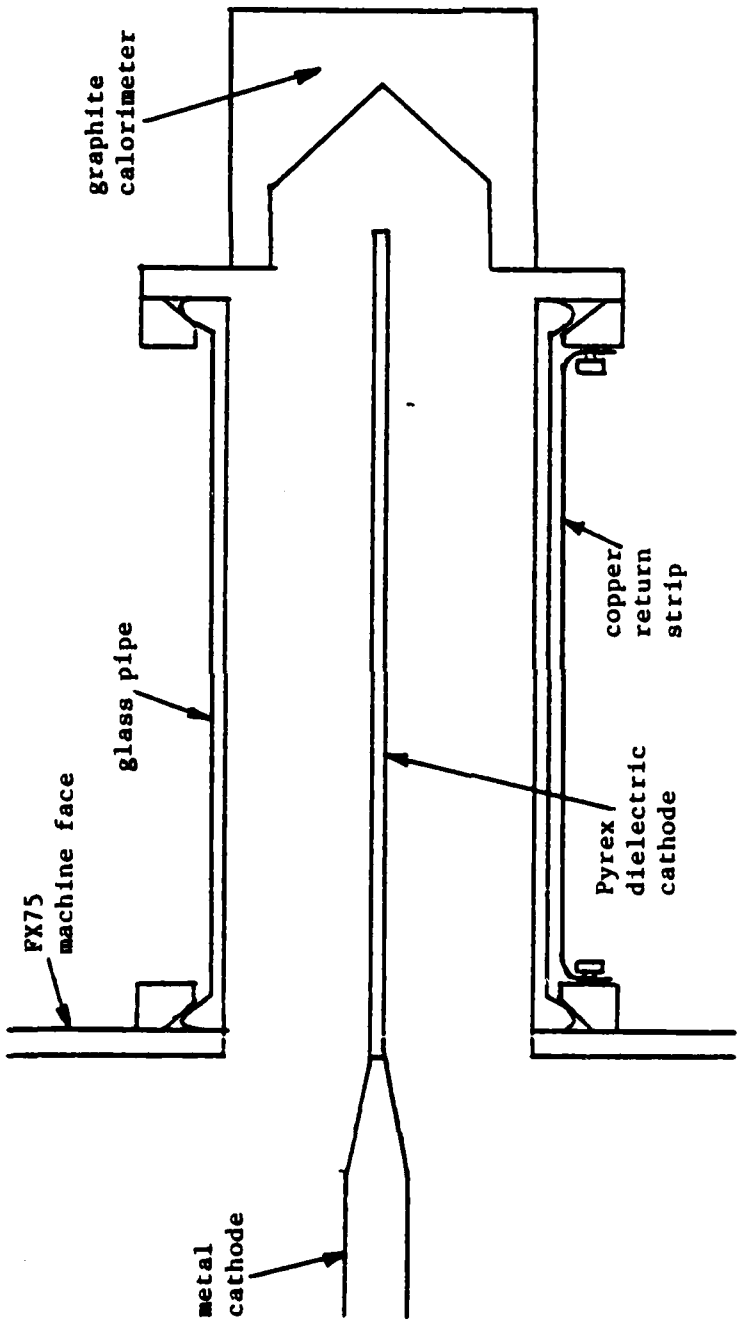

Figure 2.2 General experimental configuration

later 300 and 500 sec. Our initial count was 458,000 in 100 sec, 20 min after the activation was produced.

Analysis of this data led to the identification of the reactions producing the activity. A plot of the data is given in Fig. 2.3. For the decay of a single nuclide, the count rate decreases in time exponentially, so that a semilog plot should give a straight line with a slope proportional to the half-life of the activity. In our case the curve is of two straight lines with a knee indicating two distinct activities, one with a short half-life and one with a long half-life.

The basic analytical approach is to fit the data to a curve of the form

$$A_1 e^{\lambda_1 t} + A_2 e^{\lambda_2 t}$$

after subtracting off the background. One cannot use the usual linear least squares technique here because the fitting parameters (A_1, A_2, λ_1, λ_2) appear nonlinearly in the function. This difficulty cannot be overcome by taking the natural logarithm of the function, as it could in the case of a single species.

Instead, one must use an iterative technique. This calculation begins with an initial guess for the correct values of the fitting parameters. This guess is taken from the two slopes of the plotted data. A tentative curve is then generated and compared with the data. The parameters are modified slightly, and the process continues.

As shown in the figure, the two half-lives were eventually found to be 20.3 min and 110 min, these being produced by a $^{11}B(p,n)^{11}C$ reaction and a $^{18}O(p,n)^{18}F$ reaction respectively. Both ^{11}C and ^{18}F are positron emitters. Pyrex (borosilicate) is nominally 80% SiO_2 (with ^{18}O representing 0.2% of the total oxygen abundance) and 13% B_2O_3 (with ^{11}B representing 80% of the total boron abundance).

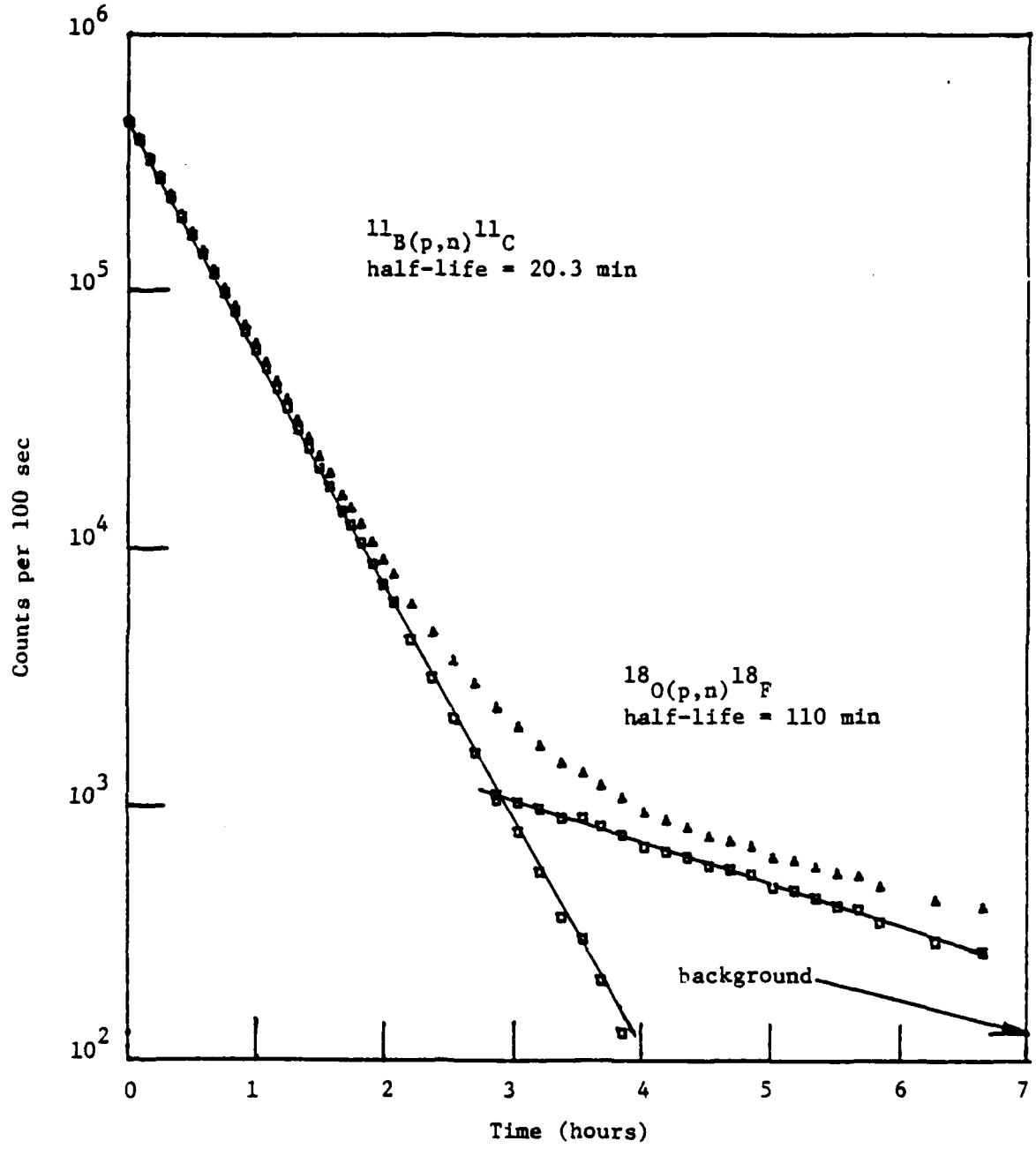

Figure 2.3 Positron activity from Pyrex rod

One may get an idea of the energy of the accelerated protons by calculating the thresholds of the reactions. These thresholds will give the least kinetic energy the proton can have and still produce the reaction. It is calculated from the difference in the masses of the constitutent particles (final masses - initial masses). When this quantity is positive, the proton must supply the difference in kinetic energy. This kinetic energy is in the center of mass frame and must be converted to the laboratory frame. In our case $^{11}B(p,n)^{11}C$ has a threshold of 3 MeV and $^{18}O(p,n)^{18}F$ of 2.6 MeV.

2.4 Investigations of Activity Versus Position

2.4.1 Experimental Method

Succeeding runs on this occasion were devoted to investigating the axial distribution of activity along Pyrex rods of various geometries. For example, a flat Pyrex strip 0.25 in. wide by 0.063 in. thick by 18 cm long was used as a dielectric cathode. The last 2 cm of the strip were sticking into the calorimeter mouth, as described above. 3 shots were fired at 6 MeV.

The strip was broken into approximately equal 2 cm segments. The segments were then counted in succession for 60 sec (in this case each segment was counted 6 times), a record of the time of each count being kept. Background counts were also taken. The detector was a 1-mm thick, Pilot B, plastic scintillator which registered the positron activity. Later, each segment was weighed.

A normalization procedure was used to compare the data of each segment. Assuming the half-life to be known, substitution in the formula,

$$R = \exp[(\ln 2)(T_o+t)/T_{1/2}](C-B)/M$$

gives R, the normalized count rate at firing per gm of material, where $T_{1/2}$ is the half-life, T_o is the time between firing and the first count, t is the time since the first count, C is the counts/min, B is the background counts/min, and M is the mass of the segment in gm. In this way, allowance is made for the variation in mass of each segment and in the decay of its activity from the firing. Multiple shots were sufficiently close in time to represent only a small error out of a 20.3 min half-life.

2.4.2 Comparison of the Collected Data

A summary of the runs in this series is given in Table 2.1. Figs. 2.4, 2.5, and 2.6 show graphs of the runs. The same vertical and horizontal scales are used in each set, distance being measured from the metal cathode tip. The dots represent the data for individual segments.

One first observes the oscillations in activity. There are cases of rough agreement in the period of oscillation. In addition, these seem to be superimposed on a slight decrease in activity as one moves downstream (from cathode to anode). In the case of the 90° bend, there is a sharp decrease in activity just beyond the bend. There was usually an initial rise in activity just moving away from the metal cathode, and a sharp drop in (or no) activity on the tip of the dielectric that extended into the metal calorimeter.

In Run I an attempt was made to depress the activity by overnight pumping and flushing with dry nitrogen. While in Run J an attempt was made to enhance the activity by washing the glass pipe with water before pumping. No systematic effect is apparent in comparing the two runs, however.

Table 2.1 Summary of runs

Code	Length (in.)	Diameter (mm)	Shape	Maximum Counts (counts/min-gm)
A	7	1/4 x 1/16[1]	flat	630,000
B[2]	6.5	4	tube[3]	-
C	13	3	rod[4]	65,000
D[2]	14	3	rod[4]	-
E	13	2	tube	996,000
F	13	3	tube	260,000
G	13	4	tube	75,000
H[2]	13	6	tube	-
I	12	3	tube	120,000
J	12	3	tube	190,000
K	24	2	tube	110,000
L	24	3	tube	70,000
M	24	4	tube	98,000
N[2]	24	10	tube	-
O	24	6	tube	25,000

1 cross section (in.)
2 incomplete data
3 segmented tube
4 90° bend, glass tee replaced glass pipe

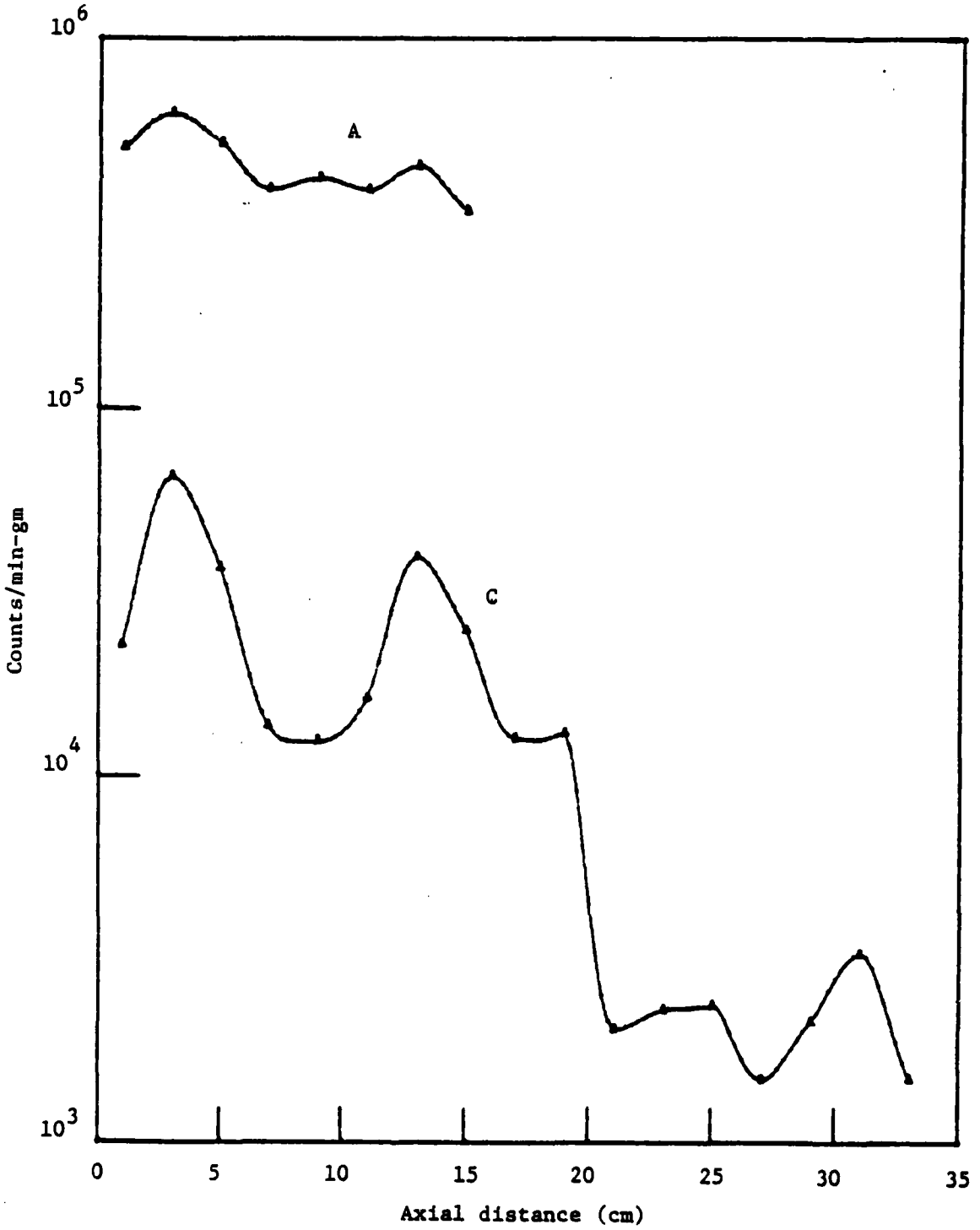

Figure 2.4 Axial variation of activity on dielectric cathodes

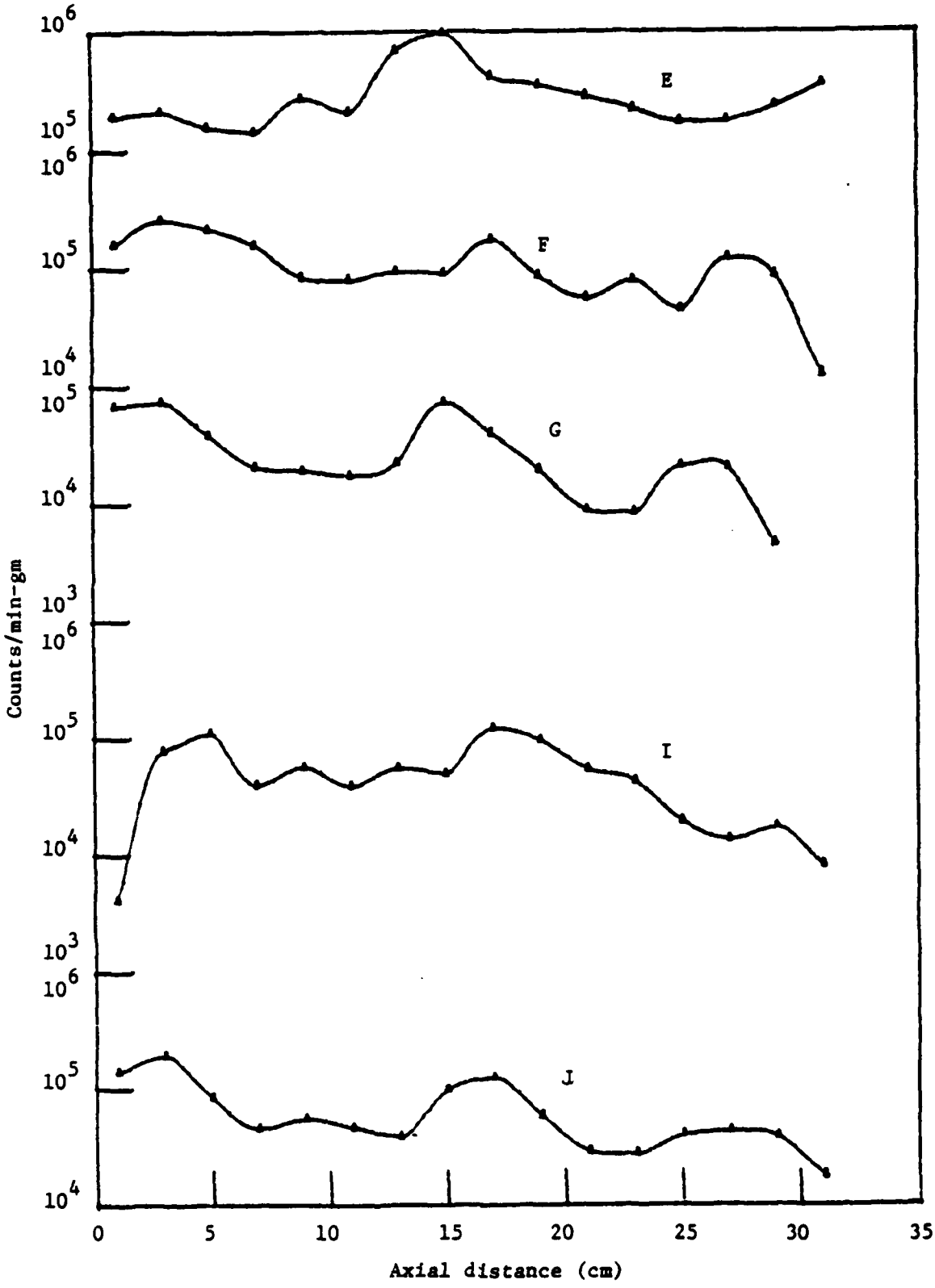

Figure 2.5 Axial variation of activity on dielectric cathodes

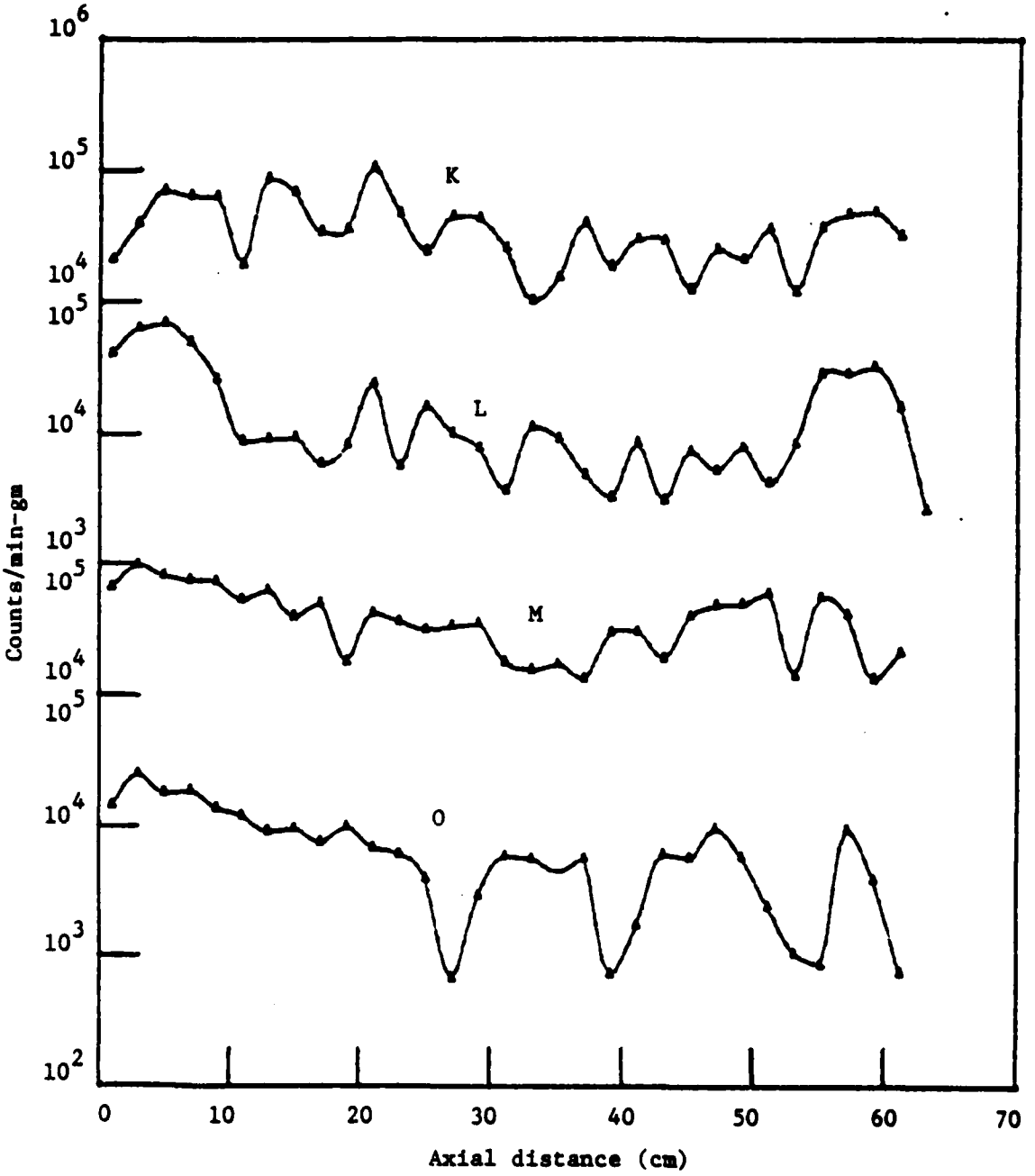

Figure 2.6 Axial variation of activity on dielectric cathodes

2.4.3 Explanation of the Observations

It is believed that the source of protons for acceleration was the wall of the glass pipe. The protons were released by electron bombardment from a coating of, perhaps, diffusion pump oil or cleaning solvent adhering to this wall. Most likely, flashover of the dielectric guide occurs quickly, and the dielectric potential approaches that of the metal cathode. This phenomenon has been studied by Stringfield in his thesis[54]. It does not seem to be necessary to invoke a collective process to account for the observed acceleration in this case.

If we consider a proton with zero velocity at the tube wall moving under the influence of a radial cylindrically symmetric electric field, its acceleration is given by

$$d^2r/dt^2 = \frac{-qV_o}{m\ \ell n(b/a)r}$$

where q is its charge, m is its mass, b is the wall radius, a is the dielectric cathode radius, and V_o is the voltage between the inner and outer radii. Using typical geometrical factors and assuming V_o to be 6 MV, a numerical integration of this equation shows that a proton could reach the axis in less than 5 ns. Thus there seems to be adequate time during the application of the voltage pulse for a proton to achieve the necessary 3 MeV activation thresholds. This process is acceleration by virtue of the intense electrostatic field of the dielectric cathode alone.

Several explanations of the periodicity of the activity are possible. There may have been an actual axial variation due to alternate focussing and defocussing of the electrons in the flashover. This behavior may have caused a periodic structure in the potential of the dielectric cathode or in the pattern of release of protons from the wall. However,

it may have been that the activity on the cathode was in a spiral pattern along its length. This spiral would have given an effective oscillation in observed count rate, due to the absorption of positrons by the dielectric material itself when the activity was turned away from the detector. The actual placement of the segments on the detector does not seem to have been a factor, since in cases of multiple counts of each segment they maintain their relative count rates.

These experiments suggest the possibility of producing a cylindrical radially-focussed ion beam, with proper adjustment of parameters effecting ion release at the walls and uniformity of potentials in the tube. Likewise, it is also evident that, with refinement, this technique may be used to explore electron beam behavior, being sensitive to these potentials and bombardment. So far, these experiments are unique in the history of ion acceleration. A later proposal by SPIRE Corporation to release ions from the walls of a dielectric liner is similar in nature and was in part investigated by Pershing in his thesis[55]. Some of the work described in this section has been previously reported[56].

3. ION ACCELERATION IN THE DIODE

3.1 Experimental Configurations

In 1970 Doggett proposed ion acceleration in the vacuum diode and in the direction of the electron beam[57]. Ions were to be provided by beam bombardment of a thin filament, membrane, or pellet suspended in the cathode-anode gap. In 1972 Luce and Sahlin achieved ion acceleration in a dielectric cylinder placed in the vacuum diode region[34]. The experiments performed in May 1974 and May 1975 by the NCSU plasma group on the FX75 combine both of these ideas.

Fig. 3.1 shows the general 1974 configuration. This diagram shows a pointed, copper cathode with a hood. The purpose of the hood was to intercept particles blasted back from the target area. As before, dielectric rods could be inserted in the end of the cathode. Alumina (Al_2O_3) ceramic rods replaced the Pyrex used previously. Alumina had been found to be more capable of surviving repeated firings. These rods were of variable length and tapered from 3 mm diameter to 1 mm. Mounted on the anode was a metal pedestal with a holder for a thick, graphite, target disk. Graphite was used because it is both conducting and durable, and does not spall, as do metal targets. This target was taken to be the actual anode. Surrounding the pedestal was a polyethylene cylinder, which was of variable length, with a 2.5 in. inner diameter. This cylinder was held in place by a slip fit over a short, interior, cylindrical support mounted in the anode. A polyethylene washer fitting into the mouth of the cylinder held the films, strings, etc. in place. The diameter of the washer opening was 4 cm.

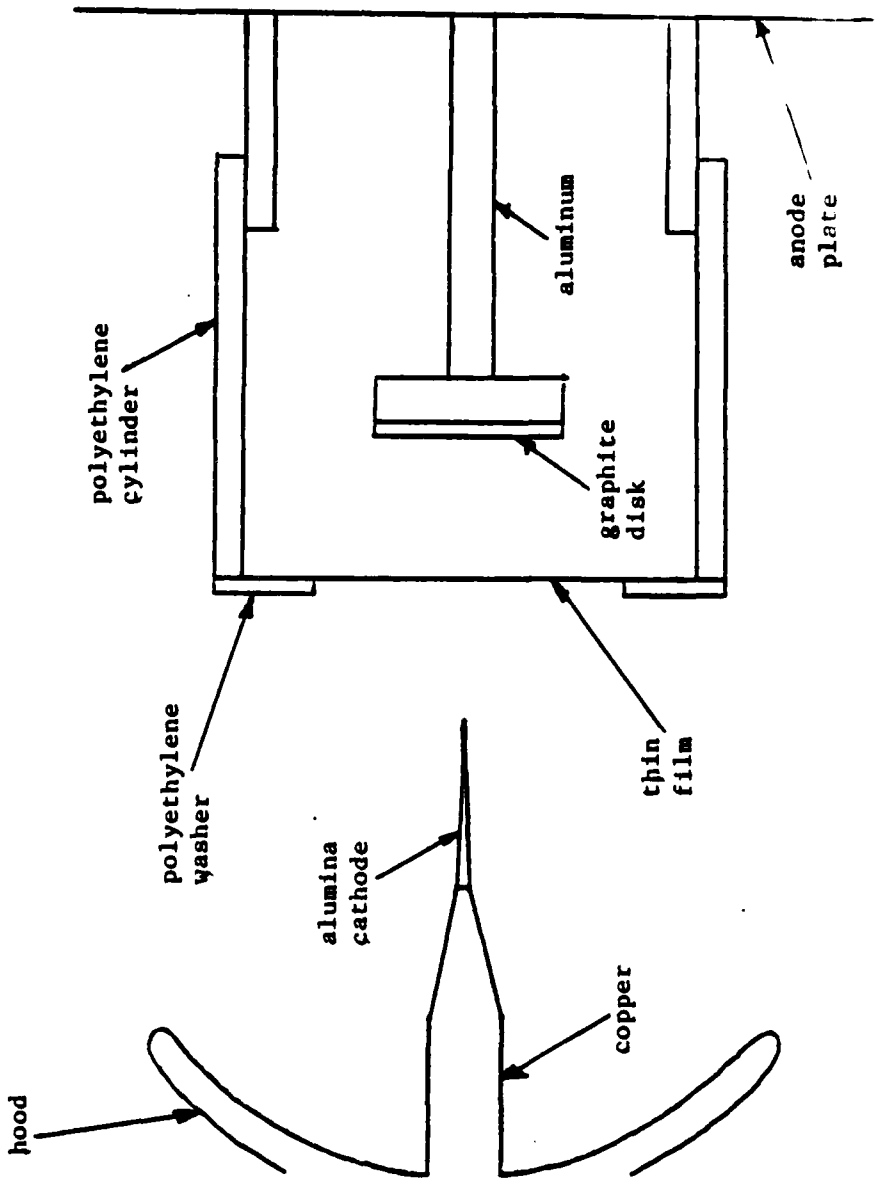

Figure 3.1 General configuration in 1974

Fig. 3.2 shows the configuration of 1975. It is substantially the same as in 1974. There was no longer a hood over the cathode. This hood may have more adversely affected cathode emission than it protected the diode from debris. The pedestal's target holder was replaced with a target holder mounted in the anode plane. This change improved the geometry and ease of access. Thick, graphite disk were still being used as targets. The polyethylene cylinder was held in place by a slightly modified support, which was more integral with the machine face and could itself be varied in length. It could also be varied in composition between graphite and polyethylene. Also, in 1975 the aperture of the washer holding the films could be varied.

3.2 Detection of Ions

Accelerated protons were detected by their activation of the graphite target. A decay curve for one such target is shown in Fig. 3.3. Computation of the half-life revealed it to be 10 min, within a few percent. This interval corresponds to ^{13}N, which has a half-life of 9.97 min and is a positron emitter. The 0.51 MeV gammas of the positron annihilation were counted by a NaI(Tl) scintillation crystal. This activity could be produced by either a $^{12}C\ (p,\gamma)^{13}N$ reaction or a $^{13}C(p,n)^{13}N$ reaction. The former reaction has no threshold, while the latter has a 3.2 MeV laboratory threshold. The $^{13}C(p,n)^{13}N$ turns out to be the dominant process for protons even just slightly above the threshold. This argument takes into account the fact that ^{13}C has only 1% relative abundance. In addition, the presence of neutrons was verified by silver activation.

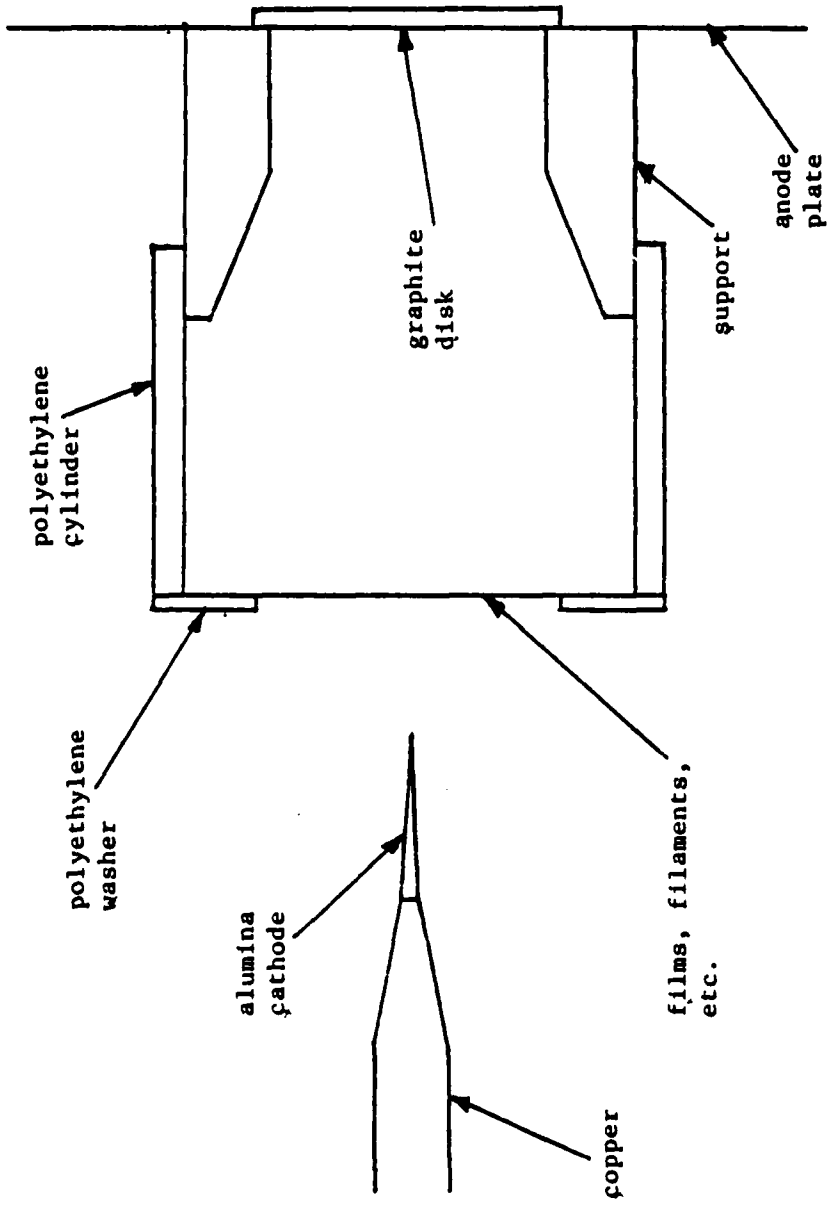

Figure 3.2 General configuration in 1975

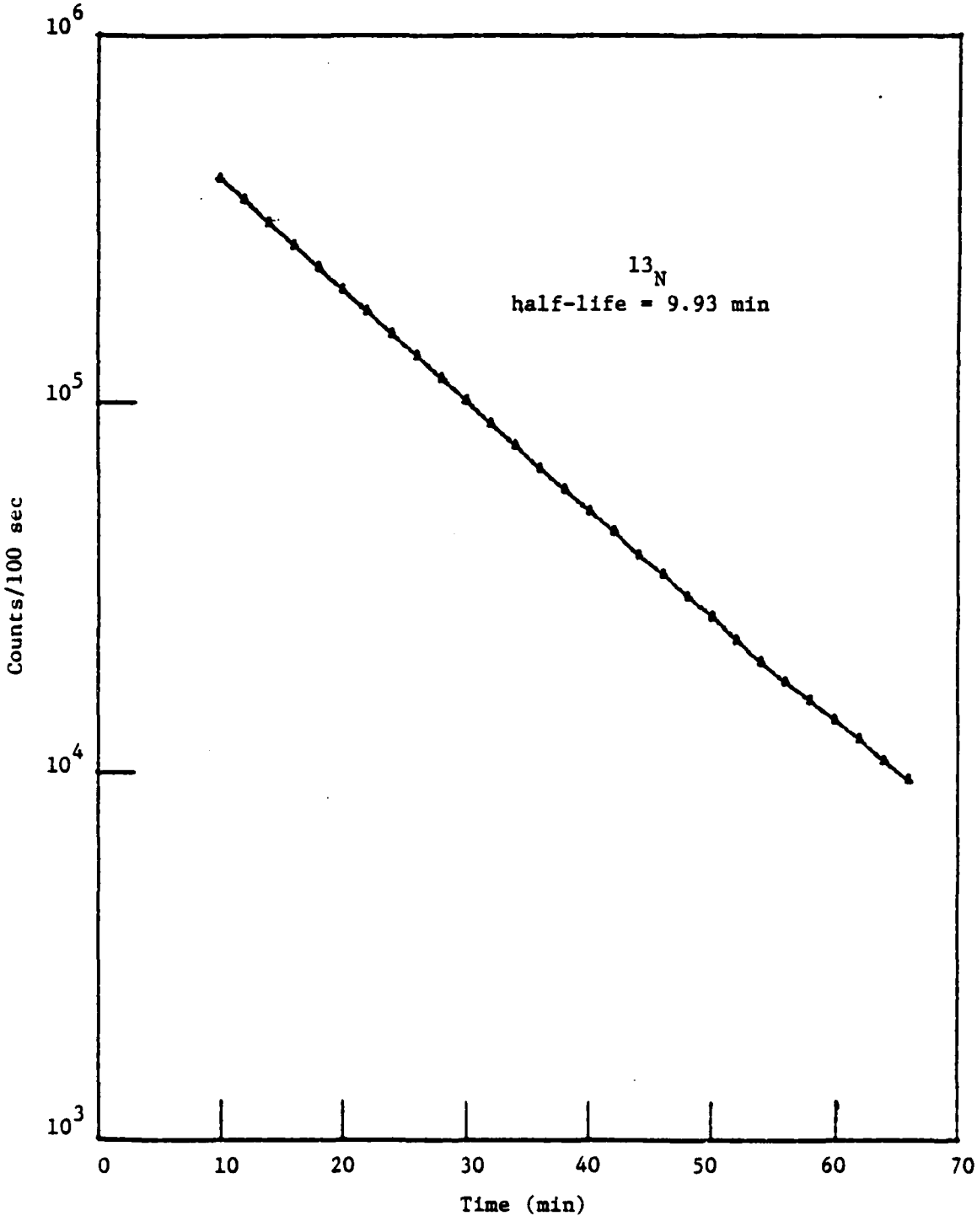

Figure 3.3 Decay of graphite target

That the (p,n) reaction dominates may be verified by a simple calculation. Theoretical considerations[58] indicate that the stopping power for charged particles should have the following form:

$$dE/dx = \frac{1}{AE} \ln (BE),$$

where E is the energy of the particle, x is its position, A and B are constants which depend on the particle parameters and the medium through which it is passing. Using tables[59] of dE/dx vs E, the following empirical fit was obtained

$$dE/dx = \frac{\ln (19E)}{1.28 \times 10^{-2} E}.$$

When E is in MeV this gives dE/dx in MeV/(gm/cm^2). The total cross section, σ, of the reaction was obtained from Ref. 60 and may be seen in Fig. 3.4. This function was approximated by a ramp which gives

$$\sigma = -2.36 \times 10^{-25} + (7.27 \times 10^{-26}) E, \quad 6.5 > E > 3.25.$$

When E is in MeV, σ is in cm^2. The probability, P, for a thick target reaction is given by

$$P = \frac{\rho N_A}{M} \int_{3.25}^{\text{initial E}} \sigma (dE/dx)^{-1} \, dE,$$

where ρ is the medium's density in gm/cm^3, N_A is Avogadro's number, M is the gm-molecular weight of the ion. For an initial E of only 3.5 MeV, a numerical integration of this quantity yields 2.6×10^{-8} for P in our case. This value is to be compared with 18.4×10^{-10} from the thick target yield of $^{12}C(p,\gamma)^{13}N$ at 2.2 MeV (see Fig. 3.5)[61]. The (p,γ) reaction yield increases stepwise because it is basically a resonance process. It has a significant cross section only at certain energies. The proton passes through these energies as it decelerates.

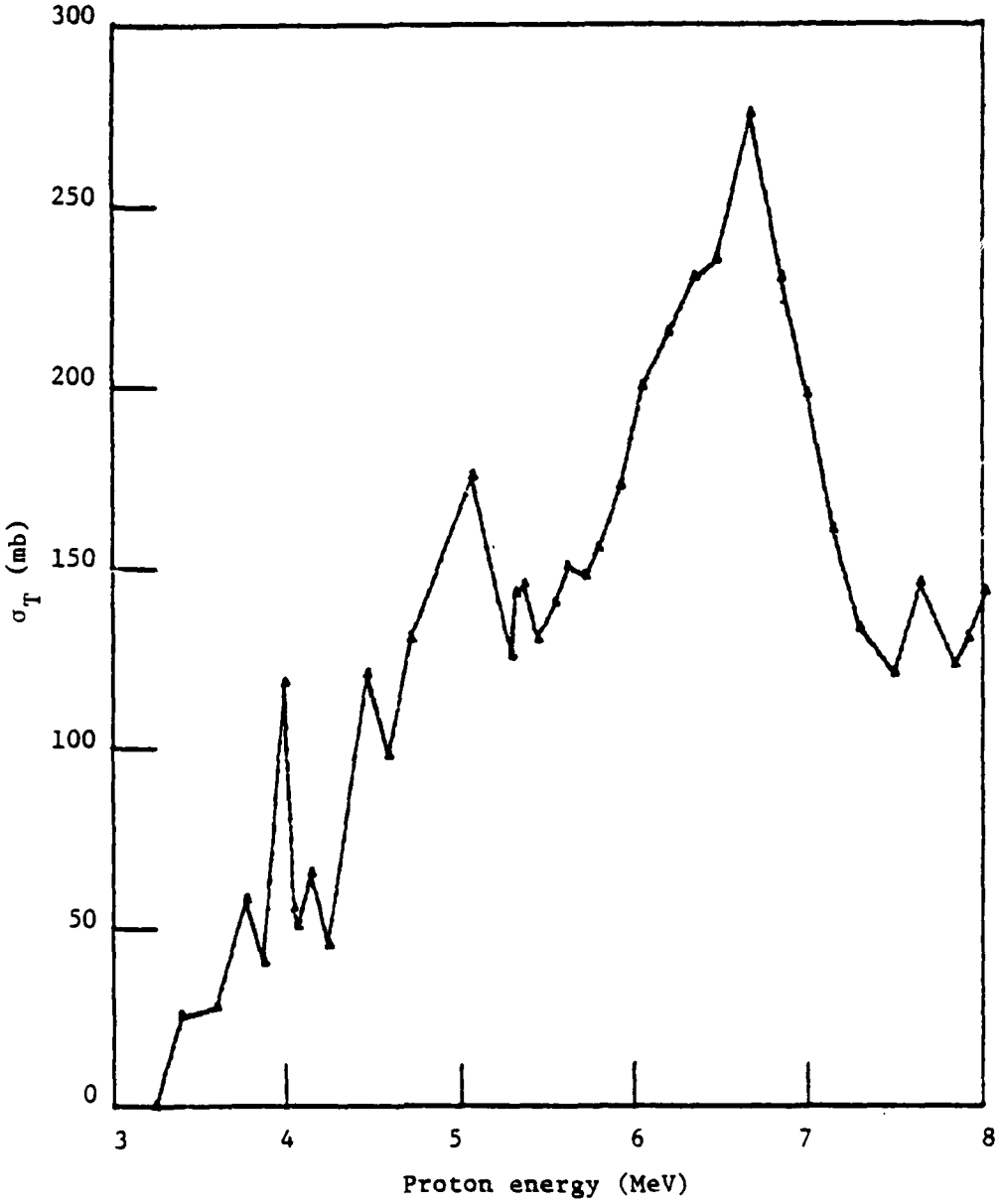

Figure 3.4 Total cross section for $^{13}C(p,n)^{13}N$

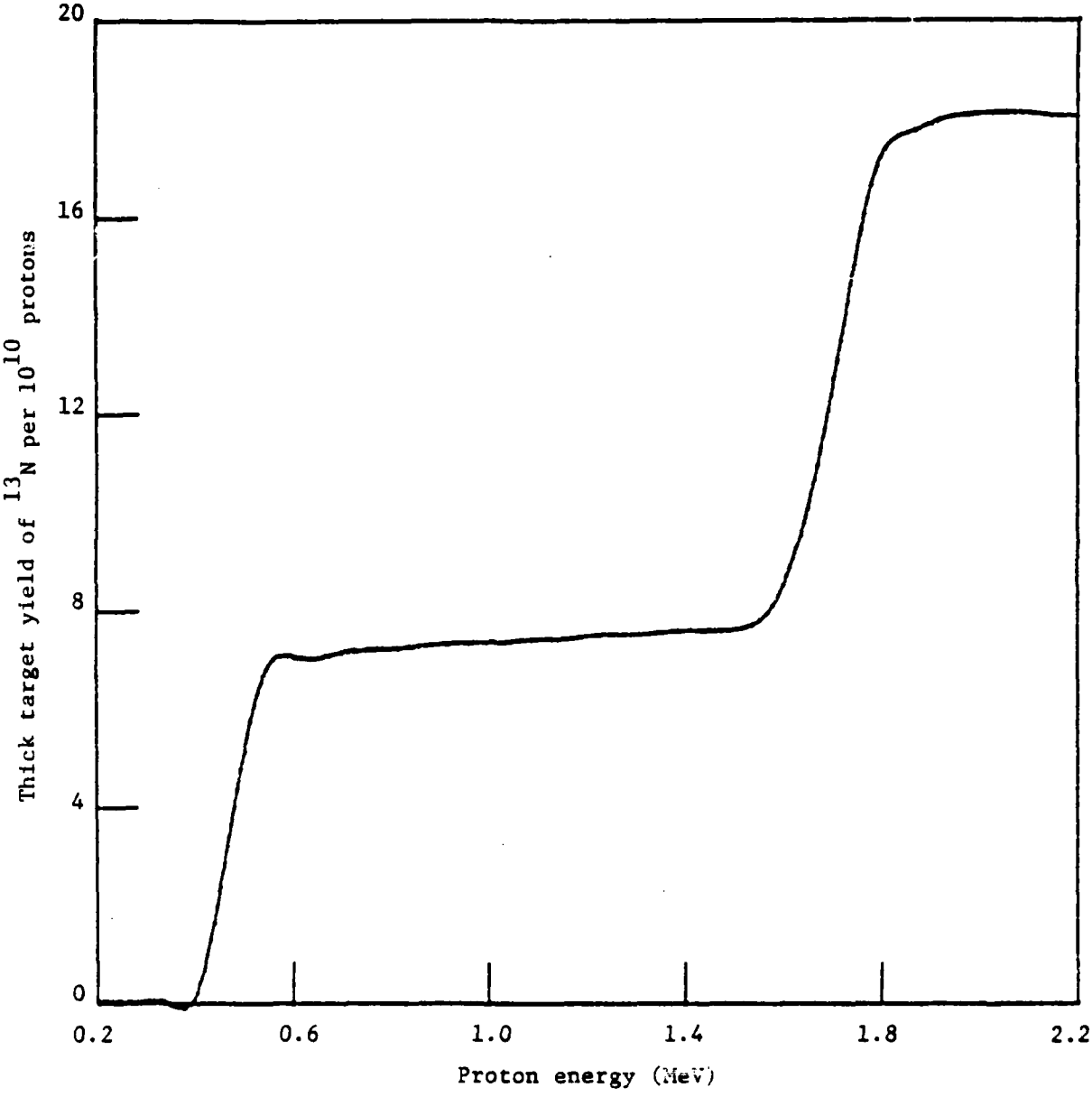

Figure 3.5 Thick target yield for $^{12}C(p,\gamma)^{13}N$

After each shot the graphite target was removed, and counting was begun, usually within 10 min of the shot. The count rate could then be extrapolated back to the instant of firing. This count rate was the basis of comparison between shots with varying parameters. No shot for shot comparison should be made, however, between the 1974 and 1975 experimental runs.

3.3 Observed Trends

The general outline of the diode phenomena is given here. The voltage pulse is applied to the metal cathode, after being transmitted from the Van de Graaff head. The metal cathode begins to emit from its tip. The bombardment of the dielectric cathode causes it to flashover, and the emission is transferred to the tip of the dielectric. It is believed that the dielectric provides some ions to neutralize and, thus, focus the electron beam. The beam then travels the gap to the film, accelerating under the applied field and expanding under its own space charge. Bombardment of the film releases ions. Some of the beam passes to the interior of the cylinder, and some may strike the outside. The film thickness was much less than the electron range. Ions are accelerated from the film region, in the beam direction, and strike the target. The films were destroyed on each shot. The polyethylene cylinders could, however, survive several shots even though they were often gouged or streaked by the electron beam. Usually the target appeared only to have been heated, not spalled or ablated.

In these experiments the variation of geometrical and material parameters was explored. When comparing shots, one must first observe that there is considerable statistical variation. On some occasions shots with

supposedly identical parameters differed by as much as a factor of 3 in radioactivity yield. It should be kept in mind that the emission process of the beam is highly erratic and spotty in detail. The process of ion production by electron bombardment suffers from similar characteristics.

The results of varying the cathode-film gap are presented in Table 3.1. The total gap (cathode-anode) was kept constant, and in 1975 the ratio of cathode-film gap and aperture was held approximately constant. A 1 cm gap consistently gave the best results. This separation seems to be a compromise between beam lost due to blow up, with larger gaps, and shorting of the voltage pulse, which was observed with smaller gaps. This spacing was used for the subsequent shots.

In 1974 little effect could be discerned regarding variation of the film-anode spacing (see Table 3.2). However, in 1975 a 4 cm spacing did best. Improved target geometry may have made it possible to tell the difference. The 4 cm spacing was used in the other tests.

In varying the machine firing voltage to lower values (see Table 3.3), detectable acceleration ceased at 4 MV. The actual energy of the electron beam will have been somewhat smaller than this. This result may indicate that, to a large extent, the ion energy is dictated by the beam voltage and has here fallen below the 3.2 MeV threshold. In another experiment at full voltage, however, protons activated the target after passing through a 20.5-mil thick Al foil. Considering the energy loss of protons in Al, this implies that their energy distribution extends up to 10 MeV.

Table 3.4 collects the data relating to film variation. One notes an overall improvement in 1975. This change, possibly, was due to the absence of the cathode hood, which may have diverted part of the electron beam by emitting electrons itself.

Table 3.1 Varying gaps with constant total gap

Shot	Film	Cathode-film gap (cm)	Film-anode gap (cm)	Aperture (cm)	Count rate (counts/min)	Voltage (MeV)
6-74	1 mil poly	1	6	4	20810	6
4-74	1 mil poly	3	4	4	low	6
5-74	1 mil poly	6	1	4	low	6
12-74	0.5 mil poly	0.5	6.5	4	6294	6
11-74	0.5 mil poly	1	6	4	40080	6
13-74	0.5 mil poly	1.5	5.5	4	22746	6
3-75	0.5 mil poly	0.5	6.5	2	0	6
4C-75	0.5 mil poly	0.75	6.25	3	46545	6
5B-75	0.5 mil poly	1	6	4	73312	6
6B-75	0.5 mil poly	1.5	5.5	4	60183	6

Table 3.2 Varying film-anode spacing with constant cathode-film gap

Shot	Film	Cathode-film gap (cm)	Film-anode gap (cm)	Aperture (cm)	Count rate (counts/min)	Voltage (MeV)
15-74	0.5 mil poly	1	4	4	44801	6
11-74	0.5 mil poly	1	6	4	40080	6
16-74	stocking	1	4	4	62829	6
7-74	stocking	1	6	4	64903	6
7-75	0.5 mil poly	1	6	4	85773	6
8-75	0.5 mil poly	1	6	4	97290	6
9-75	0.5 mil poly	1	8	4	106733	6
10-75	0.5 mil poly	1	8	4	84841	6
11-75	0.5 mil poly	1	4	4	751607	6
12-75	0.5 mil poly	1	4	4	208058	6

Table 3.3 Varying the charging voltage

Shot	Film	Cathode-film gap (cm)	Film-anode gap (cm)	Aperture (cm)	Count rate (counts/min)	Voltage (MeV)
24-75	0.5 mil poly	1	3.5	4	0	4
23-75	0.5 mil poly	1	3.5	4	78000	5
22-75	0.5 mil poly	1	3.5	4	159000	6

Table 3.4 Variation of films

Shot	Film	Cathode-film gap (cm)	Film-anode gap (cm)	Aperture (cm)	Count rate (counts/min)	Voltage (MeV)
6-74	1 mil poly	1	6	4	20810	6
11-74	0.5 mil poly	1	6	4	40080	6
15-74	0.5 mil poly	1	4	4	44801	6
7-74	stocking	1	6	4	64903	6
16-74	stocking	1	4	4	62829	6
17-74	stocking + CD_2	1	4	4	545964	6
18-74	stocking + CH_2	1	4	4	23465	6
9-74	6λ	1	6	4	100429	6
10-74	3λ	1	6	4	125306	6
8-74	nothing	1	6	4	0	6
11-75	0.5 mil poly	1	4	4	751607	6
12-75	0.5 mil poly	1	4	4	208058	6
26-75	4 stocking	1	4	4	689000	6
36-75	3 stocking	1	4	4	343000	6
27-75	2 stocking	1	4	4	1035000	6
28-75	1 stocking	1	4	4	344000	6
38-75	15 filaments	1	4	4	356000	6
29-75	8 filaments	1	4	4	408000	6
30-75	4 filaments	1	4	4	469000	6
27-75	2 filaments	1	4	4	381000	6
37-75	1 filament	1	4	4	229000	6
32-75	nothing	1	4	4	31900	6

Of the cases in which no film was present, there was no or comparatively low yield. In addition, there was target damage as illustrated in Fig. 3.6. This picture shows the beam having blasted a pit through a 3/16 in. graphite target disk and spalled the aluminum end cap behind it. There was also a dimple in the back of the end cap. Low silver activation counts in the no-film shots indicate that the activity was not merely blown away. When films were present, there was little material effect at the target, most of the electron beam striking the polyethylene cylinder. This cylinder was also becoming activated, but it was only checked with a hand monitor.

The remarkable increase in yield between shots 18-74 and 17-74 indicates the possible acceleration of deuterium. The reaction would have been $^{12}C(d,n)^{13}N$, with a threshold of 0.328 MeV. It has the advantage of interacting with the far more abundant ^{12}C. The pellets of CH_2 and CD_2 were approximately 0.1 in. in diameter and were suspended on the axis in nylon stocking material.

In 1974 the thin enamel films performed best (not counting shot 17-75). These were made by floating a drop of Pactra brand enamel on water. The film was allowed to harden and was then lifted off the water from underneath with the polyethylene washer which held it in place on the polyethylene cylinder. The thickness of the film was determined by counting interference fringes from the edge. It may be that in 1974 the beam was weaker and that more dense ion sources were overloading it.

In 1975 the nylon strings, although not always giving the best performance, did work well and did work most consistently. These strings were single filaments of 15.6 denier nylon 66. This corresponds to a diameter of 0.044 mm and a density of 1.13 gm/cm^3. The chemical

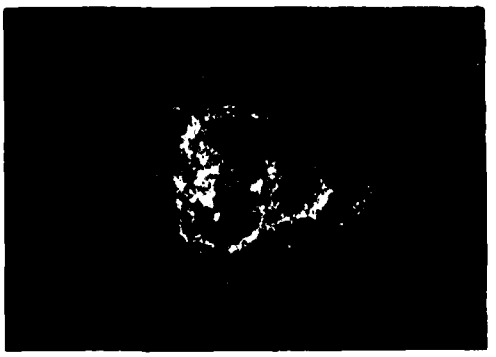

Graphite target disk

Aluminum end cap

Figure 3.6 Target damage

composition of nylon 66 is $H-(HN(CH_2)_6NHCO(CH_2)_4CO)-OH$. The filaments were arrayed in a spoke like pattern, spaced symmetrically, and intersecting on axis. A graph of the count rate vs the number of filaments is presented in Fig. 3.7. This curve indicates a maximum at 4 filaments. More copious ion sources gave more erratic results.

Besides the observation of proton acceleration, on one occasion an Al foil was activated. The decay curve of this activity is shown in Fig. 3.8. This activity has been assigned to $^{27}A\ell\ (^{12}C, n^4He)^{34m}C\ell$. Its threshold is 4.9 MeV; however, the Coulomb barrier would prevent significant activity for ^{12}C ions less that 13 MeV (see Fig. 3.9). The ion source was a nylon mat. Unfortunately, time did not allow examination of the gamma ray spectrum on a multichannel analyzer, but this reaction had been previously observed by Luce[35].

3.4 *Visual Observation*

Open shutter photography through diode ports was available in 1974 and in 1975. Additionally, in 1975 an image converter camera (Beckman and Whitley model 511) was available. This camera had a fast electronic shutter and a signal amplification capability. Exposure times of 5, 10, 50, 100, and 1000 ns were possible. We usually used a 10 ns time. The light from the object to be viewed strikes the cathode of a photodiode. Voltage is applied to the photodiode for the selected exposure time. When so applied, photoelectrons cross the gap to the phosphor-anode. A standard camera then takes an open shutter picture of the phosphor. The camera could be triggered electronically, as could the FX75. The relative timing of the machine firing and the picture taking could be adjusted by an electronic delay or by cable delays. A monitor signal from the camera indicated this timing.

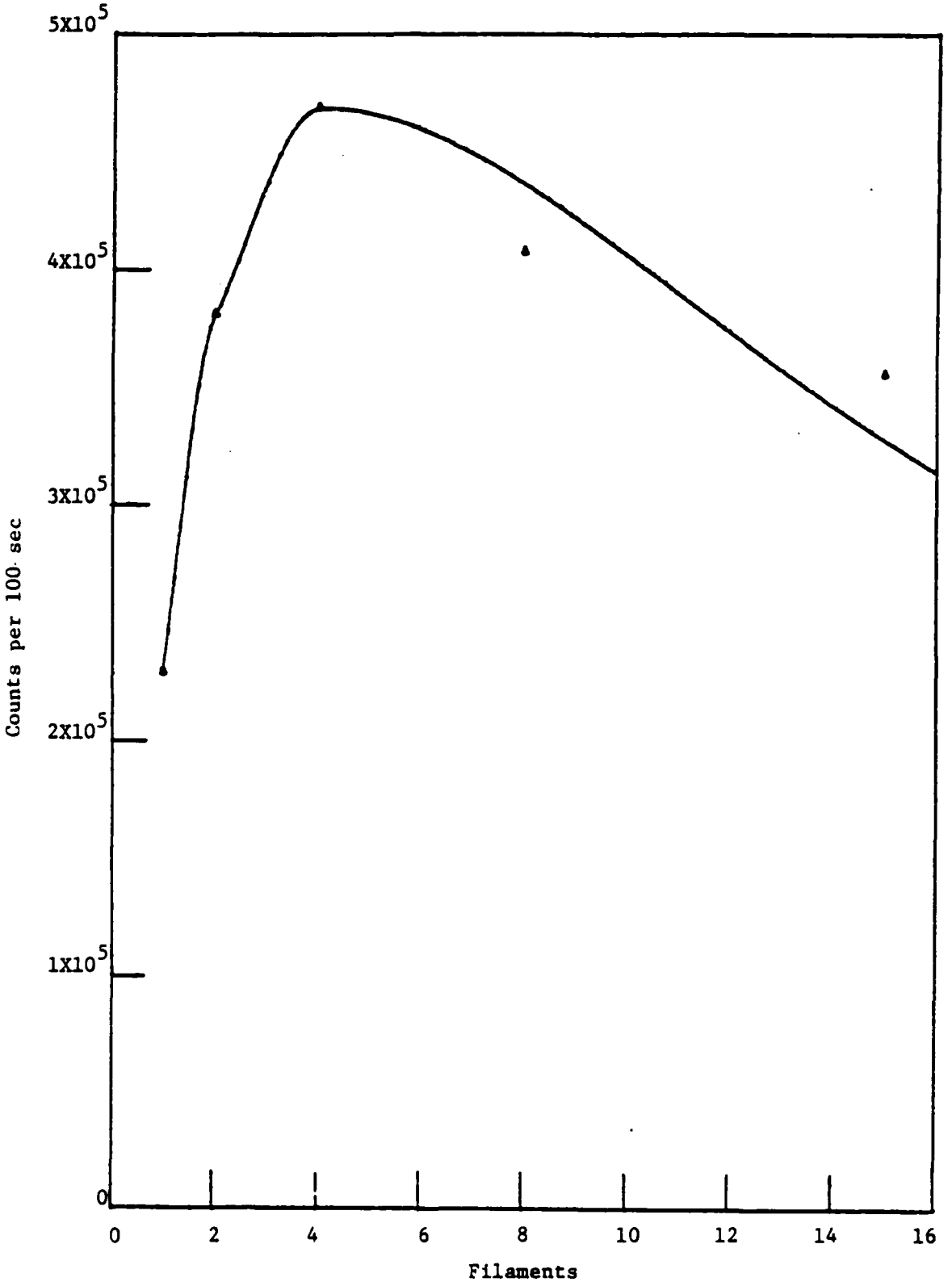

Figure 3.7 Variation in count rate with filaments

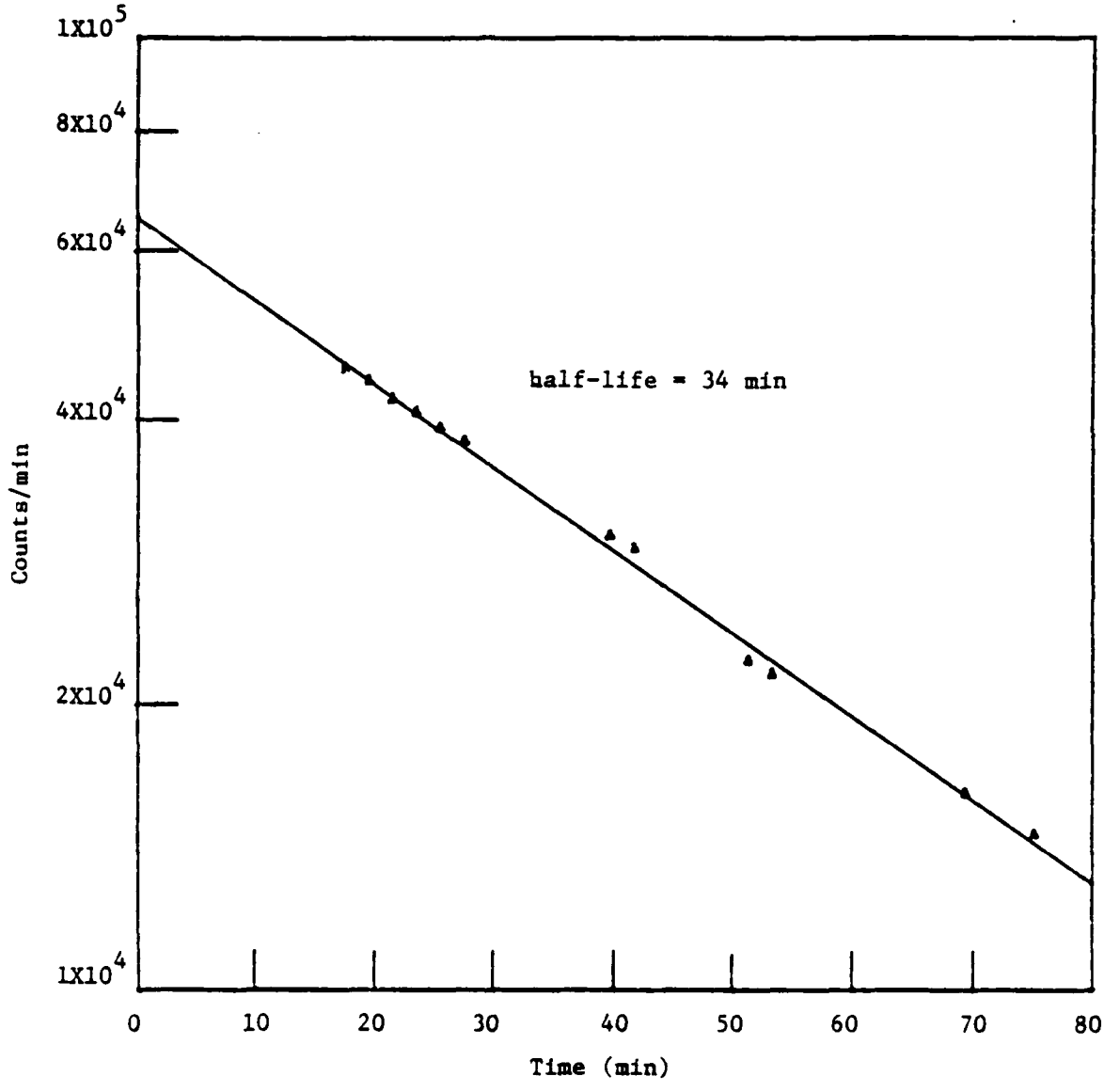

Figure 3.8 Aluminum foil activity decay

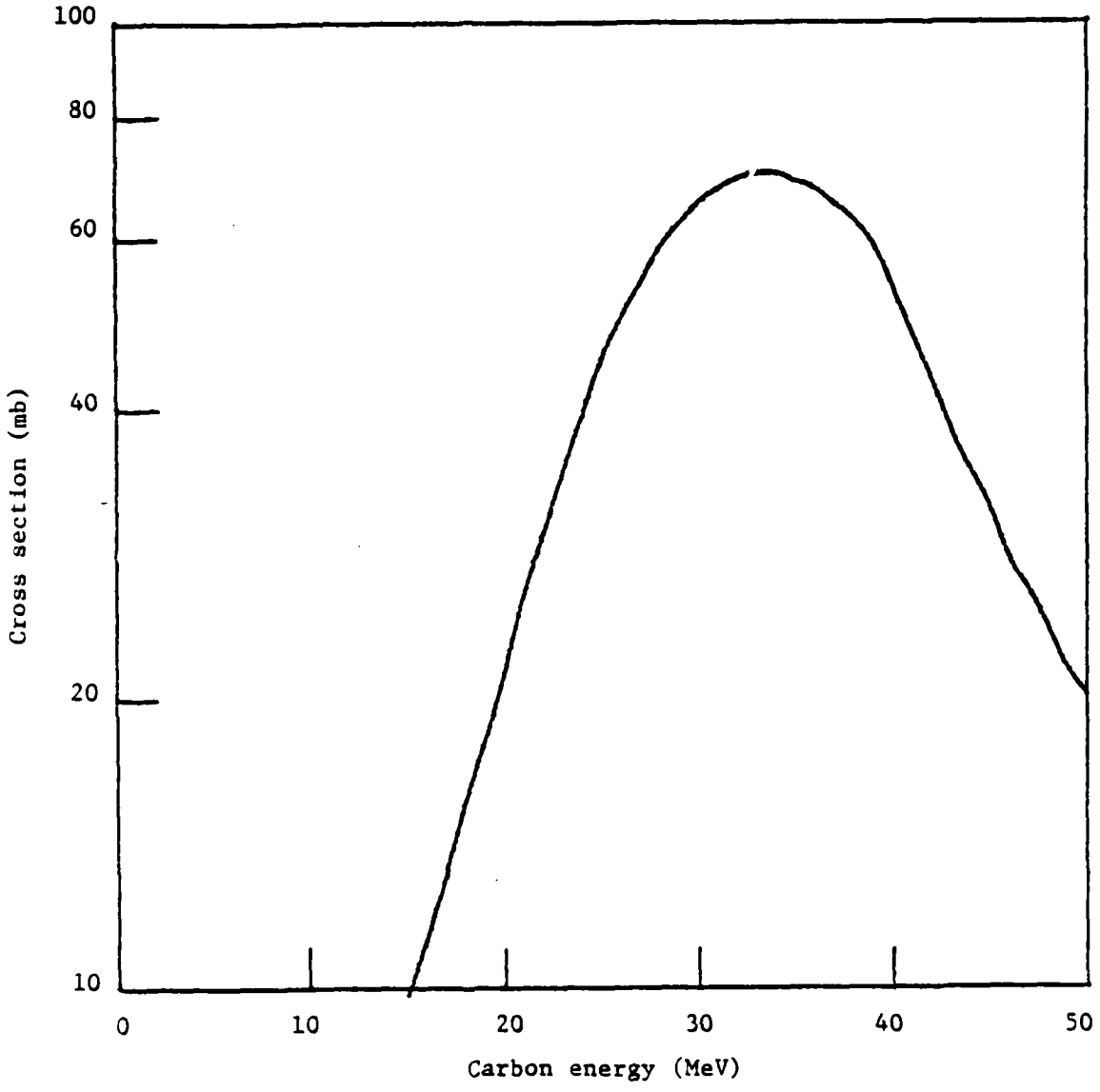

Figure 3.9 Cross section for the $^{27}Al(^{12}C,n\ ^{4}He)^{34m}Cl$ reaction

Figs. 3.10–3.12 are copies of some of these image converter pictures, open shutter shots, and set up shots. The alumina cathode can be seen on the left pointing into the aperture of the polyethylene cylinder on the right. The aperture in various pictures contains films, meshes, and filaments. Considering the spot size on the film, the beam appears to have been expanding, initially, at an angle of about 45°. One also observes the irregular channels of light on the dielectric cathodes. Corresponding channels were observed in the open shutter photographs, indicating that these features were constant during the shot or very bright by comparison. Bends in the channel may be related to the kink instability. In several cases the pattern on the film suggests that the beam may not be uniform as it leaves the dielectric cathode.

3.5 The Acceleration Process

Relatively little theoretical work has been done by people in the field of collective ion acceleration to explain these and other experiments performed in the diode region. Acceleration in the drift region has received more attention, especially the case of injection into neutral gas. Some of the difficulties encountered in the diode are (1) the presence of an applied electric field, (2) the use of pointed cathodes and the emission therefrom, and (3) the generation of plasma on the cathode and other surfaces, due to the release of adsorbed gases or bombardment by the beam.

That some collective process is necessary to explain the results is evident from the fact that acceleration was observed in a direction counter to the applied field and that proton energies exceeded that of the beam. The process currently favored is the moving potential well. This moving well is, roughly, the same mechanism that provides the acceleration in

Set up picture (film in aperture)

Image converter picture

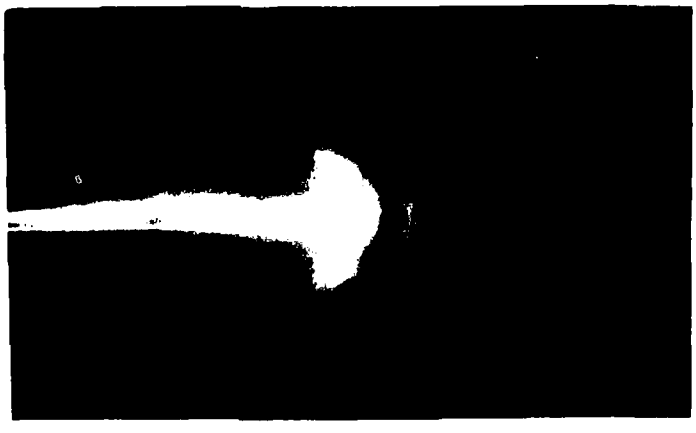

Open shutter picture

Figure 3.10 Dielectric cathode experiments

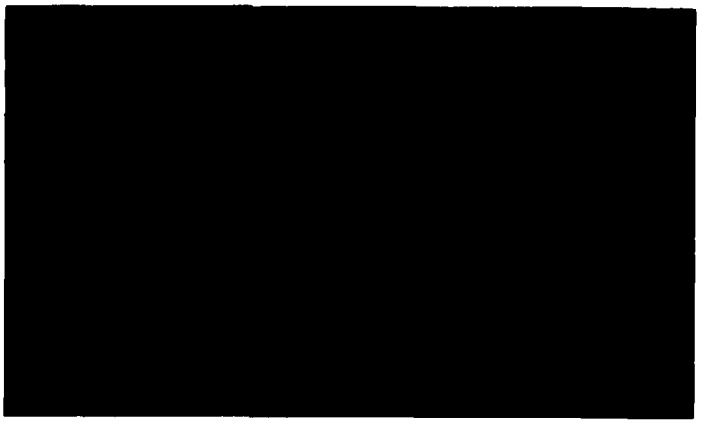

Image converter picture

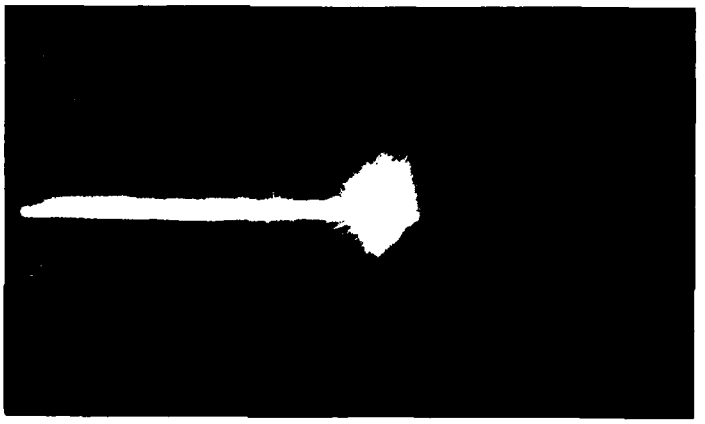

Image converter picture

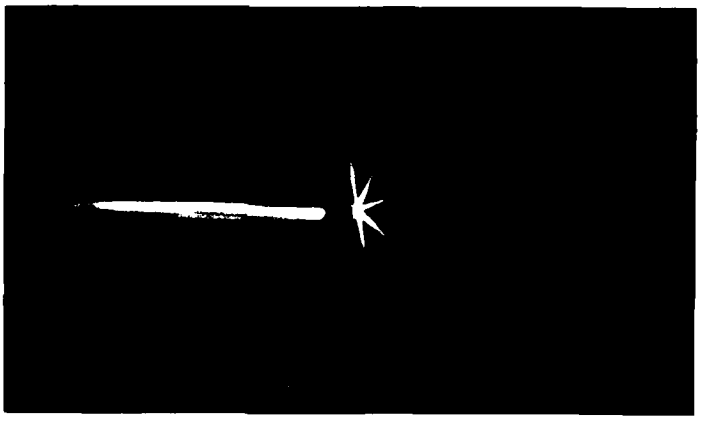

Image converter picture

Figure 3.11 Dielectric cathode experiments

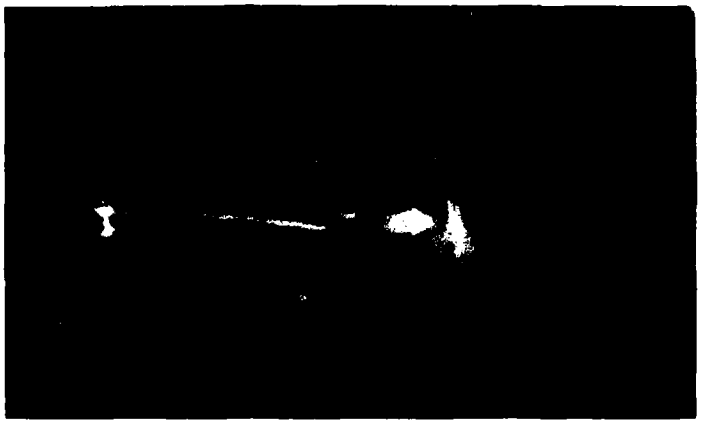

Open shutter picture

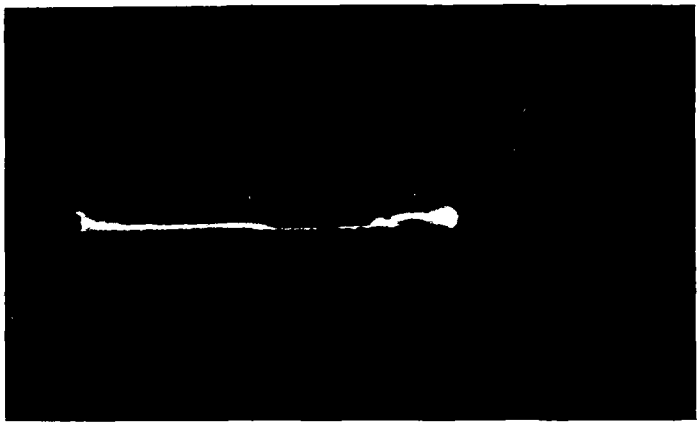

Open shutter picture

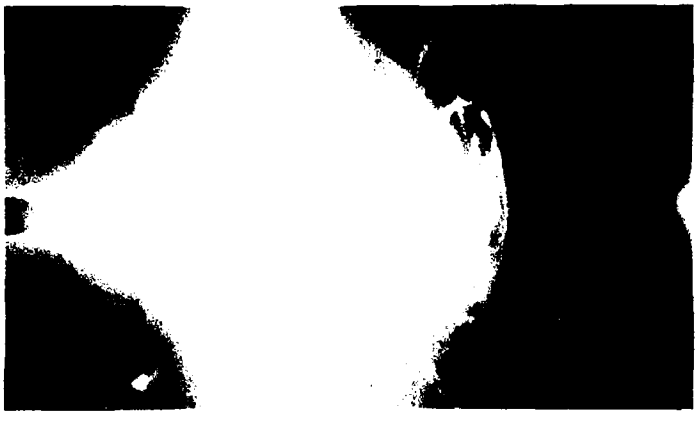

Open shutter picture

Figure 3.12 Dielectric cathode experiments

drift tube experiments. It is one of a couple of methods deemed capable of producing sufficient E_z to drag the ions along.

The following outlines what is thought to occur. The electron beam, passing into the polyethylene cylinder, releases ions from the foil at its mouth. The beam further charges up the cylinder until it, effectively, becomes an extension of the anode. Its interior becomes shielded from the accelerating field. The beam that continues to penetrate the aperture expands quickly under its space charge. This stalling of the beam just inside the cylinder produces a strong electric field, which attracts ions. As the ions are pulled into this potential well, it moves toward the anode, since its space charge is being canceled. In this manner the accelerating field is applied long enough for the ions to reach energies in excess of what a stationary field could achieve. This is a case of a great many electrons acting on a few ions to increase their velocity to some small fraction of the beam velocity. Since ions are much more massive, this results in very energetic particles.

Some of the preceding material has been presented in Refs. 62-64.

4. ION ACCELERATION IN A DRIFT TUBE

4.1 The 7 Ohm Line

The remaining ion acceleration experiments to be described were performed at NCSU on the 7 Ohm Line, which is on loan to us from the Naval Research Laboratory. This accelerator (see Fig. 4.1) consists of a vacuum diode region to which voltage is applied from a coaxial structure known as a folded Blumlein transmission line. The transmission line consists of three coaxial cylinders: the outer conductor, the intermediate conductor, and the center conductor. This region is insulated with filtered water at a resistivity of greater than 10 MΩ-cm. The large dielectric constant of the water makes it possible to store more energy in a smaller space and also yields a longer pulse with a shorter machine. The center conductor is connected to the cathode in the diode through a bulkhead which separates the water-filled from the vacuum region. The outer conductor and the anode are electrically connected by bolts through this same bulkhead. Between the center conductor and the intermediate conductor is a water switch gap. The separation of the gap may be adjusted.

The center and outer conductors are kept at the same potential, while the intermediate conductor is charged to a negative voltage of approximately 0.5 MV. This structure is effectively a capacitor which holds the energy later to be deposited in the diode. At this time, however, there is no voltage in the diode. The water switch gap breaks down spontaneously. This action initiates a series of electromagnetic waves in the transmission line which ultimately generates an intense relativistic electron beam.

The operation of the pulse forming Blumlein circuit may be more easily understood by considering the diagram in Fig. 4.2. This figure shows the

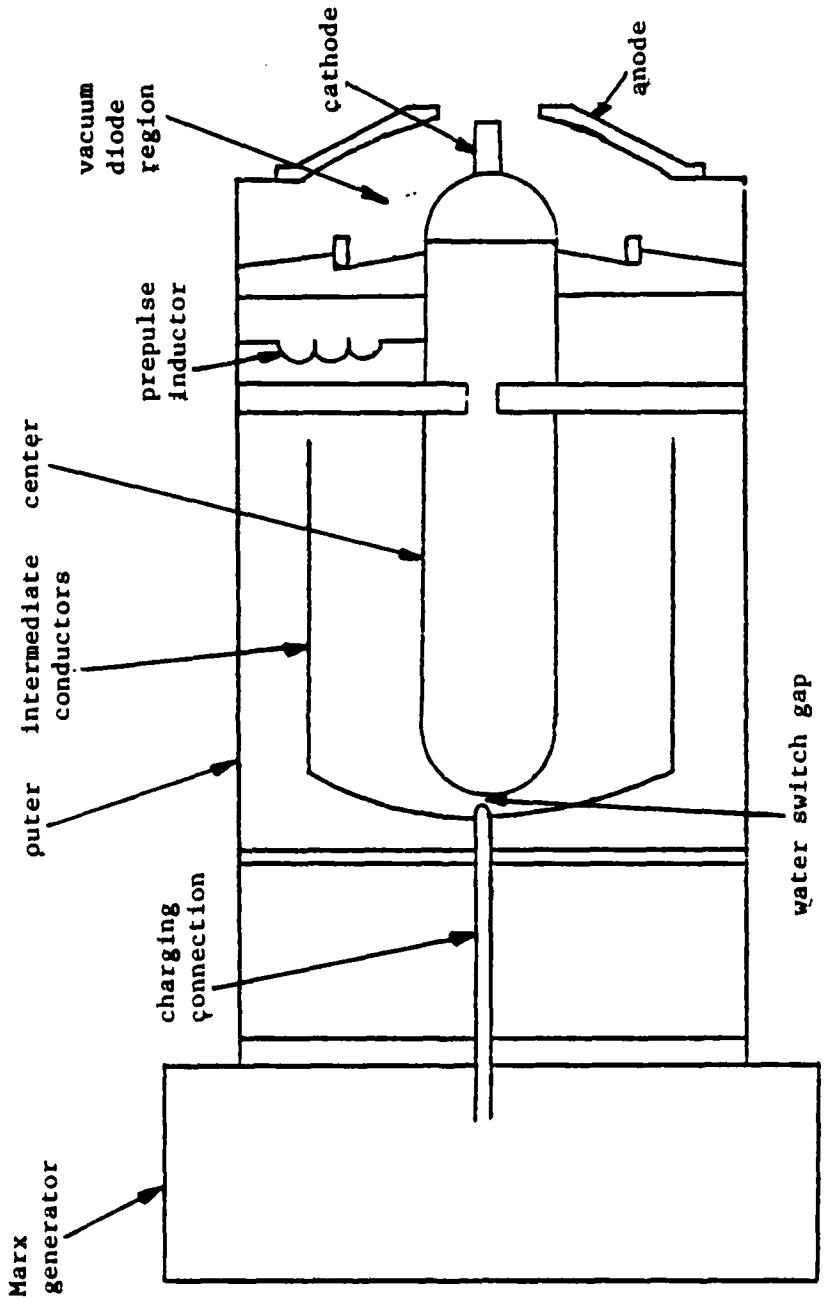

Figure 4.1 The Seven Ohm Line

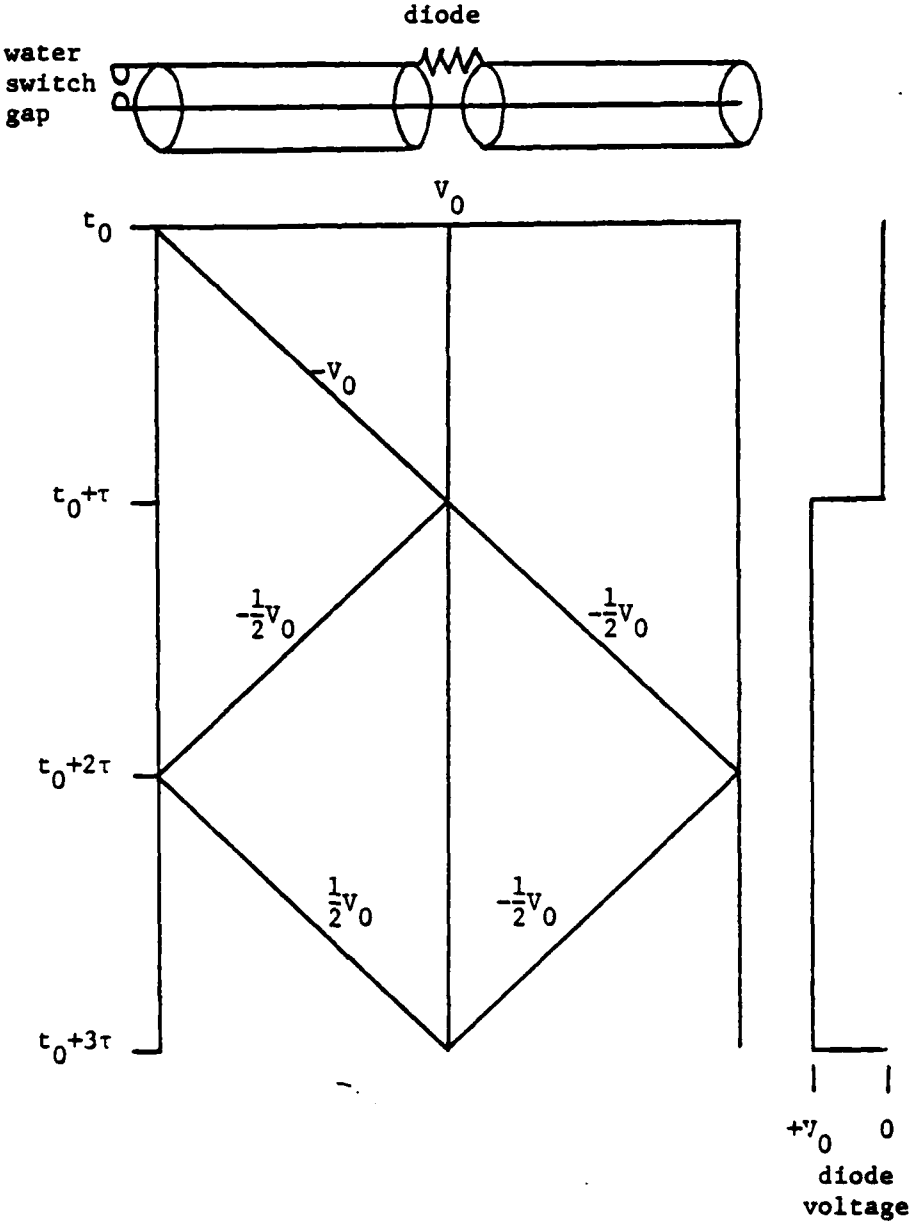

Figure 4.2 Blumlein transmission line voltages

voltages in the machine as a function of position and time, when the diode is a matched load (i.e. 7 Ω). Horizontal motion along the top of the diagram represents change of position in the 'unfolded' transmission line. Thus, at the left we begin at the water switch gap and travel along the space between the center and intermediate conductors (inner coax) to the diode. The diode is represented by a resistor in the center. To the right we are traveling away from the diode in the region between the outer and intermediate conductors (outer coax). Each individual coax has a characteristic impedance of 3.5 Ω, and each sees the other as having its characteristic impedance in series with the diode resistance. Thus, an electromagnetic wave arriving at the diode will be half reflected and half transmitted into the other coax.

The horizontal line labeled V_o at t_o represents the initial charging voltage, which at the initial instant is constant throughout the machine. At t_o the water switch gap breaks down and shorts the end of the inner coax. A traveling wave of magnitude $-V_o$ is initiated. The slope of the line is related to the velocity of the wave, which is about 3.4 cm/ns. This wave arrives at the diode at time $t_o + \tau$, where τ is known as the transit time (about 30 ns). To find the actual voltage at a given position at a given time, one must sum up all the voltages from t_o down to the given time. Thus, we see that, initially, the inner coax voltage drops to zero as the wave passes. As previously mentioned, a reflected wave and a transmitted wave are generated. The voltage on the diode is obtained by taking the difference between the inner coax and the outer coax voltages. This difference is depicted on the right. The far end of the outer coax is treated as an open circuit. Overall, a square voltage pulse is produced at the diode of magnitude equal to the charging voltage

and of duration equal to twice the transit time (about 60 ns). Of course, the actual shape of the voltage pulse will vary if the diode load is not 7 Ω or if it varies in time. In general, a higher load impedance will enhance the voltage at the expense of current, while a lower impedance will do the reverse.

Given the large voltage applied to the transmission line, even highly resistive water cannot avoid breakdown for long. Consequently, the line is pulse charged by a Marx generator. The time scale for charging (about 500 ns) is short compared to the water breakdown time but long compared to the discharge time.

A schematic of the Marx generator is given in Fig. 4.3. It consists of 9 capacitors each having 0.25 μF capacitance. They are all charged in parallel to 53 kV, which represents a stored energy of 3.2 kJ. A trigger signal to the spark column causes the capacitors to be discharged in series at a voltage, V_1, of 0.477 MV. The output is connected to the intermediate conductor, while the ground is connected to the outer conductor. Because of the Marx inductance, there is a ring-up factor, which causes the transmission line to reach a voltage of 1.4 V_1. The water switch gap is adjusted to breakdown just before peak voltage is reached.

In order to keep the center conductor at the outer conductor potential during charging, a prepulse inductor is inserted, as shown in Fig. 4.1. The inductance of the element is chosen (about 0.5 mH) so that it acts as a short circuit during the long charging phase but appears as an open circuit during the short discharge time. Nevertheless, a voltage appears at the diode prior to breakdown of the water switch gap. This voltage is known as the prepulse and, in our case, has a magnitude of about 70 kV.

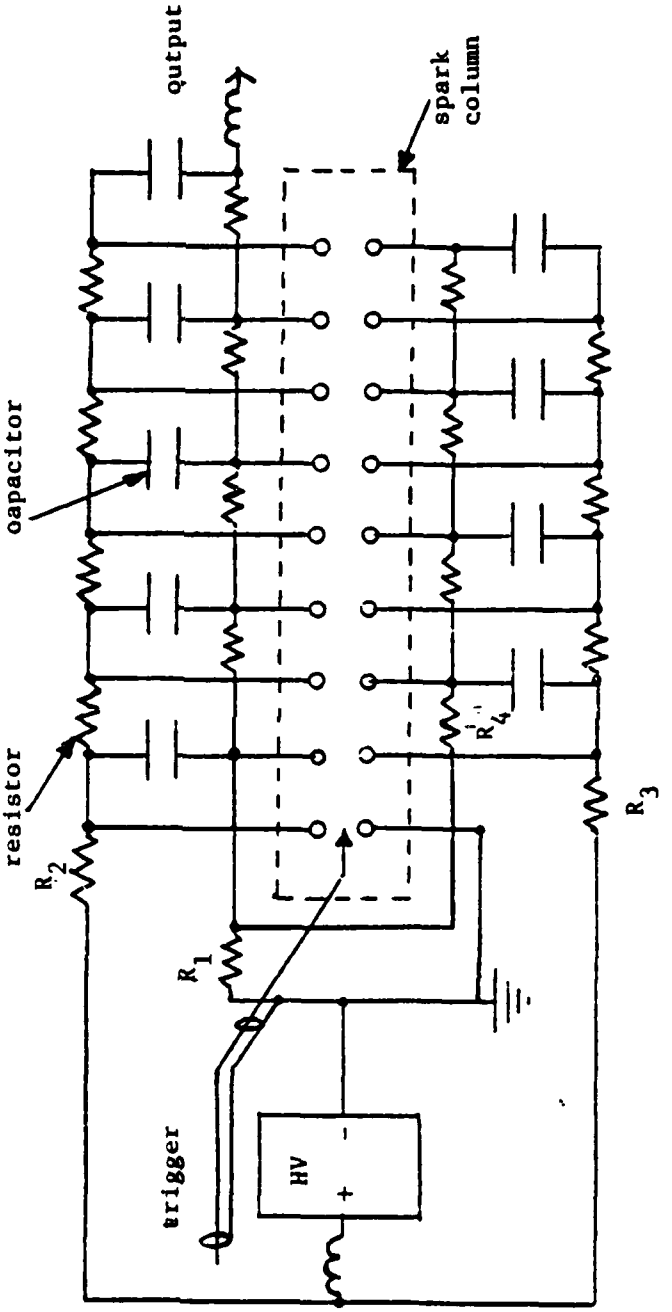

Figure 4.3 Marx generator
R_1=2800 Ω, R_2+R_3=R_4=3700 Ω, others=330 Ω, capacitors=0.25 μF

The machine is approximately 2 ft in diameter and 6.5 ft long. The actual internal transmission line is several feet shorter than this. A photograph of the machine appears in Fig. 4.4. The square Marx generator is visible in the back left. Underneath the cylindrical transmission line is the water purification and circulation system. To the right is the diode pumping manifold and diffusion pump.

4.2 Machine Diagnostics

The charging of the transmission line was monitored at the Marx by means of a simple resistive voltage divider. Part of this resistor network was a liquid resistor made from a copper sulfate solution. The waveform (see Fig. 4.5) was generally that of a ramp with a sharp cutoff, indicating the breakdown of the water switch gap. Subsequent fluctuations of the trace give an indication of the diode voltage behavior. This information, however, arrives at the Marx voltage monitor one transit time after it originates.

The diode voltage is more closely followed by a capacitive voltage divider, which is mounted in the water section just preceeding the diode region (see Fig. 4.6). Capacitive voltage monitors are preferred because they do not mechanically contact the cathode. Thus, they do not load the cathode down, distort the field, or provide a path for breakdown. However, interpretation of the output of such a monitor, as an indication of diode voltage, is based on certain geometrical assumptions. In calibration one usually takes the cathode or center conductor to be one plate of a capacitor, and the center electrode of the voltage probe (pickup) to be the other. This capacitor is then in series with the capacitance between the pickup and the machine ground wall. The probe is calibrated experimentally rather than by calculating the capacitances involved.

Figure 4.4 Photograph of the Seven Ohm Line

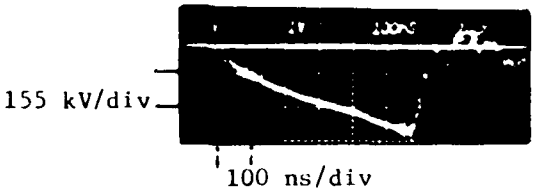

Marx voltage

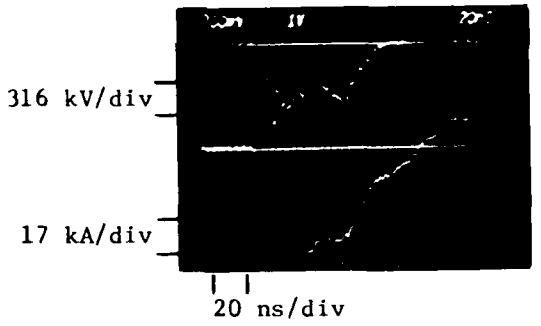

upper: diode voltage
lower: diode current

Figure 4.5 Typical machine waveforms

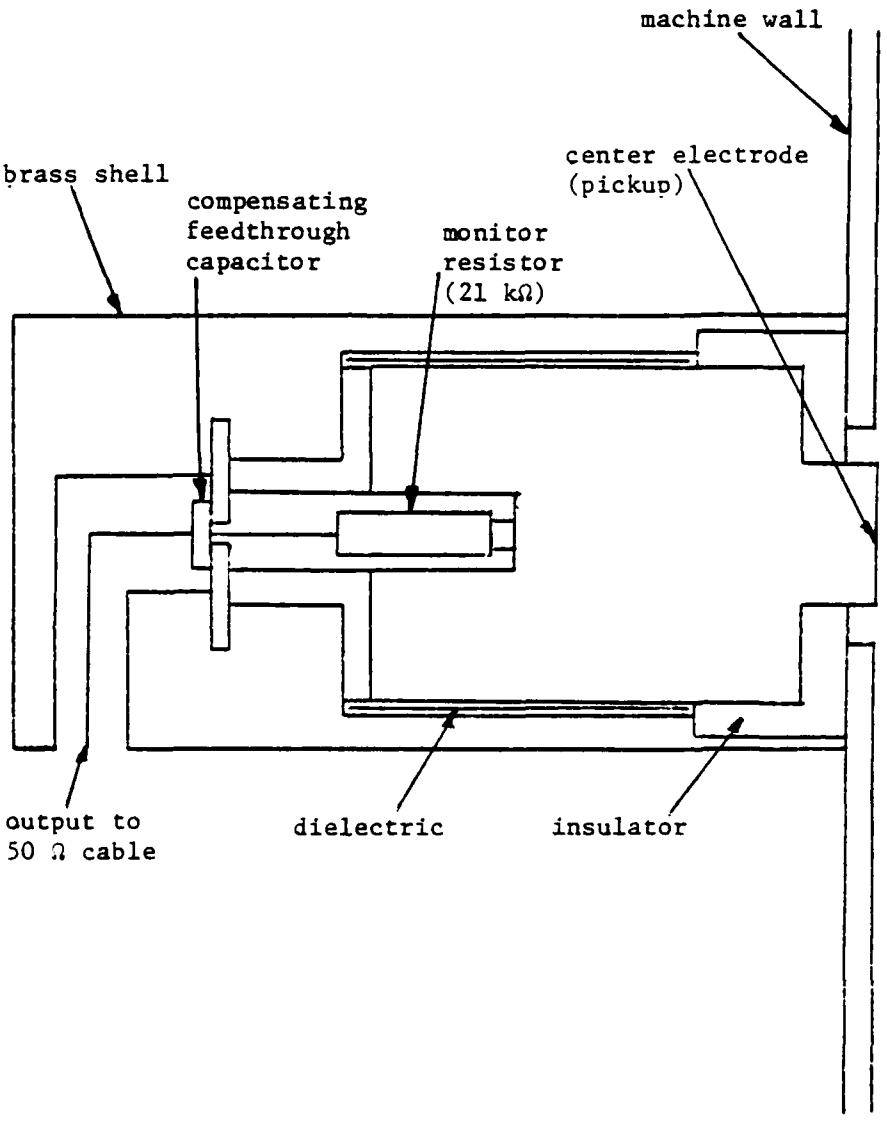

Figure 4.6 Diode voltage probe

In the case of the 7 Ω Line we are probably safe in our assumption that the center conductor is part of the circuit, but on the FX75 this was not so certain. Here the voltage probe was in the diode, where actual emission was occurring. If electrons were some distance out from the cathode closer to the probe, they could give the impression of an erroneously large voltage. Shank fire electrons striking the probe could have an even greater effect. Characteristics of the 7 Ω Line voltage monitor are further discussed in the thesis of Pershing[55]. A typical voltage trace appears in Fig. 4.5.

The diode current monitor consists of a single, shorted turn of wire. It is oriented so that its plane is perpendicular to the B field generated by axial currents (see Fig. 4.7). This B field is proportional to the axial current. Since it is shorted, this loop tries to prevent any B field from penetrating it. It thus develops a current to exclude this field. The current will be proportional to the field and, thus, to the major axial current. Finally, a Tektronix CT-2 current transformer converts the loop current to a voltage. Such current probes are simple and sturdy, but they can be deceived if they are located where plasma or direct beam can reach them. Interpretation of their signal also requires an assumption of cylindrical symmetry of the axial current.

4.3 The Diode Arrangement

Fig. 4.8 shows the basic experimental arrangement at the diode. The machine diode was 2 ft in diameter at the outer wall with a 7 in. brass plug on axis as the negative electrode. Covering this electrode was an aluminum hemispherical dome, which provided a transition down to a 1.25 in. diameter shank of variable length. The shank is terminated in the cathode.

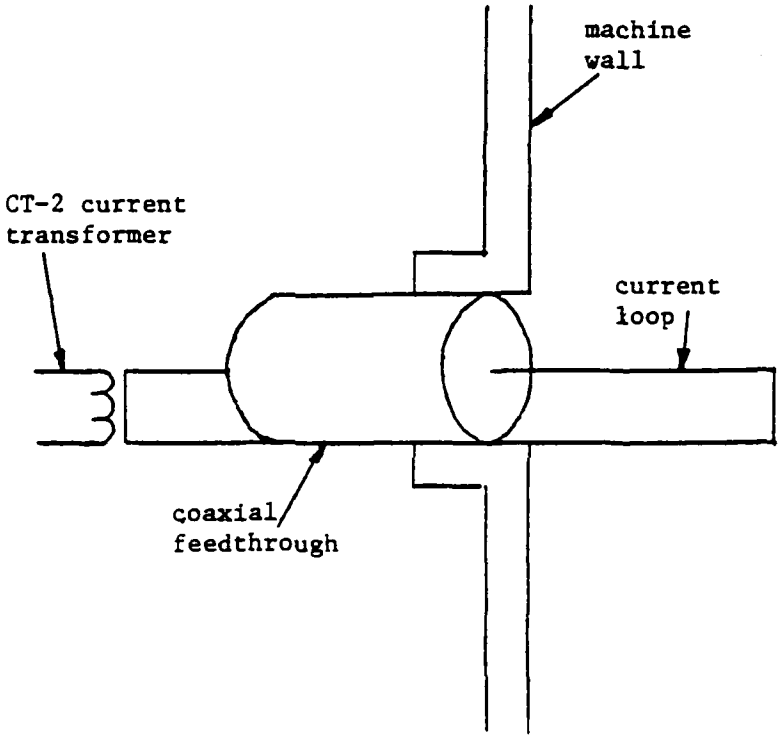

Figure 4.7 Diode current monitor

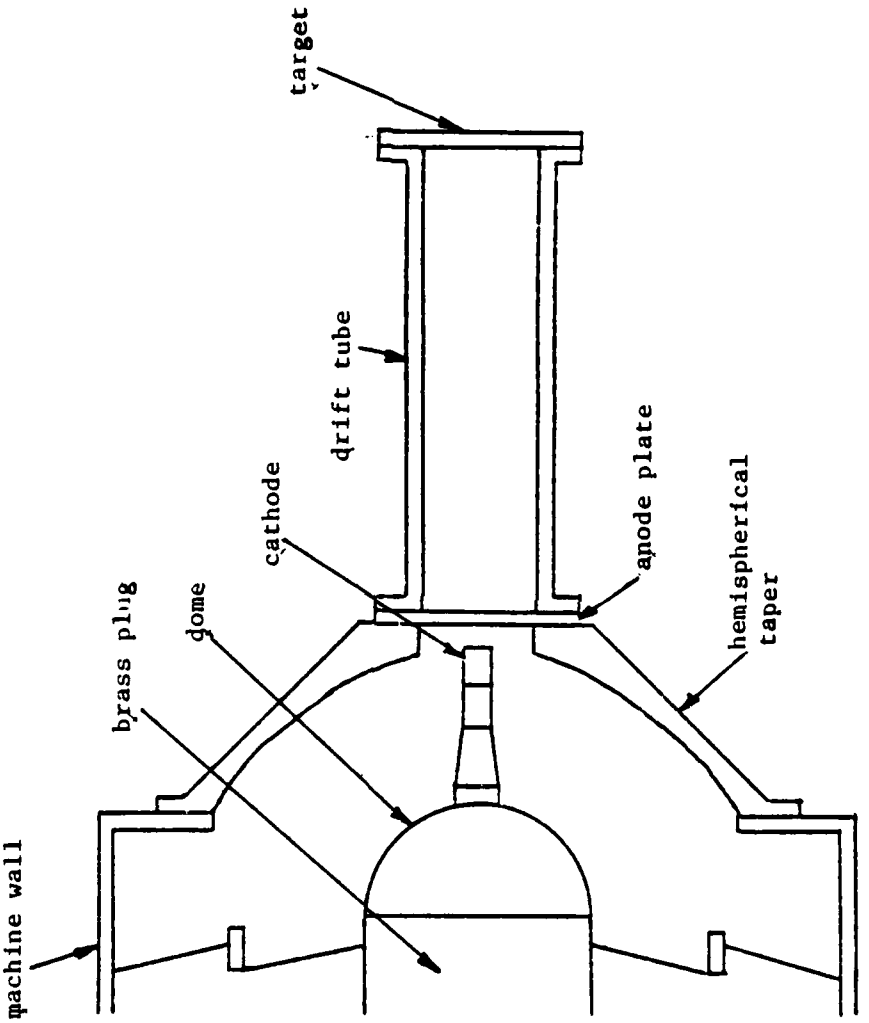

Figure 4.8 General experimental configuration

On some occasions the cathode was made of brass and tapered to a point, but usually the cathode was of graphite. One of our graphite cathodes had a flat face, while the other tapered rapidly to a point. Drawings of these may be seen in Fig. 4.9.

A tapered section attached to the machine face extended over the shank. The anode plate was attached to the end of this section. The anode contained several inserts (see Fig. 4.10). There was an outer, graphite member, which provided an aperture and protected the metal parts. It was also possible to place in the graphite aperture a polyethylene plug with its own aperture (here shown as a tapered hole). A metal plate could be attached to the downstream (in the beam direction) side of the anode to provide additional grounding.

Following the anode was the drift tube. It had a 4 in. inner diameter and was of variable length. Some of our drift tubes include a side port with a window for open shutter photography. To the end of the drift tube were attached the targets. They could take several forms, but their description will be postponed until the occasion for each arises later. The diode and drift tube were evacuated to pressures of $2\text{-}10\times10^{-5}$ Torr for firing.

4.4 Detection of Ion Acceleration

4.4.1 Coincidence Counting

Again, the presence of ion acceleration was detected by target activation. Our targets were usually thin disks of graphite or copper or nickel. The nuclear reactions one expects in such experiments result in the creation of positron emitters. The positron quickly slows down and annihilates with an electron, producing two 0.511 MeV gammas, traveling in opposite directions. These simultaneous gammas are the signature of

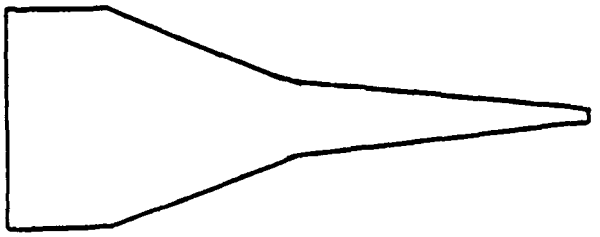

pointed, brass cathode

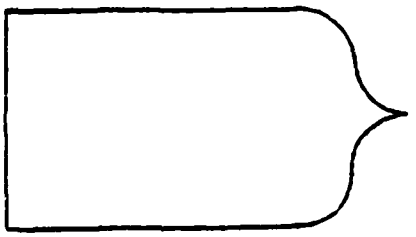

pointed, graphite cathode

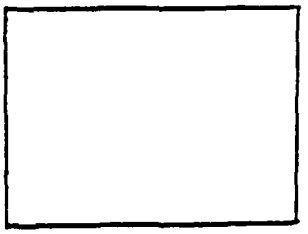

flat, graphite cathode

Figure 4.9 Three cathodes

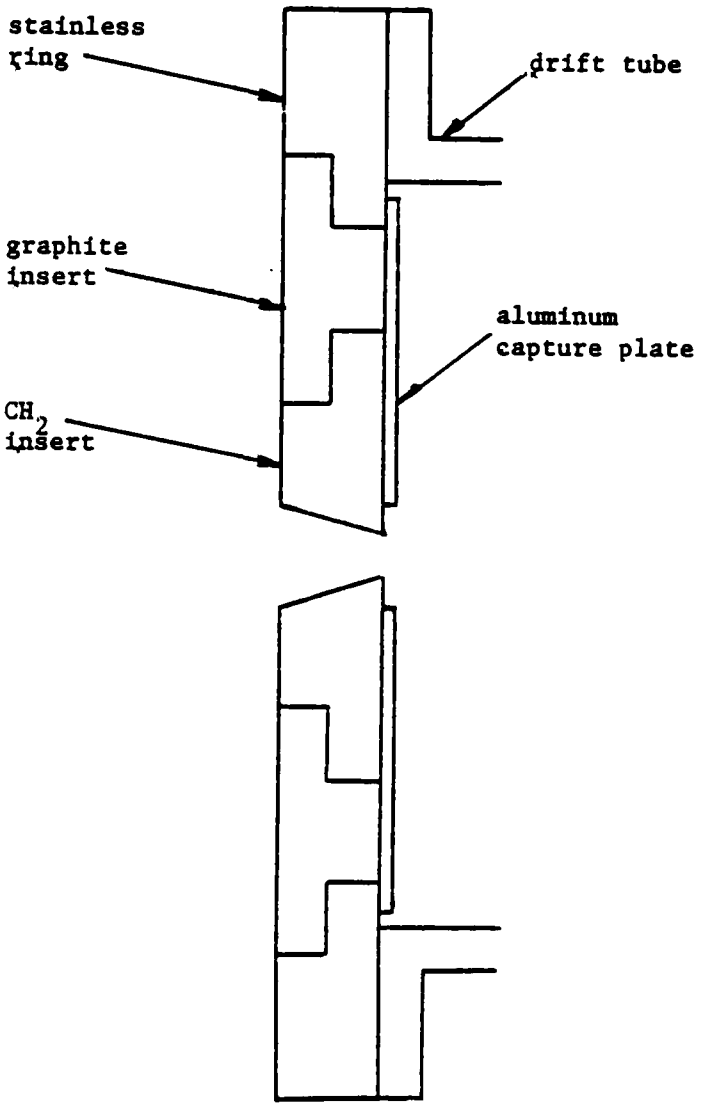

Figure 4.10 Anode plate

a positron decay. Consequently, if coincidence counting is used, a low background count rate may be achieved (2-3 counts/min) and small amounts of activity detected.

Fig. 4.11 shows the arrangement of the counting apparatus. Two NaI(Tl) scintillation detector crystals were mounted vertically with 1/4 in. gap between their faces. The target was placed in the gap for counting. The upper crystal was 2 in. in diameter (Bicron model 2MW2Q/2) with a well (the same one used in 1974-75), and the lower crystal was 3 in. in diameter (Bicron model 3M3/3). These crystals are housed in an opaque metal cover. A photomultiplier picks up the light generated in the crystals.

These crystals are intended to be gamma ray detectors. A gamma from the target passes through the metal cover and transfers its energy to energetic electrons by means of the photoelectric effect or Compton scattering, These electrons, in slowing down in the crystal, produce a flash of light. The light intensity is proportional to the energy dissipated in the crystal. If a photoelectron is generated, all the gamma energy will be captured. However, in the event of only Compton scattering, some of the energy may escape the detector. This effect would give an anomalous low energy tail to a spectrum which would otherwise be a single peak.

The photomultiplier signals are fed to their respective amplifiers and pulse height analyzers (PHA). The window and level on each PHA were set to produce a signal only when a gamma with an energy in the neighborhood of 0.511 MeV was detected. This adjustment was done using a ^{22}Na source. The spectrum of pulses may be observed on an oscilloscope, and the annihilation gamma pulses readily distinguished. If these same pulses

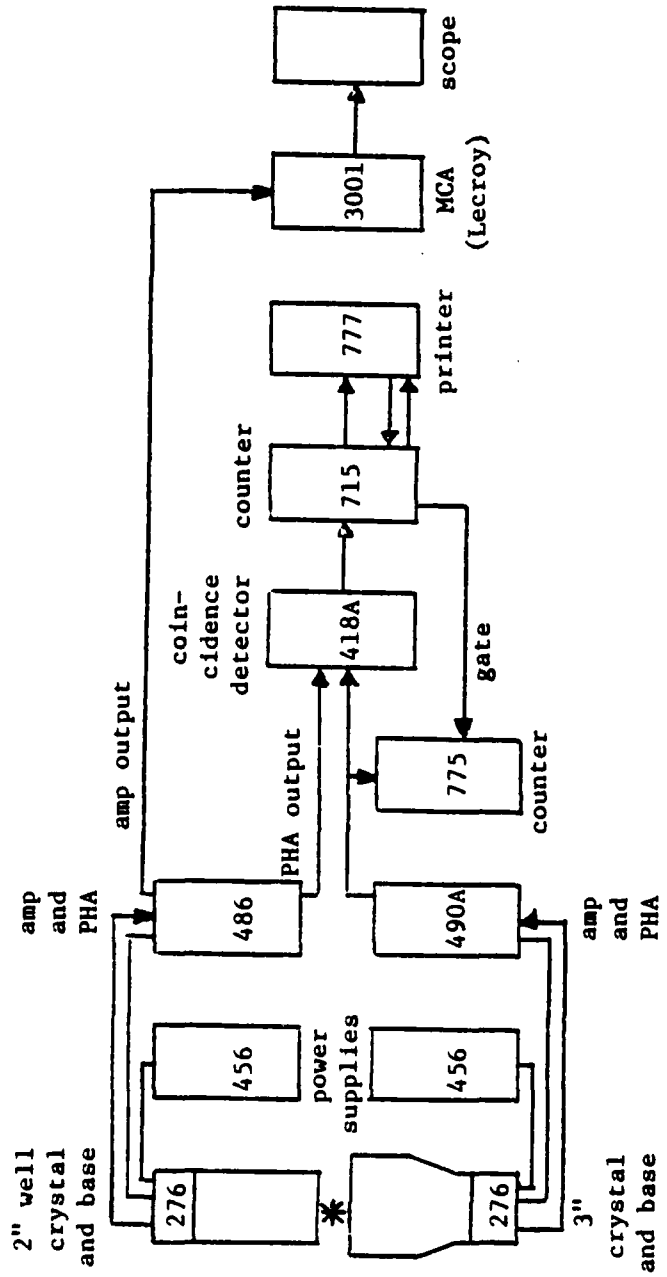

Figure 4.11 Counting apparatus
(model nos. for ORTEC)

are fed to the PHA and if the scope is triggered from its output, then one can adjust the window and level until all pulses are excluded except those desired.

The PHA outputs were processed by a coincidence detector. This device was set to give an output pulse only when two 0.511 MeV gammas were observed approximately simultaneously. The coincidences were totaled by a counter-timer, and the count for each time interval was automatically recorded by a printer.

4.4.2 Calibration of the Coincidence Counter

Since the counting rates are low, a weak positron emitter was needed to properly calibrate our detector. The standard ^{22}Na source which was available was too strong. Instead, it was used to establish the strength of a weaker ^{22}Na source. This measurement was done on a system which was not as susceptible to dead time counting losses as was ours.

The strength of the standard was 11.01 μCi on August 1, 1974. The calibration was performed on April 18, 1979. This is an elapsed time of 4.71 yr. Using 2.58 yr as the half-life of ^{22}Na, we concluded that the source strength had diminished to 3.10 μCi. Comparison of this source with the weaker gave 0.00355 as the ratio of their count rates. This ratio means that the weaker source corresponded to 0.0110 μCi. Thus, decays were occurring at the rate of 407 disintegrations per second. Counting this source on our own set up for 19 h gave a count rate of 15.3 positrons detected per second. Allowing for the fact that in the case of ^{22}Na there are 0.89 positrons per disintegration, we calculated an efficiency of 0.0424 positrons detected per positron decay. Thus, our detection system is approximately 5% efficient.

The background count rate was monitored on a daily basis. Thirty minute background counts were taken. Fig. 4.12 is a cumulative probability distribution of 66 such counts. Each count was plotted with an ordinate that represents the fraction of the total population (i.e. 66 samples) having counts less than or equal to the given count. Statistical considerations dictate that these points should have a Gaussian distribution. The integral of the best such fit is given. This curve was arrived at by using the noncumulative distribution and doing a second order linear least squares fit to the natural logarithm of the ordinates. Also shown are the 90% confidence limits at selected points. Our average 30 min count for this set of samples was 65.31. Thus 2.18 counts/min was our background rate. We found that this rate fluctuated up to a level just under 3 counts/min. Most of our targets gave count rates at least several times this level.

4.4.3 Silver Activation

Silver activation could also be used to detect the neutrons produced by the (p,n) reactions of accelerated protons. This method gives a prompt indication of the amount of activity produced. It is, in addition, less sensitive to where the activity is produced. If the accelerated protons should strike the drift tube wall, for example, this detector would still function. Although little or no target damage was usually experienced, a silver activation detector could, even in this case, reveal the presence of accelerated protons. Usually, our two methods of detection correlated well.

The silver activation detector consisted of a solid, cylindrical block of polyethylene 7 in. in diameter and 7.5 in. high. It was encased

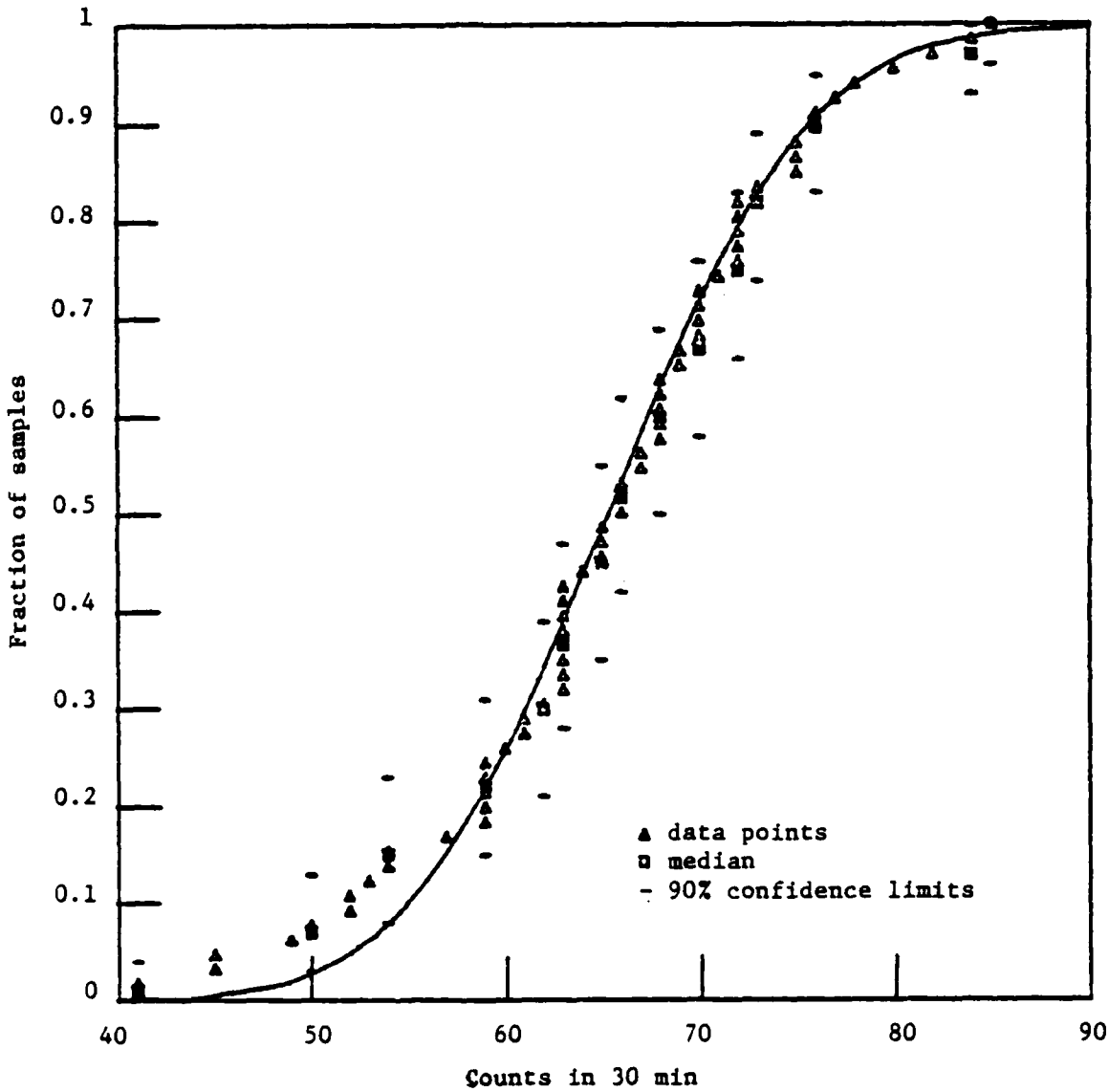

Figure 4.12 Analysis of background counts

in a layer of cadmium. A hole drilled along the axis of the cylinder received a rod shaped Geiger tube wrapped with a thin, silver foil. Pulses from the Geiger tube could be counted on our counter-timer.

Prompt neutrons from the target in the drift tube would pass into the polyethylene cylinder sitting nearby. Here they would thermalize and be captured by the silver, specifically, $^{109}Ag + ^{1}n \rightarrow ^{110}Ag$. The isotope thus formed begins to decay with a half-life of 24.6 sec. Immediately after the shot, the Geiger tube voltage would be turned on, and this decay would be counted for about 2 min. The counter would later be switched to record the target activity, when it had been removed.

The purpose of the cadmium cover was to prevent neutrons thermalizing outside the detector from reaching the silver foil. This arrangement gives a better defined geometry.

4.4.4 Target Material

By proper selection of target material, one can get a rough idea of the ion energies and the amount of ions. Table 4.1 is a list of some popular reactions with their half-lives and thresholds. It is necessary to select a target material giving a reaction whose half-life is sufficiently long to allow for the time necessary to remove the target and get it to the counting equipment. On the other hand, the half-life should not be so long as to give only a very low count rate. Since our targets are not isotopically pure, it is important to consider possible reactions with all the stable isotopes. Hopefully, the various half-lives thus obtained are all much shorter or longer than the one of interest.

As can be seen from the table, different reactions enable one to conclude that ions were or were not accelerated up to a particular energy level. Stacked foils are another method of establishing the energy spectrum.

Table 4.1 Some reactions used to investigate ion acceleration

Reaction	$T_{1/2}$	E_{thres} (MeV)
$^{13}C(p,n)^{13}N$	10 min	3.2
$^{63}Cu(p,n)^{63}Zn$	38 min	4.2
$^{52}Cr(p,n)^{52m}Mn$	21 min	6.0
$^{12}C(d,n)^{13}N$	10 min	0.328
$^{18}O(p,n)^{18}F$	110 min	2.6
$^{11}B(p,n)^{11}C$	20.3 min	3
$^{12}C(p,\gamma)^{13}N$	10 min	0.457 res 1.7
$^{14}N(p,\gamma)^{15}O$	124 sec	0.278 res 1.06
$^{10}B(p,\gamma)^{11}C$	20.3 min	>0.4
$^{10}B(d,n)^{11}C$	20.3 min	>0.2
$^{14}N(d,n)^{15}O$	124 sec	0.143
$^{16}O(d,n)^{17}F$	66 sec	1.83
$^{14}N(p,n)^{14}O$	70.6 sec	6.35

In this technique ions pass through a series of foils, slowing down and activating the foils as they go, until their energy falls below the threshold. By examining the activity in each foil, one can conclude that ions with the threshold energy plus the energy lost in preceding foils were present. In addition, by using the reaction cross section as a function of energy, a determination of the number of ions can be made.

Ion yield can be most conveniently established if the target reaction has resonances, rather than thresholds. This is the case for (p,γ) reactions. We have previously seen this for $^{12}C(p,\gamma)^{13}N$. The thick target yield is conveniently flat over the energy range between resonances. More usually, one must integrate the cross section, which involves an assumption about the initial ion energy.

4.5 Production of Accelerated Ions

4.5.1 Preliminary Experiments

The aim of the experiments on the 7 Ω Line was to determine whether ion acceleration was possible and to what extent. By extent we mean the type of ion, the energy, and the number of ions. To this end, various material and geometrical factors were varied, much as was done on the FX75. With the 7 Ω Line, however, we are dealing with a much lower voltage beam and a somewhat lower energy beam. We are also accelerating ions in a drift tube beyond the field of the diode. In the FX75 we were able to accelerate protons to about 2.5 times the beam energy in a distance of 4 cm. With the 7 Ω Line a factor of 2.5 would only have given us 1.25 MeV protons, but we also had the capability of maintaining the acceleration for a greater distance. Working at NCSU had the additional advantage of more experimental flexibility and the opportunity

of repeating experiments more, since statistical variability was still a concern.

The first successes occurred using a pointed, brass cathode, an anode with graphite insert but no polyethylene plug, and a target of BN (boron nitride). The cathode-anode gap was 28 mm, measured from the tip of the cathode to the anode ion source. The target, in the form of a ceramic tube, was attached to the face of a graphite calorimeter-Faraday cup. This cup was mounted at the end of 6 in. drift tube. Deuterium was used, initially, as an ion source, in the form of a CD_2 coating on a film held against the anode aperture by a capture plate. This choice of ion and target was motivated by its zero threshold, high yield, and by the interest in accelerating deuterium for fusion applications. Activity was observed in the BN, but it did not seem to have the correct half-life to have been produced by $^{10}B(d,n)^{11}C$.

Even more activity (3 times more) was subsequently generated when the CD_2 film was replaced with a half-mil CH_2 film. The count rate, initially, was 240 times background. The decay rate was also consistent with this having been derived from either $^{10}B(p,\gamma)^{11}C$ or $^{11}B(p,n)^{11}C$.

An attempt was also made to accelerate protons from a polyethylene plug in the anode. There was a 1/2 in. hole drilled through its axis. The anode-cathode gap was 15 mm. On the first shot no activity was found at the target. Nine more shots were fired without opening the diode. Activity levels were then found to have a count rate about twice that of the CH_2 film. However, it is not known whether this activity was accumulated over several shots or produced on a single shot. Further, the exact anode geometry was in doubt, since the beam had opened up the upstream side of the aperture to 1 in. (see Fig. 4.13).

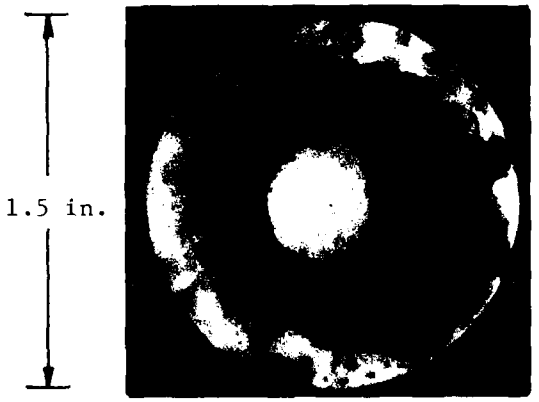

Figure 4.13 Damage to polyethylene anode

The polyethylene surface was very rough and flaky.

These initial trials indicated that it would be best to focus on proton acceleration, rather than deuterium. Our deuterated films were of an irregular quality. It was also decided to use anode films, rather than polyethylene plugs, as an ion source. The latter tended to blow particles all over the diode. Finally, the target was changed to graphite. Our graphite targets were thin disks with a 3.5 in. diameter. They were fastened to the calorimeter face. They presented a much greater area to the ions, and their proton activation characteristics were similar to boron's.

4.5.2 Tests with Films and Filaments

Fig. 4.14 shows a closer view of the cathode-anode arrangement for the experiments with films. The aluminum capture plate (used to hold the films to the downstream side of the anode) had a 2 in. diameter aperture, while the graphite aperture was 1.5 in. As before, the basis for comparison was the counts per min in the graphite target disk, extrapolated back to the time of firing. The 9.97 m ^{13}N half-life was used for this purpose. The graphite disk was always centered in the scintillation detectors.

Table 4.2 shows the effect of varying the cathode-anode gap using a polyethylene film (CH_2) and a polycarbonate film ($C_{16}H_{14}O_3$). Table 4.3 shows the effect of varying the film thickness at two different gaps. The variations observed must be viewed in the light of Table 4.4, which shows the variation in count rate for a single experiment repeated four times. This variation makes it essentially impossible to distinguish between these two films over the range of gap spacings used. However, a considerable increase in count rate was observed when filaments were

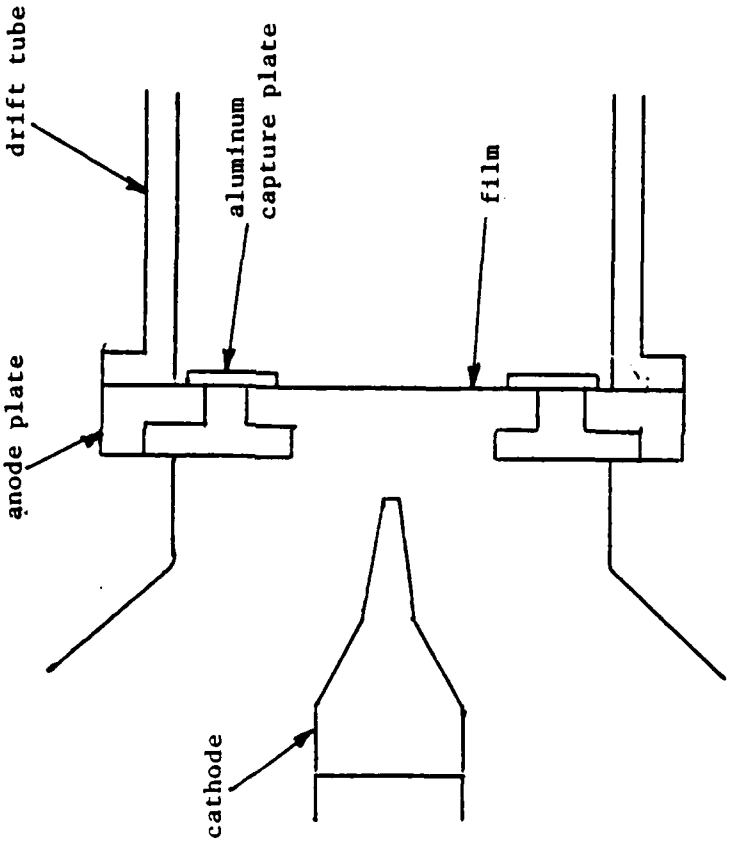

Figure 4.14 Cathode-anode arrangement for films

Table 4.2 Variation of the cathode-anode gap

Film	Thickness (microns)	Gap (mm)	Count rate (counts/min)
CH_2	13	38	18
CH_2	13	28	53
CH_2	13	23	21
$C_{16}H_{14}O_3$	2	28	30
$C_{16}H_{14}O_3$	2	23	41
$C_{16}H_{14}O_3$	2	18	19-70
$C_{16}H_{14}O_3$	2	13	-

Table 4.3 Variation of the film thickness

Film	Thickness (microns)	Gap (mm)	Count rate (counts/min)
$C_{16}H_{14}O_3$	2	18	19-70
$C_{16}H_{14}O_3$	4	18	43
$C_{16}H_{14}O_3$	6	18	13
$C_{16}H_{14}O_3$	2	28	30
$C_{16}H_{14}O_3$	4	28	20
$C_{16}H_{14}O_3$	6	28	17

Table 4.4 Reproducibility of the count rate

Film	Thickness (microns)	Gap (mm)	Count rate (counts/min)
$C_{16}H_{14}O_3$	2	18	70
$C_{16}H_{14}O_3$	2	18	52
$C_{16}H_{14}O_3$	2	18	26
$C_{16}H_{14}O_3$	2	18	19

used for an ion source.

Fig. 4.15 shows a view of the diode set for the use of filaments. The cathode is shown as the flat, graphite cylinder; and the anode is shown without the graphite insert; but, initially, the pointed, brass cathode and the insert were present. The filament pattern shown is a particular one which would be described as having 3 strands. The number of filaments per strand could also vary. This was the same nylon filament material used on the FX75.

Table 4.5 shows the variation in count rate for a single filament at a single gap. The same cathode and anode structures were used as for the film shots. Even though there is still considerable fluctuation, it shows a dramatic improvement by about a factor of 10. It may be that, with our less energetic electrons, the beam is easily overloaded.

It was observed that, when the anode graphite insert was removed, the count rate dropped to much lower levels. This drop was remedied by replacing the pointed, brass cathode with the graphite cylinder. Table 4.6 shows the count rates for a variety of filament configurations. Again, statistical considerations make it impossible to distinguish between these, except that the larger gap of 19 mm appears to have had an adverse effect. Thus, it was necessary to move in closer when using the flat, graphite cathode to achieve the previous levels of activity.

One should note that the activity on the target was not spread uniformly over its surface. There was usually a broad hot spot instead, frequently off to one side. This wandering of the activity may account for some of the observed variability for shot to shot. On occasion a graphite sheet was placed so as to line the inside of the drift tube. Localized activity could be observed on this as well. As for loss of

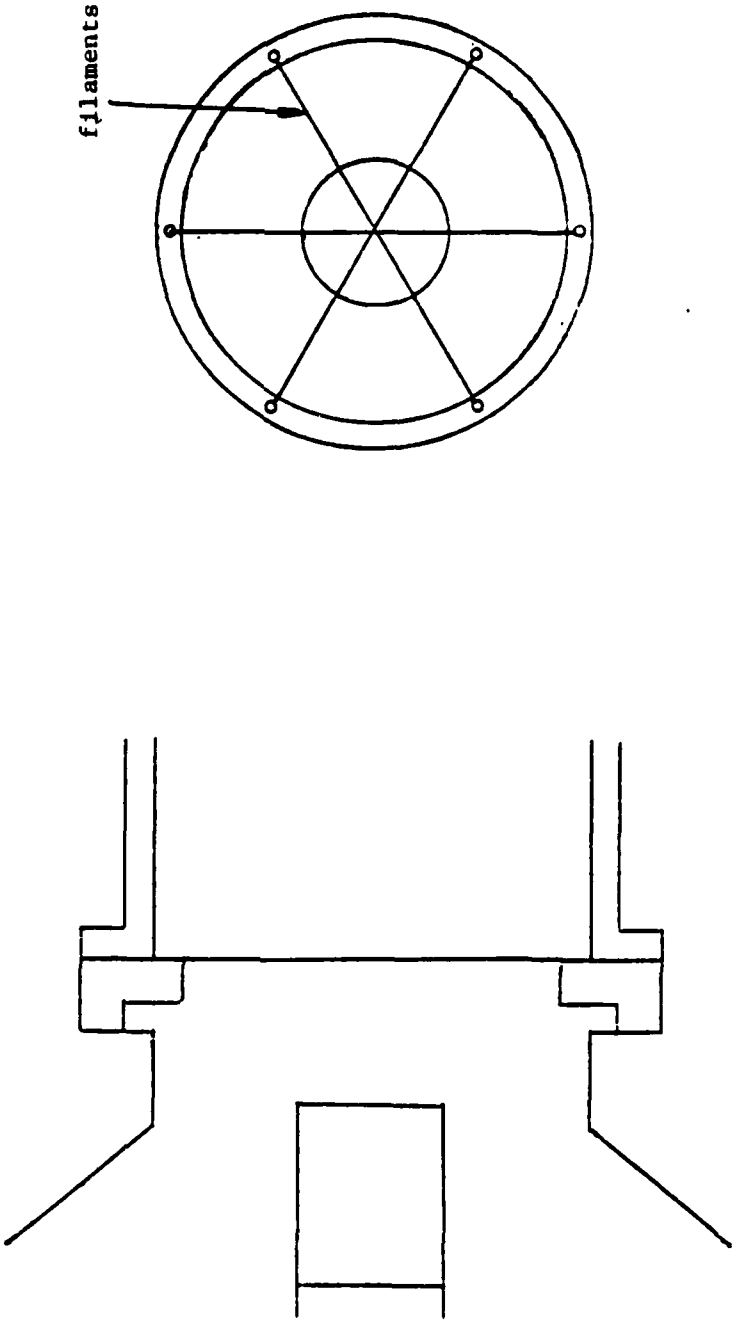

Figure 4.15 Cathode-anode arrangement for filaments

Table 4.5 Variation in count rate for a single filament

Strands	Filaments each	Gap (mm)	Count rate (counts/min)
1	1	18	730
1	1	18	188
1	1	18	102
1	1	18	62

Table 4.6 Variation of the filament configuration

Strands	Filaments each	Gap (mm)	Count rate (counts/min)
3	5	13	730
3	5	13	237
3	2	13	165
3	1	13	118
3	5	19	84

activity due to target blow off, visual inspection indicated only target heating in most cases.

Calorimeter current traces showed electron current levels of up to 13 kA at the drift tube end when the brass cathode was used with filaments. This current increased dramatically to 18-32 kA when the graphite cylinder was used. The diode current also increased similarly. Otherwise, these current levels could not be correlated with activity levels.

4.5.3 Activating Metals

The original decision to use a graphite target was, in part, based on the belief that the ions accelerated would be of rather low energy. The activity produced was expected to be due to the resonance (p,γ) reactions. It was discovered, in the course of some spectroscopic work, that a stainless steel foil was being activated.

Fig. 4.16 is a graph of the decay curve of this activity. The activity was the total produced after several shots. This curve appears to represent the decay of two species. Accordingly, a nonlinear, least squares fit of that type was performed, as earlier described. The adjustable parameters were the amount and half-life of each species. The half-lives thus derived were 21.1 min and 4.44 h. A χ^2 test indicated that the probability was 0.9 of the fit actually corresponding to the data.

The basic constituents of stainless steel are Fe, Ni, and Cr. If we consider (p,n) and (p,γ) reactions on the stable isotopes of these elements, then the best candidates for giving the activity are ^{60}Cu and ^{61}Cu, with 23 min and 3.37 h half-lives, respectively. Assuming this to be the case, a fit was performed with the given half-lives, adjusting only the amounts. Unfortunately, the χ^2 test associated a probability

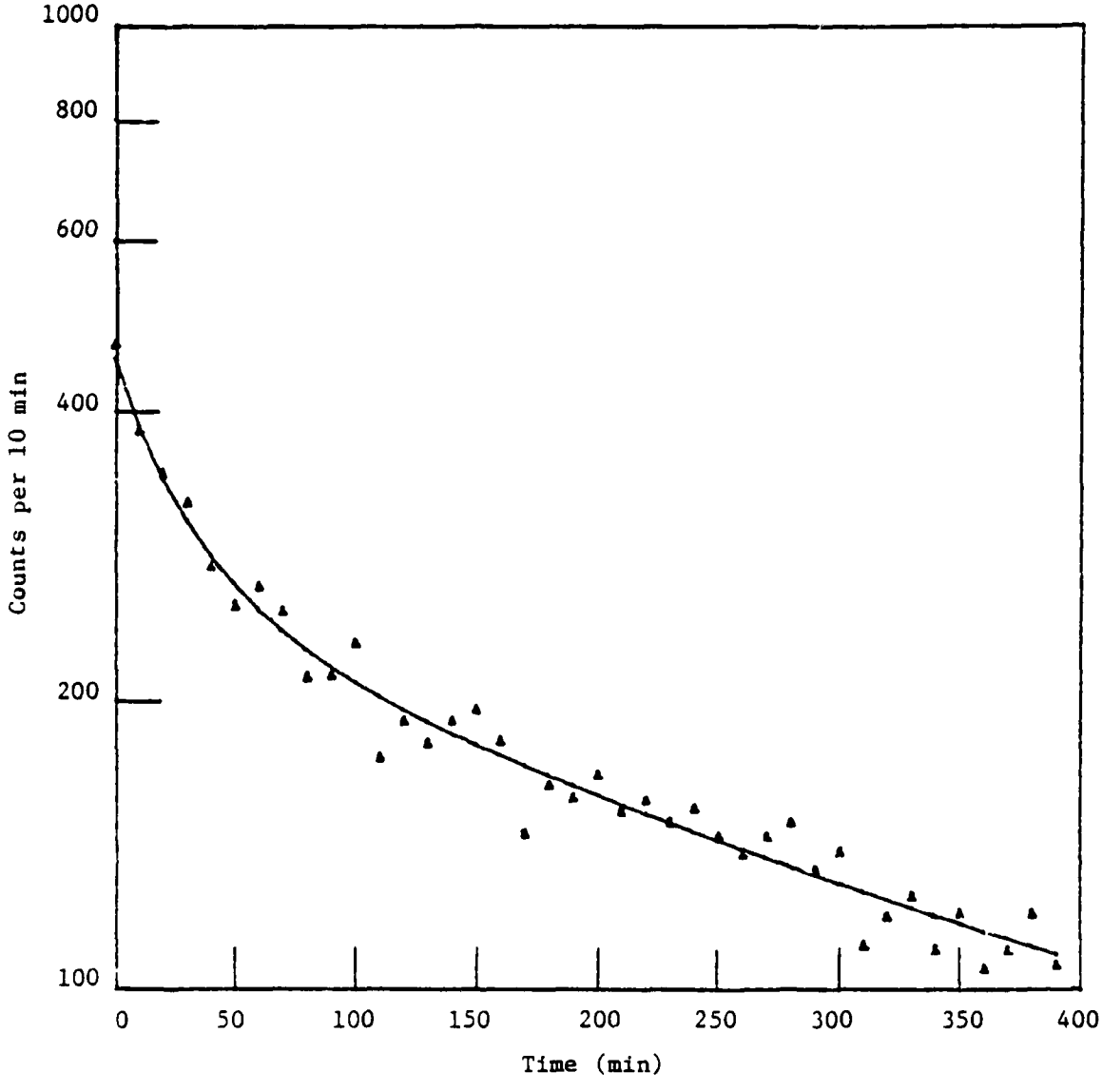

Figure 4.16 Decay curve of stainless activity

of only 0.01 with this fit.

This difficulty can be overcome by observing that ^{62}Cu and ^{64}Cu may also be produced from Ni isotopes. The half-lives of these nuclides are close enough to the others to confuse the simple two species decay scheme. This hypothesis was tested by doing another fit. All 4 half-lives were used and considered fixed. Only the amounts were varied. The relative proportions of ^{60}Cu, ^{61}Cu, ^{62}Cu, and ^{64}Cu predicted were 6:55:1:55. The χ^2 probability was 0.97.

The pertinent data respecting these activities is given in Table 4.7. ^{60}Cu and ^{64}Cu must be produced by (p,n) reactions. The former requires 7 MeV ions. This would be 14 times the beam electron energy. One might be surprised to observe that more ^{60}Cu was present than ^{62}Cu, since ^{62}Cu has a threshold of only 4.8 MeV. It must be remembered, though, that this activity was accumulated over a period of time and that the ^{62}Cu was decaying faster. This effect may account for their ratios when the counting began.

Nickel foil was obtained, and these same activities were produced in a purer substance. On two other occasions, for example, the relative proportions were 1:21:3.5:6.3 and 1:89:2.6:56. The foils were checked by x-ray flourescence to see if contaminants could be interfering. Overnight gamma ray spectra were taken. The two most prominent peaks of ^{61}Cu were found (0.284 and 0.656 MeV). This observation seemed to definitely indicate that at least 3 MeV ions were present, if not even more energetic ones.

The experimental configuration in use consisted of the cylindrical flat, graphite cathode with a filament pattern of 3 strands, 1 filament per strand. The anode-cathode gap was 18 mm. There was a graphite

AD-A118 515 NORTH CAROLINA STATE UNIV RALEIGH DEPT OF PHYSICS F/G 20/7
OBSERVATIONS OF COLLECTIVE ION ACCELERATION.(U)
1981 D L MORROW AFOSR-80-0051
UNCLASSIFIED AFOSR-TR-82-0641 NL

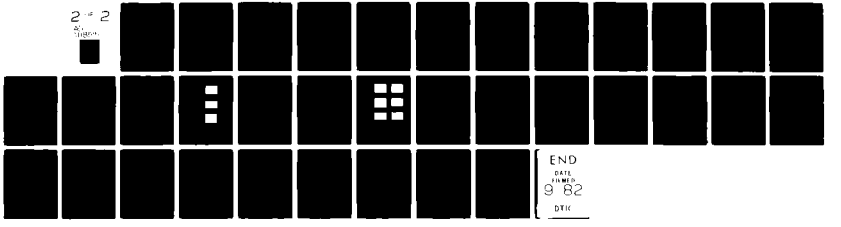

Table 4.7 Data on Ni isotope activation

Reaction	Relative abundance of Ni isotope (%)	$T_{1/2}$	E_{thres} (MeV)
$^{60}Ni(p,n)^{60}Cu$	26	23 min	7.018
$^{61}Ni(p,n)^{61}Cu$	1	3.37 h	3.07
$^{62}Ni(p,n)^{62}Cu$	3.6	9.78 min	4.80
$^{64}Ni(p,n)^{64}Cu$	0.9	12.74 h	2.50

in the anode with a 2.25 in. diameter aperture. The target foil was held at the end of a 1 ft drift tube. The exposed foil area was 3.5 in. in diameter.

To further clarify matters a copper foil was used. The only activity that can be observed in a copper foil is $^{63}Cu(p,n)^{63}Zn$, with a 38.5 min half-life and a 4.2 MeV threshold. ^{63}Cu is 69% abundant. We were consistently able to activate single sheets and stacks of this 1-mil copper foil.

On our best shot a stack of 5 foils became active. This stack consisted of 1 1-mil Al foil, 3 1-mil Cu foils, and 1 5-mil Cu foil (the Al foil was not activated). Assuming that some ions had at least 4.2 MeV when they reached the last foil, one can calculate from range-energy tables what their initial energy was before being slowed down by the preceding foils. 3 mils of Cu corresponds to 68 mg/cm^2, and 1 mil of Al to 6.86 mg/cm^2. 4.2 MeV protons have a range of 51.954 mg/cm^2 in Cu. The preceding 3 foils increase the necessary range to 120 mg/cm^2, which gives an energy of 7 MeV. In aluminum 7 MeV protons have a range of 91.05 mg/cm^2. Finally, this calculation gives an initial proton energy of 7.3 MeV. This is over 12.3 times the beam energy indicated for that shot. A 1 ft drift tube was used on this occasion.

4.6 Stacked Foil Analysis

As indicated previously, a foil stack can give a rough picture of the energy spectrum. First, one must know how much activity is created in each foil by an incident proton of a given energy. This computation involves keeping track of the proton energy as it slows down and computing the probability of its reacting in a particular foil as a function of energy. This is essentially the same calculation as was described in

Section 3.2.

For better accuracy, a computer program was written which steps the proton through the foil stack. At each step the energy loss was computed, to give the current proton energy. The probability of reacting during that step was added to the total probability for the foil which contained the proton. In this way, the relative levels of activity for each foil could be determined. Slowing down values[59] and reaction cross section values[65] were obtained by interpolating in tabulations of these quantities, rather than by relying on an emperical fit.

The number of reactions in each foil was determined by extrapolating the count rate back to the instant of firing and by allowing for the detection efficiency (previously determined to be 5%). This process gave 1.25×10^{7}, 3.55×10^{6}, 5.35×10^{5}, and 2.32×10^{4} as the number of ^{63}Zn atoms created in each foil. The ratio of the activities in the last two foils was 23.

Various incident proton energies were tried until one was found which gave a probability ratio of 23 for these two foils. Thus, 7.48 MeV protons had activation probabilities of 35×10^{-6}, 27×10^{-6}, 14×10^{-6}, and 0.59×10^{-6}. If we assume that there were 3.9×10^{10} protons with this energy, then they could account for all the activity in the last two foils and some of the activity in the other two. This process can be repeated after subtracting off all of the activity due to the 7.48 MeV protons. It was found that a 5.2×10^{11} member bunch of 6.25 MeV protons could account for the rest of the activity. Total ion energy amounted to 0.57 J, while the total electron beam energy, estimated from current and voltage traces, was 800 J. 0.07% of the beam energy went into ions producing activation.

This analysis gives an energy spectrum of two peaks, 7.49 and 6.25 MeV. In actuality, the ions in these peaks should probably be spread

over a much broader energy range. The analysis gives only one possible spectrum out of an infinity of others.

4.7 Distribution of the Activity

Two types of targets were available. One had a 3.5 in. diameter aperture and held the target foils tightly at their perimeter by means of a screw-in ring. This target, called the foil holder, was bolted to the end of the drift tube. Thus, its location could be varied only in 6 in. jumps by changing the drift tube length.

The other type (see Fig. 4.17) was called the pedestal. It had a 2.88 in. diameter aperture. The foils were held against a flat plate by means of a ring at the perimeter, which screwed over the foils and onto the plate. The plate was mounted on a long rod. The rod was held in a vacuum tight sliding o-ring seal, in which it could be positioned independently of changing the drift tube. However, it was much more inductive electrically than the foil holder and had a smaller aperture.

It was possible to activate foils with either target, and in view of the erratic occurrence of the activity, it was not clear that one was necessarily superior. The best shot was with the foil holder at a distance of 12 in. from the anode (10,785 counts/min initially). The best pedestal shot was almost half this level and occurred at a distance of 18 in. (4749 counts/min.

Count rates exceeding 1000 counts/min occurred frequently. These rates could be obtained with either the pedestal or the foil holder at distances ranging from 7 in. to 24 in. Activity was not observed, when using metal foil targets, at distances less than 7 in. Much closer than this distance resulted in target damage. The cathode configuration con-

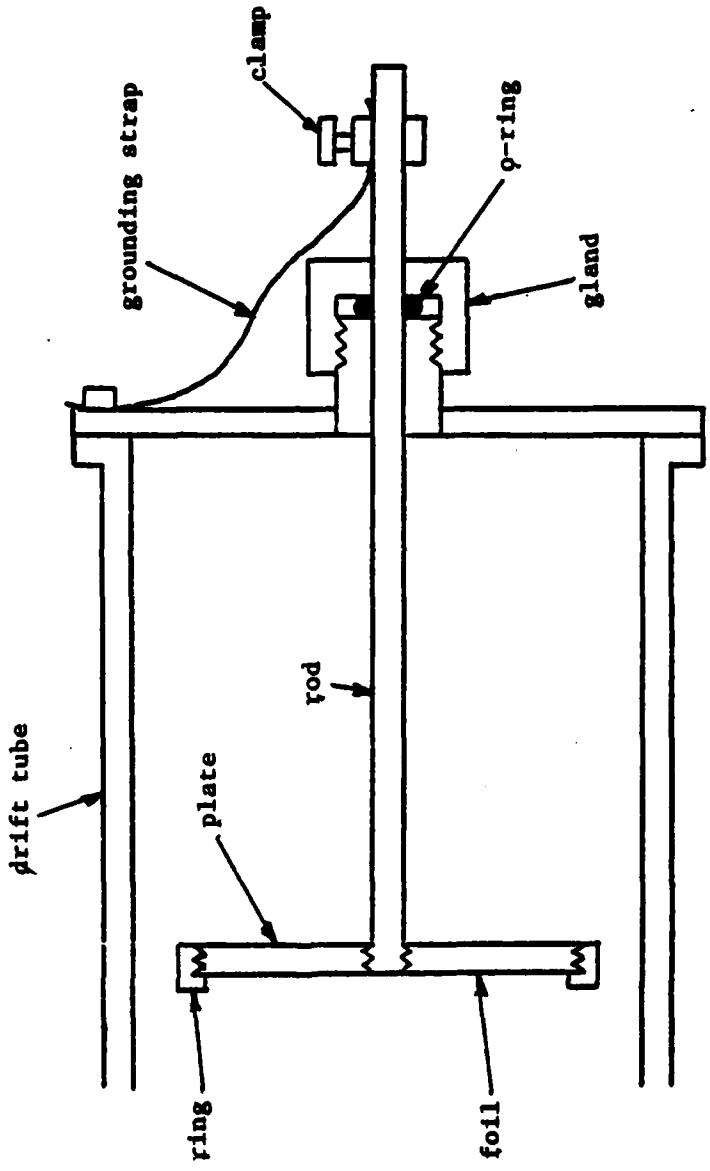

Figure 4.17 Pedestal target assembly

sisted of the cylindrical, graphite block, 3 filament strands of 1 filament each, and an anode-cathode gap of 18-20 mm.

A hand Geiger counter with a 1.25 in. diameter window was available to indicate the location of the activity on the target. The activity was usually confined to a spot which appeared to be about the size of the counter window. The actual spot size could thus have been considerably smaller, but the counter resolution could not permit this determination. The activated spot was usually located off center near the foil perimeter.

On several occasions a sheet of Cu foil was used to line the downstream end of the drift tube. This liner was 7 in. wide and long enough to just encircle the 4 in. diameter drift tube. The pattern of activity on these liners consisted of a narrow band aligned axially. The band appeared on the side of the tube to which the activated spot on the target was displaced. The band activity was almost always greater at its upstream end and, sometimes, exceeded the activity of the target.

Once, the band activity increased, as usual, when proceeding upstream but dropped rapidly to zero about 2 in. before the end of the liner. The liner for this shot occupied the last 7 in. of a 12 in. drift tube. Thus, the activity ceased at a point 7 in. from the anode. Prior to reaching this cutoff, the activity level had almost doubled, as compared to the downstream end of the band. As mentioned earlier, activity has not been observed closer to the anode than this. Similar measurements have been described in the case of a dielectric guide by Pasour et al[66].

Finally, it was found that the accelerated ions could activate the pedestal holder behind the pedestal. To do this the ions had to travel

18 in. to the pedestal, pass through the 0.5 in. gap between the pedestal rim and the drift tube wall (4 in. inner diameter), and travel another 6 in. to reach the pedestal holder.

4.8 Electron Beam Observations

4.8.1 Diagnostics

An unsuccessful attempt was made to correlate electron beam behavior with ion acceleration. The presence or absence of filaments in the anode did have an effect, but the subsequent occurrence of acceleration could not be associated with a particular beam character. Besides the diode current and voltage traces, there were available two PIN diodes and a Rogowski coil to monitor the beam.

Our PIN diode (Quantrad model 100-PIN-250N) was an x-ray detector with a nanosecond risetime. It consists of a silicon wafer, 100 mm^2 in area and 250 μ thick. The name PIN implies that the device is a sandwich of a heavily p-doped region, an intrinsic region, and a heavily n-doped region. In fact the intrinsic region is actually a fully depleted p-doped region. It was biased to 300 Volts. An x ray passing through the active region will deposit some energy in the form of charge pairs (3.72 eV per charge pair). These are quickly swept out by the bias voltage and produce a current into 50 Ω, which is seen on the scope.

The PIN diodes were set to pick up the bremsstrahlung x rays produced in the drift tube wall when struck by the electron beam. To insure that the diode received only those x rays generated in the wall immediately in front, it was surrounded by a 1 in. thick lead shield with a 0.25 in. diameter aperture drilled through the front (see Fig. 4.18).

A calculation was performed to determine the sensitivity of the diodes.

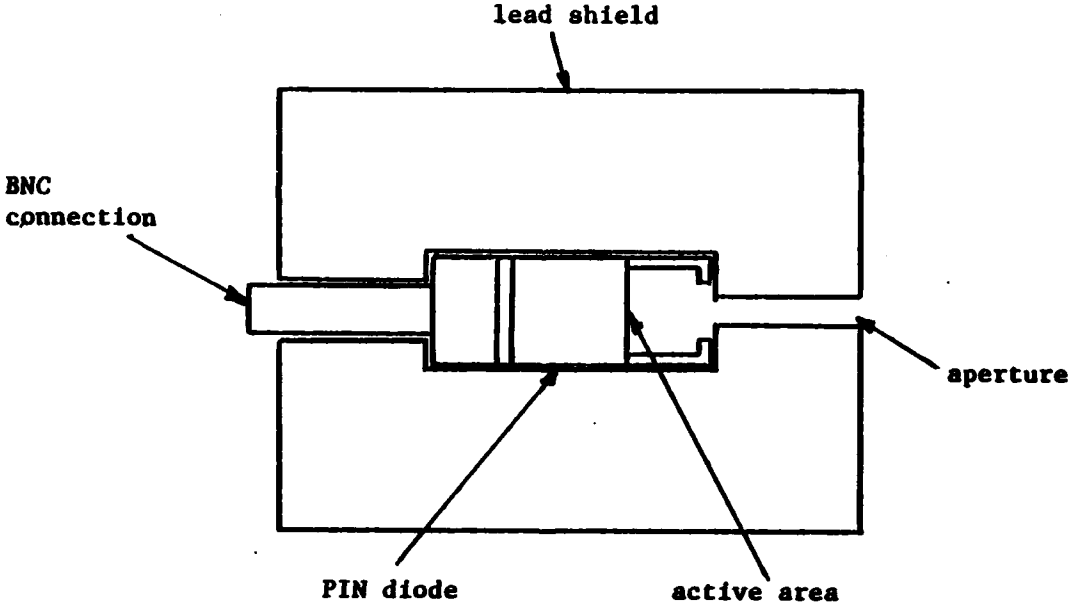

Figure 4.18 PIN diode and shield

Given the current and energy of a beam incident on the interior tube wall, what would be the signal from the diode? This calculation was attached in two parts. First, given x rays of a known energy, how many would get through the tube wall and deposit energy in the detector? Second, given an electron beam, what x rays and how many would it produce in the wall?

The mass attenuation and absorption coefficients in iron and silicon for x rays as a function of energy were obtained from tables[67]. Using the formula

$$\frac{\Delta E}{E_o} = \frac{\mu_{ASi}}{\mu_{Si}} [1-\exp(-\mu_{Si} \Delta x_{Si})]\exp(-\mu_{Fe} \Delta x_{Fe})$$

the fraction of incident energy finally deposited in the silicon could be obtained. μ_{ASi}, μ_{Si}, and μ_{Fe} are the mass absorption coefficient, mass attenuation coefficient of silicon, and the mass attenuation coefficient of iron, respectively, in cm^2/g. Δx_{Si} and Δx_{Fe} are the thicknesses of the silicon and iron, respectively, in cm^2/g. In our case the iron was 1/8 in. or 2.55 g/cm^2, and the silicon was 0.0583 gm/cm^2. This relation is plotted in Fig. 4.19. For purposes of further calculation, it was approximated by the square function shown. Thus, we see that, for incident x-ray energies above 100 keV, the response is relatively constant.

The bremsstrahlung spectrum for electrons of a given energy passing through iron was also found in tables[68], as was the data for electron slowing down[69]. Then, given an initial electron energy, its progress could be followed numerically as it moved through the iron. As the electron lost energy, the total bremsstrahlung emitted in the sensitive region of the detector was accumulated as a function of incident electron energy. This sum could then be multiplied by the previously calculated

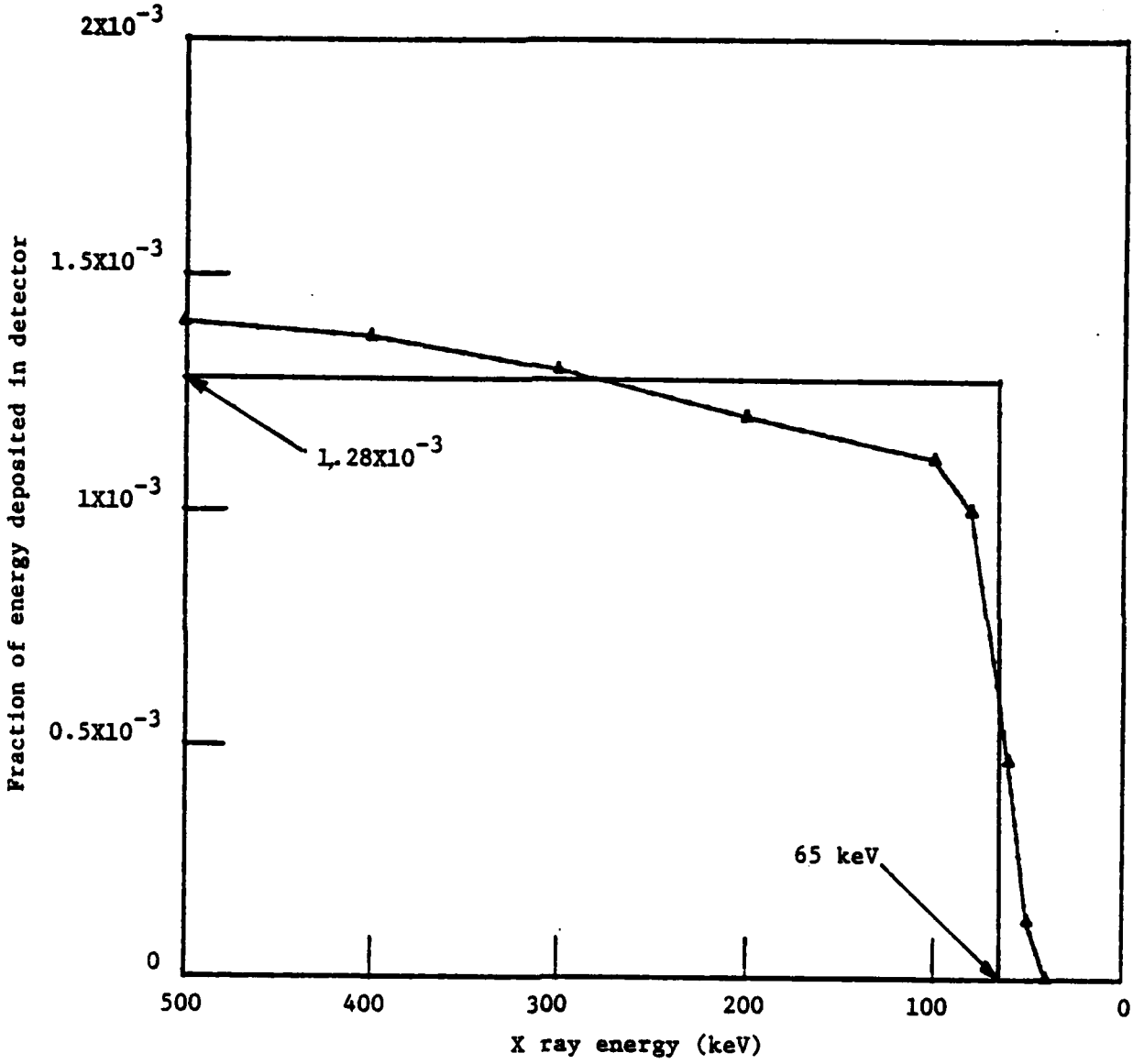

Figure 4.19 Bremsstrahlung absorbed

detector sensitivity. The ultimate result is seen in Table 4.8. The calibration factor is in Amps/cm^2 of beam electrons incident in front of the detector window (0.32 cm^2) per volt of signal seen at the scope. Unless the beam energy is well known, the PIN diode can only give an approximate picture of the current density. It can also be used to give an idea of the timing of events in the drift tube.

The Rogowski coil is, essentially, a toroidal solenoid which wraps around the drift tube just inside the wall. It is shielded from direct beam bombardment. The B field of a current passing through the coil is picked up. The coil sends out a voltage pulse proportional to dB/dt, but this is integrated at the probe by an L-R circuit. Thus, a signal proportional to B, and thus to the axial current, reaches the scope. The calibration factor was 9.04×10^{-5} V(out)/Amps(in)[55].

4.8.2 Currents in the Drift Tube

A series of several experiments was performed to determine what fraction of the emitted current was reaching the pedestal when it was located at various drift tube positions. This measurement was accomplished by placing the Rogowski coil at the end of the drift tube, encircling the pedestal support rod. The emitted current was taken from the diode loop signal. The ratio of pedestal current to loop current is plotted in Fig. 4.20. Loop current levels ran between 27 and 43 kA.

In all cases a 3 strand filament pattern was used. However, for the 5-9 in. data the graphite, cylinder cathode at a gap of 20 mm was used, while for the 12-21 in. data the pointed, graphite cathode at a gap of 5 mm was used. Nevertheless, the two groups seem to be in general agreement. A shot with the pedestal at 12 in. and no filaments gave no

Table 4.8 PIN calibration

Initial energy (keV)	Bremsstrahlung produced above 65 keV (keV)	Calibration ((Amp/cm^2)/Volt)
500	2879.9	16.3
450	2294.5	20.4
400	1772.6	26.5
350	1314.1	35.7
300	919.7	51.0
250	590.6	79.4
200	329.2	142
100	27.1	1730

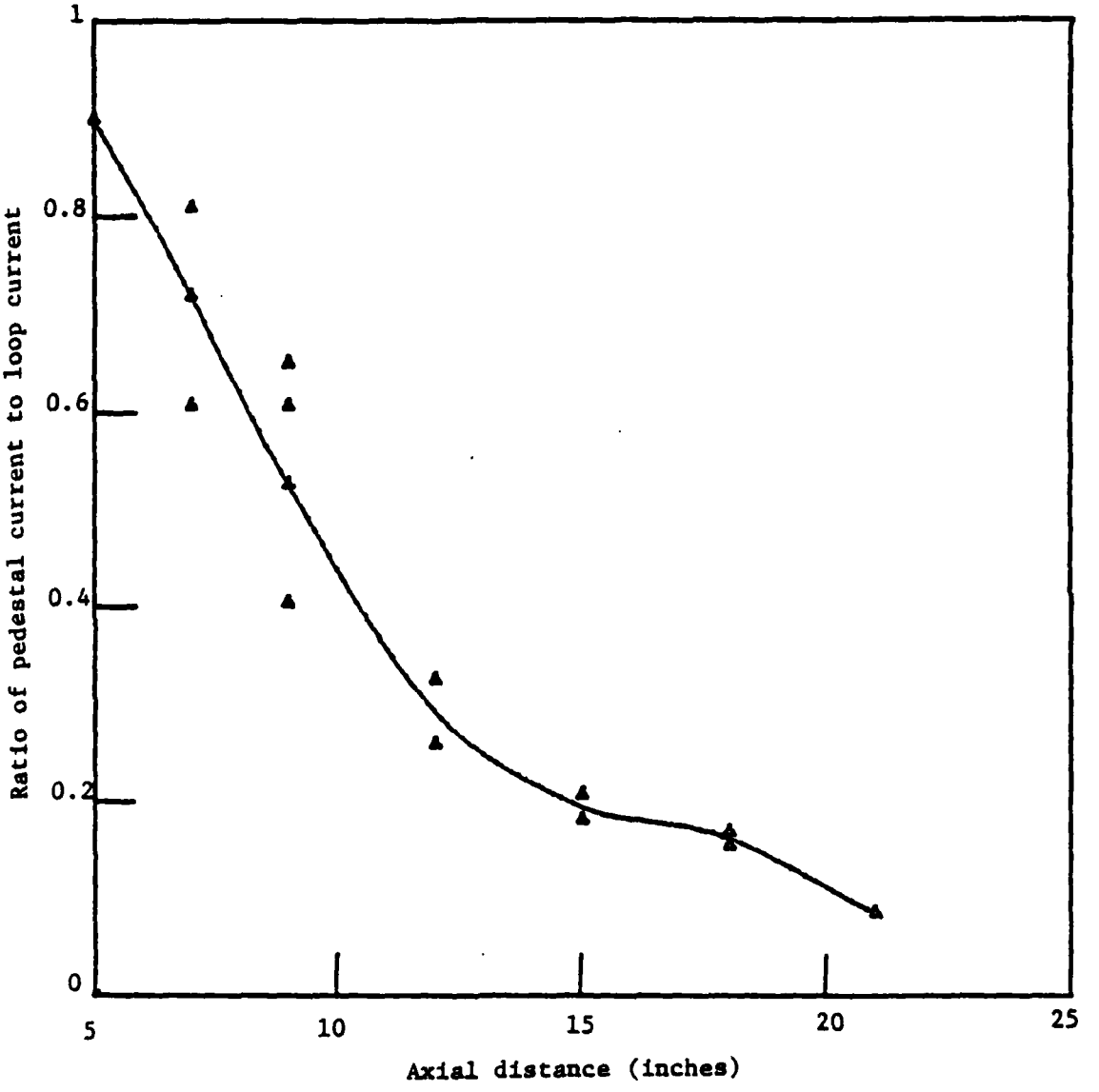

Figure 4.20 Loss of current in drift tube

Rogowski signal. The diode loop current was also considerably reduced.

When the Rogowski was placed immediately following the anode with filaments present, it showed about 22 kA entering the drift tube, out of 27 kA generated. Without filaments the signal was very narrow and erratic.

On the other hand, without filaments the PIN diode signals were relatively uniform and reproducible. Apparently, what beam got into the tube was regular in structure. Fig. 4.21 shows a plot of the peak PIN voltage vs position from the anode. We notice that the presence of filaments enhances the signal. The enhancement factor was greater further downstream, indicating less loss of beam as it travels the drift tube.

4.8.3 Timing of the Signals

Fig. 4.22 shows several PIN signals taken at different locations from the anode. These traces were taken without filaments being present but with an anode graphite aperture. One first observes that the PIN signals all began simultaneously, regardless of location. When the PIN was close to the anode (2.5 in.), a single initial peak was seen. As the PIN was moved downstream, the peak occurred later in time, and an initial plateau developed. This delay, between the signal beginning and the peak, is plotted in Fig. 4.23. Near the anode the peak velocity is approximately 0.02c. Between 6 and 12 in. its velocity appears to have increased to 0.06c. Beyond this point signals occur simultaneously in the tube. 0.5 MeV electrons have a velocity of 0.87c. This behavior gives a picture of an electron beam expanding into the drift tube and then focussing slightly. This action would cause a pattern of increased x-ray generation to move along the wall.

Besides the timing in the tube, it was found that an additional delay of 30 ns existed between the appearance of diode voltage and the

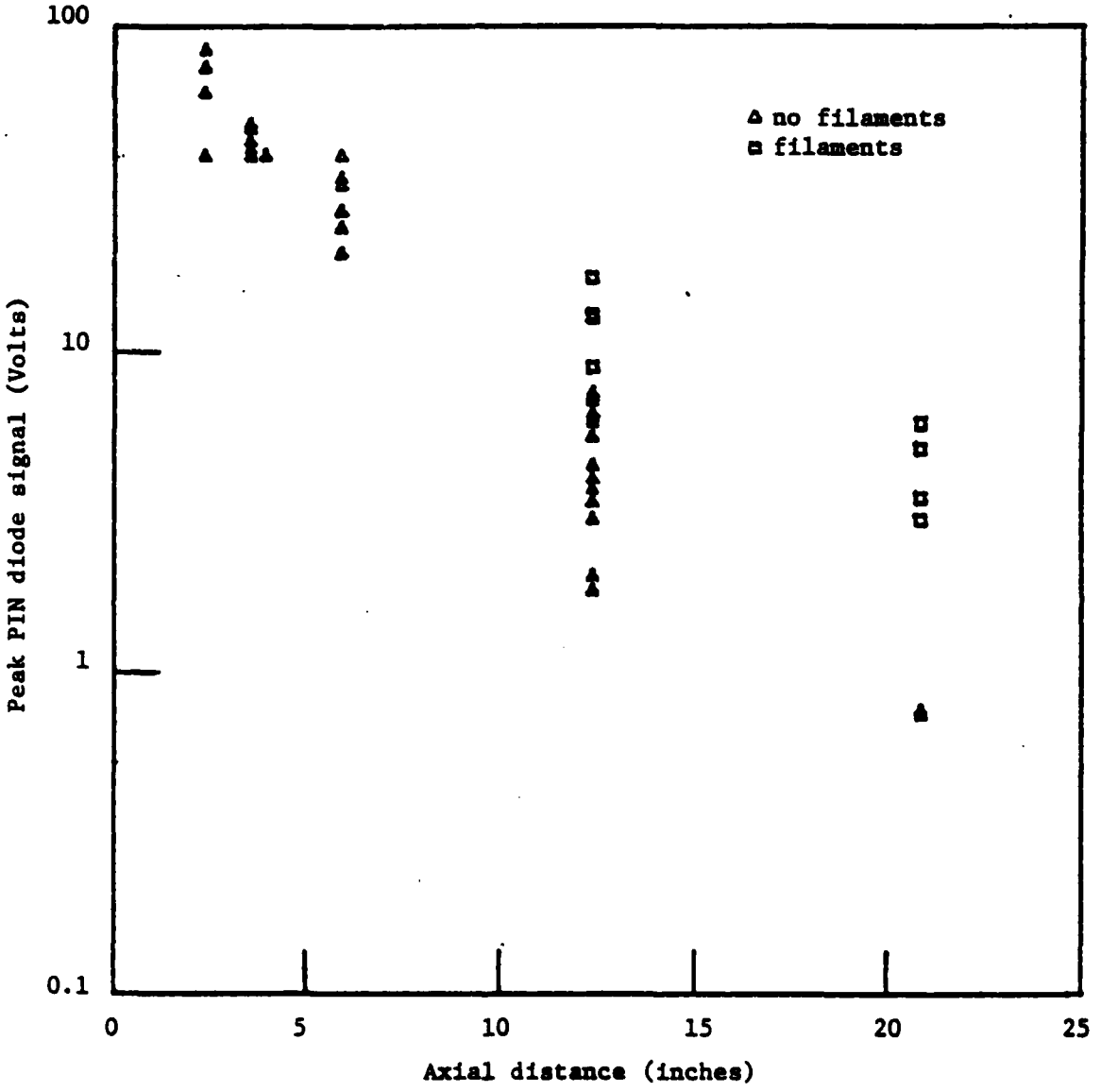

Figure 4.21 PIN signal vs position along drift tube

upper at 2.5 in.
lower at 12.5 in.

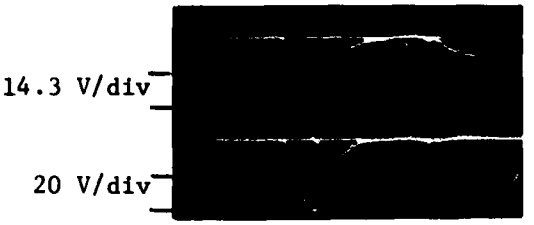

both at 3.5 in.

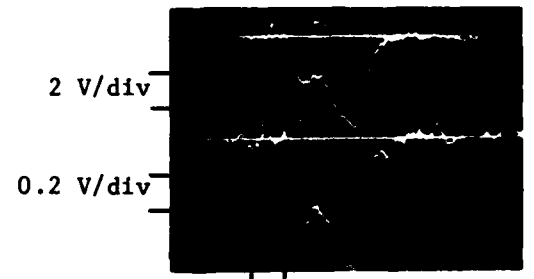

upper at 12.5 in.
lower at 21 in.

Figure 4.22 PIN diode signals, with no filaments.
The indicated locations are axial positions measured downstream from the anode.

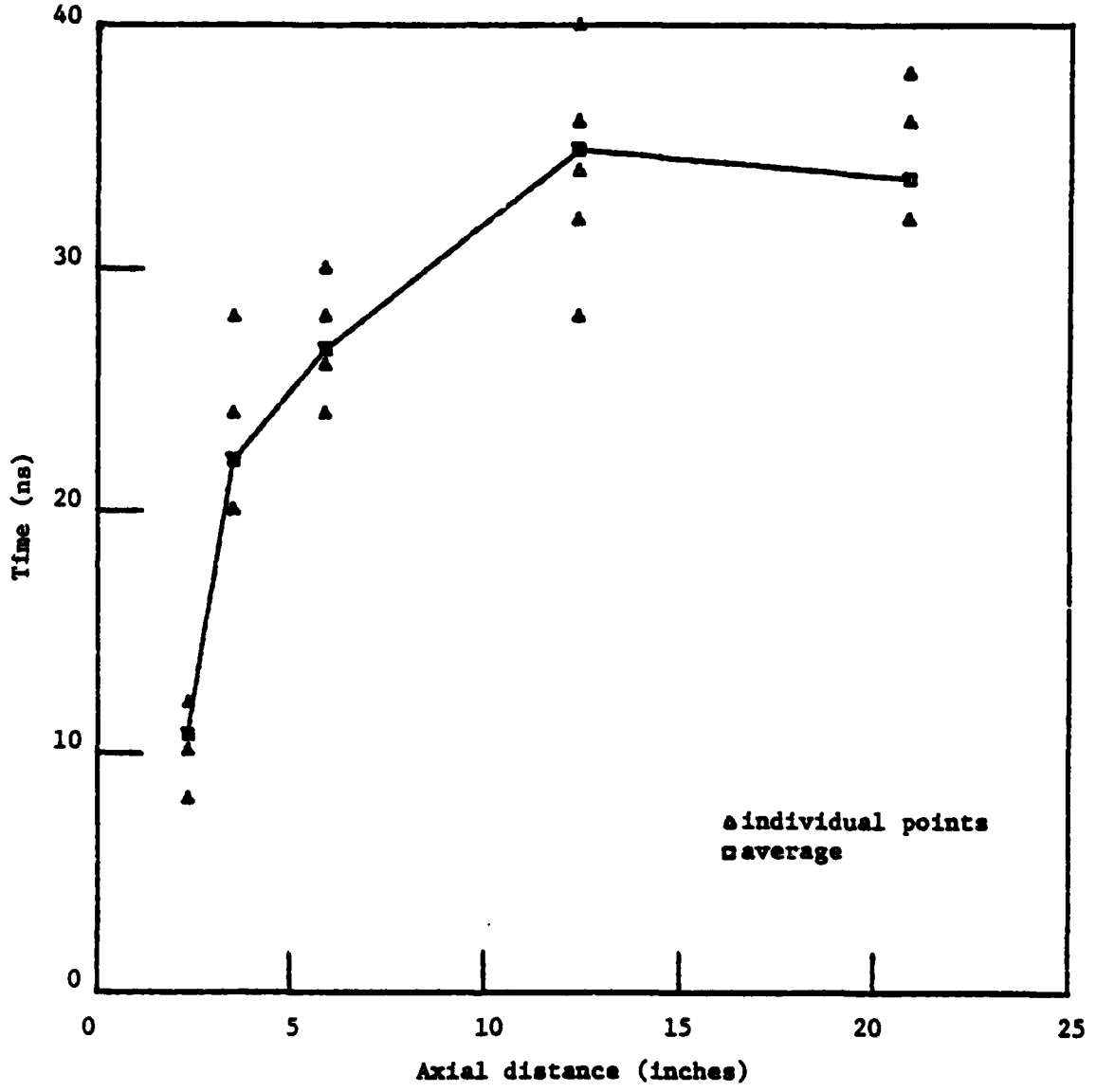

Figure 4.23 PIN diode signal delays

beginning of the PIN signals. This delay was determined by delaying a PIN signal by a known amount and adding it to the voltage signal. In this way the PIN signal could be seen beyond the end of the voltage pulse. If the beam initially expands rapidly, this delay may be the time required for it to become more forward directed.

When filaments were present, the PIN signals became rather unpredictable. The only constant feature seemed to be the time the signals began and ended. The 30 ns delay with respect to the diode voltage was still present also. Fig. 4.24 shows a sequence of PIN signals all taken at the same drift tube position (9 in. from the anode). We see that PIN's on opposite sides of the drift tube did not even track each other, as they did when filaments were not present. This behavior gives a picture of a beam which may be pulsing or wandering in the drift tube. There was no progression of a peak to later times as the PIN was moved downstream.

Comparison of the PIN signals (at 9 in.) and the Rogowski signal (at the anode) shows that they begin simultaneously when no filaments are present but that there is a 20 ns delay in the PIN signal with filaments. It was also observed that, when the pedestal was at a position of 1 ft and beyond, its current signal began after the PIN signal by 10-20 ns. The velocities associated with these various signal delays are all too slow to be synchronized with protons of energy above 2 MeV. In any event, it appears likely that all the ion acceleration occurs in the first few centimeters of the drift tube.

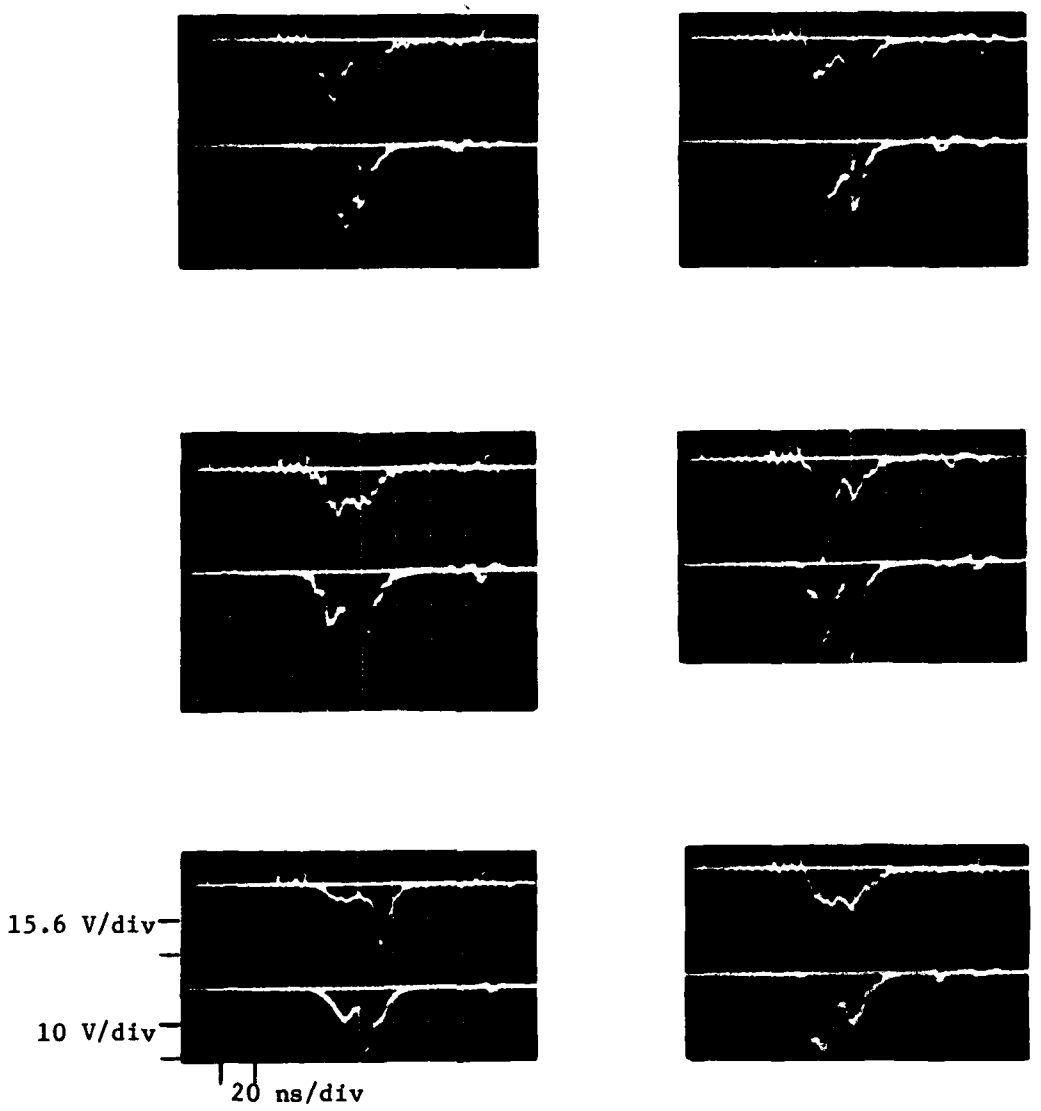

Figure 4.24 PIN diode signals, filaments present
The detectors are at 9 in. on opposite sides of the drift tube.

5. THEORETICAL CONSIDERATIONS

5.1 Aspects of the Problem

Olson[9] lists seven collective ion acceleration mechanisms which have been proposed by various researchers. They are net space charge, inductive, inverse coherent drag, linear waves, nonlinear waves, stochastic, and impact. These may further be rated by the size of the accelerating fields associated with each. Impact acceleration, while able to impart enormous energies to the ions, also seems to be one of the most difficult mechanisms to establish in practice. The net space charge and nonlinear wave methods are capable of large accelerating fields. The linear wave method is capable of moderate fields, and the others produce only small or very small fields.

In accounting for the ion acceleration observed in the experiments described herein, it is necessary to find a process which occurs naturally. No attempt was made to grow waves on the beam, or inject ions, or otherwise control the acceleration by external means. The acceleration derives only from the presence of the electron beam and its interaction with various passive films, filaments and apertures in its path.

There are numerous difficulties obstructing the development of a quantitative analytical treatment of ion acceleration in vacuum diodes and drift tubes. The geometries are irregular, often consisting of pointed cathodes and apertures. Various insulating plastics may be present. There is an applied E_z in the diode (i.e. the beam is not merely drifting). Moving plasmas are being generated by beam bombardment, and their production may be irregular. The ions are also produced in a localized region, rather than being available through out the beam, as when a gas filled drift tube is used. The entire phenomenon is very dynamic in

character. Thus, it seems that the most convincing theory of ion acceleration is likely to come from a particle simulation computer code, while analytical theories will have to examine simpler cases and try for more qualitative results. However, it must be remembered that more symmetry is usually built into simulation codes than actually exists.

Overall, the most attractive acceleration mechanism is the net space charge. One must certainly deal with space charge effects when analyzing the behavior of nonneutral electron beams. Further, electrostatic effects, when present, tend to dominate the magnetic effects. Thus, if ion acceleration can also be accounted for in terms of net space charge, a great theoretical economy will be achieved.

An early attempt to give a theoretical account of collective ion acceleration with a beam injected into a vacuum drift tube was that of Poukey and Rostoker[70]. This theory was one-dimensional, including relativistic effects but excluding magnetic effects. They performed a computer simulation supported by analytical results. Basically, it was found that, when the beam is injected through a grounded metal foil, a potential well is formed which oscillates in depth and position but has an average depth of 2.5 times the beam electron energy (for β=0.8). Presumably, protons merely falling into such a well could achieve energies 2-3 times that of the electrons. However, this mechanism cannot account for observations of ions accelerated to a much greater extent by ourselves and others.

Their theory does not predict a propagating beam (in vacuum), since all electrons are eventually turned around. The distance to which the electrons penetrate, x_m, is of the order c/ω_b, where $\omega_b^2=4\pi ne^2/m\gamma$, n, e, and m are the injected electron density, charge, and mass (cgs-Gaussian units).

A limiting current may be derived for this theory[67]. We observe that the 1D theory will apply if $r_b > 2c/\omega_b$, where r_b is the beam radius. The associated current is $I = e\pi r_b^2 n\beta c$. Thus, we find that the theory holds when

$$I > \beta\gamma mc^3/e \text{ (statamps)} = \beta\gamma(17000) \text{ (Amps)}$$

and, as a result, no beam propagation occurs due to the potential well formation. However, for currents less than this, the 1D approximation may fail. This limiting current is the same as the Alven limiting current, but the latter is a purely magnetic effect, while the former is electrostatic.

Two-dimensional potential wells and limiting currents were discussed in a paper by Olson and Poukey[71]. They derived

$$I_\ell = \beta(\gamma-1)(mc^3/e)[1+2\ln(R/r_b)]^{-1}(1-f_e)^{-1} \text{ (cgs units)},$$

where I_ℓ is the limiting current, R is the drift tube radius, and f_e is the fractional space charge neutralization. This formula was derived by computing the potential at the beam center and equating it to the injected electrons' kinetic energy. Thus, for currents greater that I_ℓ, the electrons do not have sufficient energy to form a beam, and a potential well forms just inside the drift tube. Ion acceleration is not expected to occur unless the injected current exceeds I_ℓ. When $f_e=0$, the current I_ℓ is always less than the previously derived limiting current and so will dominate. For our machine ($\gamma=2$, R=2 in., $r_b=0.625$ in., $f_e=0$) $I_\ell=4430$ Amps, which we exceed in our experiments by a factor of 5-10. For a force neutral beam $f_e=1/\gamma^2$, which gives $I_\ell=5900$ Amps. Thus, even force neutral beams are prevented from propagating.

Swain et al.[72], building on Olson's work, theoretically examined the case of injecting the beam into vacuum with ions supplied by an anode foil.

Prior to charge neutralization they found a potential well created which was 2-3 times the beam energy. The well remained near the anode until enough ions were drawn in to neutralize the space charge. At this time the beam began to propagate, producing a drawn out, dynamic, ion background. The highest proton energies were predicted to be 2-3 times the beam energy.

Other 1D simulations by Destler et al.[73] and by Taylor[74] essentially confirm the earlier work of Poukey and Rostoker. These latter also take into account the presence of an additional grounded plane at the far end of the drift region. Taylor's simulation included injected ions, which were found to be accelerated to an average of 1.4 times the beam energy, but little comment was made regarding his maximum ion energy. Destler et al. considered the acceleration with respect to the beam front. They found, for example, that a beam with $\gamma=2$ (0.5 MeV) and current density of 13 kA/cm^2 could accelerate protons to 20 MeV in 4 nsec. Much depends on the length of time during which the ambipolar process is effective. A calculation is performed in the next section which parallels this one.

To summarize, it seems that, while a moving potential well can, in principle, accelerate ions to high energies, this phenomena has not been entirely born out by numerical simulations. The simulations chiefly find ions accelerated to the depth of the potential well. This observation indicates that proper synchronization of the well and ion motion is not achieved. This latter problem needs to be investigated more fully before it can be determined if net space charge effects alone are capable of explaining all the ion acceleration observed.

5.2 A Simple Acceleration Model

Consider a uniform electron beam injected through a grounded anode foil into a vacuum drift region (see Fig. 5.1). Only one-dimensional motion is allowed. The beam is injected with an initial energy, KE_o, and an outgoing current density, J. In the steady state the actual current density will be zero, since all electrons return to the anode. Using cgs-Gaussian units, Poisson's equation reads

$$dE/dx = 4\pi\rho, \tag{1}$$

where E is the electric field, and ρ is the charge density. The charge density may be related to the outgoing current density by

$$2J = \rho\beta c, \tag{2}$$

where $\beta=v/c$, and the factor of 2 allows for the increase in charge density due to the return current. Letting $E=-dV/dx$, we obtain

$$d^2V/dx^2 = -8\pi J/\beta c. \tag{3}$$

At a given position the beam velocity is determined by KE_o and the potential energy at that position. Thus,

$$KE_o = \gamma_o mc^2 = \gamma mc^2 + eV, \tag{4}$$

where $\gamma^{-2}=1-\beta^2$, m and e are the electron rest mass and charge. Eliminating V from (3), we obtain

$$\beta d^2\gamma/dx^2 = 8\pi \frac{eJ}{mc^3} \tag{5}$$

or

$$\sqrt{1 - 1/\gamma^2}\, d^2\gamma/dx^2 = 8\pi \frac{e J}{mc^3} \tag{6}$$

Let $\gamma'=d\gamma/dx$, then (6) may be written

$$\gamma' d\gamma' = \frac{8\pi\, e\, J\, \gamma d\gamma}{mc^3 \sqrt{\gamma^2-1}}. \tag{7}$$

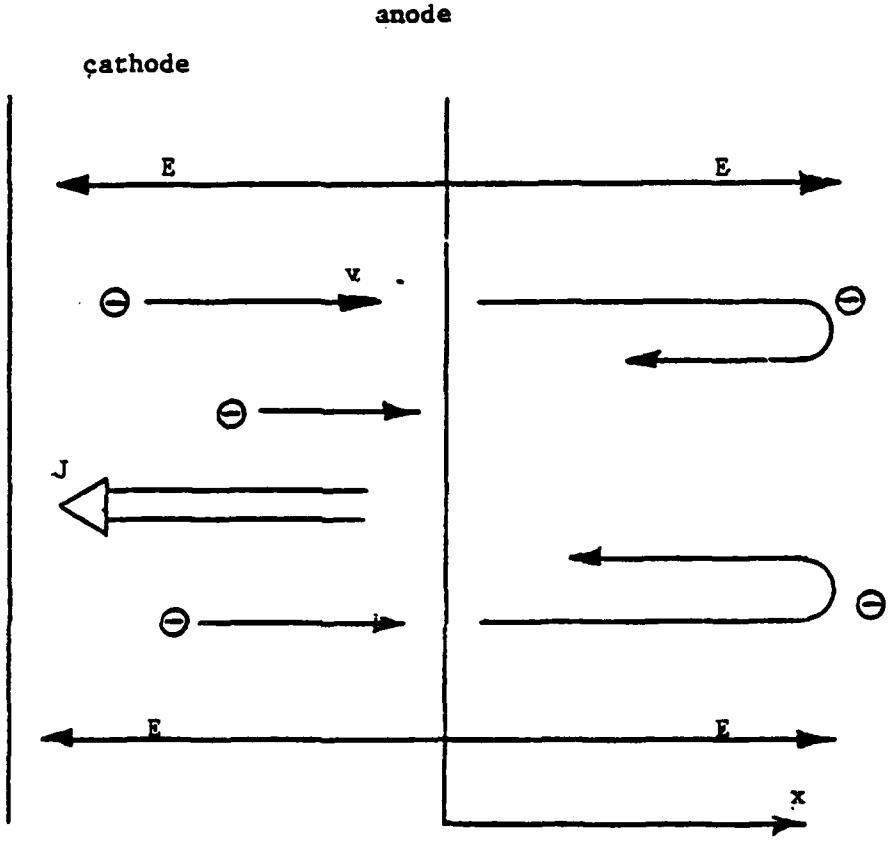

Figure 5.1 Model for collective acceleration

Integrating yields

$$(\gamma')^2 = \frac{16\pi e}{mc^3} J \sqrt{\gamma^2-1}. \tag{8}$$

Integrating again yields

$$\frac{16\pi e}{mc^3} J x^2 = \left(\int_{\gamma}^{\gamma_o} \frac{d\gamma}{(\gamma^2-1)^{1/4}} \right)^2. \tag{9}$$

This formula gives a relationship between the velocity of the electrons and their distance from the anode foil.

We may use this expression to find the turning point of the beam (γ=1). Suppose, for example, that γ_o=2 (0.5 MeV beam) and J=5 kA/cm^2 (corresponds to 40 kA beam with 1.25 in. diameter), then the beam will stop at x=0.28 cm.

We would like to know the electric field, particularly at the anode. We may write

$$E = -dV/dx = -\gamma' dV/d\gamma \tag{10}$$

and
$$V = (\gamma_o-\gamma)mc^2/e. \tag{11}$$

Thus, $dV/d\gamma = -mc^2/e$.

Using γ' from (8), we find

$$E^2 = \frac{16\pi mc}{e} J \sqrt{\gamma^2-1} \tag{12}$$

The field at the anode foil, E_o, for the values above will then be E_o=8620 statvolt/cm=2.59 MV/cm.

This field can accelerate a proton at the rate of

$$a = eE_o/2M = 1.24 \times 10^{18} \text{ cm/sec}^2,$$

where M is the proton mass, and the factor of 2 allows for the fact that a sheet of charge is being accelerated, and thus the entire electric field is not effective. A proton can then be accelerated to 7 MeV in

2.94 ns and a distance of 5.35 cm. The actual acceleration achieved depends on how long the potential well and ions remain synchronized, but 3 ns and 6 cm do not seem to be severe constraints.

There is good reason to believe the field E_o may be much stronger. Its value depends on J, which was calculated without allowing for electron beam pinching. A reflexing process may further increase the effective J. In this process the electrons which return to the anode pass back into the diode region, where they are again turned around, thus adding to the initial current density. In any event, forces are apparently available to provide the observed acceleration. The only question that remains is how effectively and reproducibly they may be brought to bear.

Recently[47] the two-stream instability has again been proposed to explain collective ion acceleration. The effect of this instability is to generate space charge bunches in an otherwise smooth beam. The fields of these bunches then accelerate the ions. However, in our case it does not seem to be necessary to invoke this phenomena in view of the large space charge already present at the beam front. In addition, the instability fields cannot be significantly greater than those already calculated because these alone are sufficient to turn the electron beam.

6. CONCLUSIONS

It has been demonstrated that protons can be accelerated in the direction of an electron beam in both the vacuum diode and vacuum drift tube. In the latter case protons have been accelerated to 7 MeV in 1 ft in quantities of a few times 10^{10}. This energy was 12 times the electron energy of the beam.

The number of ions accelerated for a given geometry varies considerably. This variation prevented distinguishing between most geometries and ion sources. However, in the drift tube experiments, filaments gave distinctly better performance. This improvement supports the contention that it is important not to overload the beam with ions if high energies are desired. It is also clear that some anode ion source is necessary, because its absence gave no ion acceleration.

There seems to be an inverse relationship between ion acceleration and target damage. This was particularly apparent in the Seattle work where the cathode to target distance was necessarily very small.

In the drift tube protons with energies greater than 4 MeV were found at distances from the anode ranging between 7 in. and 24 in. (the maximum tried). The ion energy spectrum seems to increase dramatically toward lower energies. Activity was usually confined to an off-center spot on the target and a corresponding streak on the drift tube wall.

No direct correlation between the electron beam and ion acceleration was identified. However, the presence of filaments in the anode did increase electron beam current and its transport into the drift tube. In addition, PIN diode signals indicated that the beam may be pulsing or wandering off axis.

The intense fields necessary for such collective acceleration have been shown to be present in the moving potential well model. However, the degree of synchronization between ions and the well is still in question.

Activation of dielectric cathodes has also been observed. This activity reveals the radial acceleration of protons from the drift tube wall. The pattern of activity on the cathodes was found to be spatially oscillatory, indicating either a periodic release of ions from the wall or a periodic potential along the cathode.

7. REFERENCES

1. A. M. Sessler, "The Acceleration of Particles by Collective Fields," Comments on Nuclear and Particle Physics 3, 93 (1969).

2. J. D. Lawson, "Collective and Coherent Methods of Particle Acceleration," Particle Accelerators 3, 21 (1972).

3. A. A. Kolomensky, "Particle Acceleration by Electron Beams," Particle Accelerators 5, 73 (1973).

4. M. S. Rabinovich and V. N. Tsytovich, "Prospects for the Development of New Collective Methods of Acceleration," Particle Accelerators 5, 99 (1973).

5. G. Yonas, "Acceleration of Charged Particles by Intense Electron Beams," Particle Accelerators 5, 81 (1973).

6. A. A Kolomensky, "Other Collective Methods," in Proceedings of the Ninth International Conference on High Energy Accelerators, SLAC, Stanford, Calf., May 2-7, 1974 (NTIS CONF-740522) p. 254.

7. G. Wallis, K. Sauer, D. Sunder, S. E. Rosinskii, A. A. Rukhadze, and V. G. Rukhlin, "Injection of High-Current Relativistic Electron Beams into Plasma and Gas," Sov. Phys.-Usp. 17, 492 (1975).

8. C. L. Olson, "Collective Acceleration with Intense Electron Beams," IEEE Trans. Nucl. Sci. NS-22 #3, 962 (1975).

9. C. L. Olson, "Collective Ion Acceleration with Linear Electron Beams," Springer Tracts in Modern Physics 83 (Springer-Verlag, 1979).

10. W. Raudorf, "An Electronic Ram," Wireless Engineer 28, 215 (1951).

11. H. Alfven and O. Wernholm, "A New Type of Accelerator," Arkiv For Fysik 5, 175 (1956).

12. G. J. Budker, "Relativistic Stabilized Electron Beams," Proceedings of the CERN Symposium on High Energy Accelerators vol. 1, 68 (1956).

13. Ya. B. Fainberg, "The Use of Plasma Waveguides as Accelerating Structures in Linear Accelerators," Proceedings of the CERN Symposium on High Energy Accelerators vol. 1, 84 (1956).

14. V. I. Veksler, "The Present State of the Problem of Acceleration of Atomic Particles," Sov. Phys.-Usp. 66, 54 (1958).

15. V. I. Veksler, "The Principle of Coherent Acceleration of Charged Particles," Sov. J. Atom. En 2, 525 (1957).

16. A. A. Plyutto, "Acceleration of Positive Ions in Expansion of the Plasma in a Vacuum Spark," Sov. Phys-JETP 12, 1106 (1961).

17. E. D. Korop and A. A. Plyutto, "Acceleration of Ions of Cathode Material in Vacuum Breakdown," Sov. Phys.-Tech. Phys 15, 1986 (1971).

18. E. D. Dorop and A. A. Plyutto, "Plasma Effects in the Emission of a Needle Cathode," Sov. Phys.-Tech. Phys. 16, 830 (1971).

19. S. E. Graybill and J. R. Uglum, "Observation of Energetic Ions from a Beam-Generated Plasma," J. Appl. Plys. 41, 236 (1970).

20. J. R. Kerns, C. W. Rogers, and J. G. Clark, "Production of Neutrons in a Deuterated Polyethylene Target by an Intense Relativistic Electron Beam," Bull. Am. Phys. Soc. 17, 690 (1972).

21. T. E. McCann, C. W. Rogers, and D. N. Payton, "Neutron Production in Electron Beam Targets," Bull. Am. Phys. Soc. 17, 690 (1972).

22. D. L. Morrow, J. D. Phillips, R. M. Stringfield, Jr., W. O. Doggett, and W. H. Bennett, "Concentration and Guidance of Intense Relativistic Electron Beams," Appl. Phys. Lett. 19, 441 (1971).

23. L. P. Bradley and G. W. Kuswa, "Relativistic High Current Diode Characteristics Associated with Collective Ion Acceleration," Bull. Am. Phys. Soc. 17, 980 (1972).

24. G. W. Kuswa and L. P. Bradley, "Neutron Production by Collective Ion Acceleration in Field Emission Diodes," Bull. Am. Phys. Soc. 17, 980 (1972).

25. J. G. Clark, J. R. Kerns, and T. E. McCann, "Neutron Production via Intense Relativistic Electron Beams," Bull. Am. Phys. Soc. 17, 1031 (1972).

26. L. P. Bradley and G. W. Kuswa, "Neutron Production and Collective Ion Acceleration in a High Current Diode," Phys. Rev. Lett. 29, 1441 (1972).

27. G. W. Kuswa, "Neutron Production Mechanisms in E-Beam Diodes," Bull. Am. Phys. Soc. 18, 1310 (1973).

28. J. R. Kerns and D. J. Johnson, "Study of an Electron-Beam Discharge into a Vacuum Diode with Polyethylene Anode," J. Appl. Phys. 45, 5225 (1974).

29. J. G. Clark and J. R. Kerns, "Neutron Production with High-Current Relativistic Electron Beams and Deuterated Polyethylene Targets," Annals New York Academy of Sciences 251, 273 (1975).

30. G. W. Kuswa, "Experimental Studies of Collective Ion Acceleration," Annals New York Academy of Sciences 251, 514 (1975).

31. B. Freeman, H. Sahlin, J. Luce, O. Zucker, T. Crites, and C. Nelson, "Enhanced Neutron Yield from a Relativistic Electron Beam-Deuterated Polyethylene Target Interaction," Bull. Am. Phys. Soc. 17, 1030 (1972).

32. H. Sahlin, B. Freeman, J. Luce, and O. Zucker, "Theoretical Discussion of the Neutron Yield Produced by Electron Beam-Deuterated Target Interaction," Bull. Am. Phys. Soc. 17, 1030 (1972).

33. B. Freeman, R. Gullickson, O. Zucker, W. Bostick, and H. Klapper, "Phenomena Relating to Relativistic Electron Beam-Deuterated Target Interactions," Bull. Am. Phys. Soc. 18, 1351 (1973).

34. J. S. Luce, H. L. Sahlin, and T. R. Crites, "Collective Acceleration of Intense Ion Beams in Vacuum," IEEE Trans. Nucl. Sci. NS-20 #3, 336 (1973).

35. J. S. Luce, "Neutrons and Radioisotopes Produced by Collective Effect Acceleration," Annals New York Academy of Sciences 251, 217 (1975).

36. G. T. Zorn, H. Kim, and C. N. Boyer, "Experimental Investigation of Linear-Beam Collective Ion Acceleration in Vacuum," IEEE Trans. Nucl. Sci. NS-22 #3, 1006 (1975).

37. G. T. Zorn, H. Kim, and C. N. Boyer, "Experimental Investigation of Linear-Beam Collective Ion Acceleration in Vacuum," Bull. Am. Phys. Soc. 20, 1381 (1975).

38. R. F. Hoeberling, R. B. Miller, D. C. Straw, and D. N. Payton 3rd, "Collective Ion Acceleration in the Evacuated Drift Tube Geometery," Bull. Am. Phys. Soc. 21, 1059 (1976).

39. R. F. Hoeberling and D. N. Payton 3rd, "Ion Acceleration in the Evacuated Drift-Tube Geometry," J. Appl. Phys. 48, 2079 (1977).

40. R. Williams, J. A. Nation, and M. E. Read, "Measurements of Ion Acceleration in Relativistic Electron Beams, "Bull. Am Phys. Soc. 21, 1059 (1976).

41. O. Zucker, J. Wyatt, H. Sahlin, J. S. Luce, B. Freeman, and R. Gullickson, "Collective Field Acceleration by the Interaction of a Relativistic E-Beam with an Apertured Solid Dielectric Anode (Luce Geometry)," in N. Rostoker and M. Reiser (eds.) Collective Methods of Acceleration (Harwood Academic Publishers, 1979), p.475.

42. W. W. Destler, L. Floyd, and M. Reiser, "Experimental Studies of Heavy Ion Collective Acceleration at the University of Maryland," IEEE Trans. Nucl. Sci. NS-26 #3, 4177 (1979).

43. W. W. Destler, R. F. Hoeberling, H. Kim, and W. H. Bostick, "Collective Acceleration of Carbon Ions to 170 MeV," Appl. Phys. Lett. 35, 296 (1979).

44. L. E. Floyd, W. W. Destler, M. Reiser, A. Sternlied, H. M. Shin, and S. E. Graybill, "Collective Acceleration of Heavy Ions," Bull. Am. Phys. Soc. 24, 1026 (1979).

45. W. W. Destler, L. E. Floyd, and M. Reiser, "Collective Acceleration of Heavy Ions," Phys. Rev. Lett. 44, 70 (1980).

46. R. J. Adler and J. A. Nation, "Collective Acceleration of Metallic Ions," Appl. Phys. Lett. 36, 810 (1980).

47. R. J. Adler, "Collective Acceleration of Ions in Vacuum," Ph.D Thesis, Cornell University (1980).

48. U. Schumacher, "Collective Ion Acceleration with Electron Rings," Springer Tracts in Modern Physics 83 (Springer-Verlag, 1979).

49. M. L. Sloan and W. E. Drummond, "Autoresonant Accelerator Concept," Phys. Rev. Lett. 31, 1234 (1973).

50. S. Humphries, J. J. Lee, and R. N. Sudan, "Generation of Intense Pulsed Ion Beams," Appl. Phys. Lett. 25, 20 (1974).

51. R. A. Mahaffey, J. A. Pasour, J. Golden and C. A. Kapetanakos, "Collective Ion Acceleration in Reflecting Electron Systems," in N. Rostoker and M. Reiser (eds.) Collective Methods of Acceleration (Harwood Academic Publishers, 1979), p. 521.

52. N. Camarcat, P. L. Dreike, C. B. Eichenberger, S. Glidden, M. Greenspan, D. A. Hammer, S. Humphries, Jr., J. Maenchen, J. Neri, R. N. Sudan, and L. G. Wiley, "Progress in the Production of Intense Proton Beams with Magnetically Insulated Diodes," in N. Rostoker and M. Reiser (eds.) Collective Methods of Acceleration (Harwood Academic Publishers, 1979), p. 413.

53. Richard L. Copeland, Herbert P. Neff, Jr., Willard H. Bennett, David L. Morrow, and John L. Adamski, "A Simulation Model for the FX-75 Relativistic Electron Beam Accelerator," IEEE Trans. Nucl. Sci. NS-25 #3, 1017 (1978).

54. R. M. Stringfield, Jr., "Surface Flashover Characteristics of Alumina Dielectric Guide Cathodes in an Intense Relativistic Electron Beam Accelerator," Ph.D. Thesis, North Carolina State University (1978).

55. Dean Eugene Pershing, "Intense Relativistic Electron Beam Propagation in Evacuated Dielectric Guides," Ph.D Thesis, North Carolina State University (1980).

56. Wesley O. Doggett, "Coherent Acceleration of Ion Bunches by Intense Relativistic Electron Beams," Proposal No. RDRD-P-10633 submitted to the U. S. Army Research Office - Durham, October 25, 1971.

57. Wesley O. Doggett, "Proposed Method for Achieving Coherent Acceleration of Ion Clouds by Relativistic Electron Beams," Physics Department Seminar, North Carolina State University, November 18, 1970.

58. Irving Kaplan, Nuclear Physics (Addison-Wesley Publishing Company, 1962), p. 315.

59. W. H. Barkas and M. J. Berger, Tables of Energy Losses and Ranges of Heavy Charged Particles, NASA SP-3013 (1964).

60. P. Dagley, W. Haeberli, and J. X. Saladin, "The $C^{13}(p,n)N^{13}$ Reaction Cross Section from Threshold to 13 MeV," Nuclear Physics 24, 353 (1961).

61. F. C. Young, J. Golden, and C. A. Kapetanakos, "Diagnostics for Intense Pulsed Beams," Rev. Sci. Instrum. 48, 432 (1977).

62. Wesley O. Doggett, Ray M. Stringfield, Jr., David L. Morrow, and Willard H. Bennett, "Ion Acceleration in the Diode Region of a Relativistic Electron Beam Machine," Bull. Am. Phys. Soc. 20, 585 (1975).

63. Wesley O. Doggett, David L. Morrow, Ray M. Stringfield, Jr., Stanley P. Converse, Willard H. Bennett, and Pax S. P. Wei, "Ion Acceleration Using Thin Mats, Meshes, and Filaments," Bull. Am. Phys. Soc. 20, 1234 (1975).

64. W. O. Doggett and W. H. Bennett, "Collective Ion Acceleration Experiments," Proceedings 2nd Symposium on Collective Methods of Acceleration (JINR Dubna, USSR, 1977), p. 127.

65. R. Colle, R. Kishore, and J. B. Cumming, "Excitation Functions for (p,n) Reactions to 25 MeV on ^{63}Cu, ^{65}Cu, and ^{107}Ag," Physical Review C 9, 1819 (1974).

66. J. A. Pasour, R. K. Parker, R. L. Gullickson, W. O. Doggett, and D. Pershing, "Collective Ion Acceleration and Intense Electron Beam Propagation Within an Evacuated Dielectric Guide," in N. Rostoker and M. Reiser (eds.) Collective Methods of Acceleration (Harwood Academic Publishers, 1979), p.383.

67. J. H. Hubbell and M. J. Berger, "Photon Attenuation," in R. C. Jaeger (ed.) Engineering Compendium on Radiation Shielding (Springer-Verlag, 1968), vol. 1, p. 167.

68. R. H. Pratt, H. K. Tseng, C. M. Lee, and Lynn Kissel, "Bremsstrahlung Energy Spectra from Electrons of Kinetic Energy 1 keV <= T_1 <= 2000 keV Incident on Neutral Atoms 2 <= Z <= 92," Atomic Data and Nuclear Data Tables 20, 175 (1977).

69. Lucien Pages, Evelyne Bertel, Henri Joffre, and Laodamas Sklavenitis, "Energy Loss, Range, and Bremsstrahlung Yield for 10-keV to 100-keV Electrons in Various Elements and Chemical Compounds," Atomic Data 4, 1 (1972).

70. J. W. Poukey and N. Rostoker, "One-Dimensional Model of Relativistic Electron Beam Propagation," Plasma Physics 13, 897 (1971).

71. C. L. Olson and J. W. Poukey, "Force-Neutral Beams and Limiting Currents," Phys. Rev. A 9, 2631 (1974).

72. D. W. Swain, G. W. Kuswa, J. W. Poukey, and C. L. Olson, "Collective Ion Acceleration in Linear Electron Beams," in Proceedings of the Ninth International Conference on High Energy Accelerators, SLAC, Stanford, Calif., May 2-7, 1974 (NTIS CONF-740522), p.268.

73. W. W. Destler, H. S. Uhm, H. Kim, and M. P. Reiger, "Study of Collective Ion Acceleration in Vacuum," J. Appl. Phys. 50, 3015 (1979).

74. Peter L. Taylor, "Relativistic Electron-Beam Propagation in Vacuum with Ion Acceleration," J. Appl. Phys. 5, 22 (1980).